Effect of Heat Treatment and Silver Deposition on the Corrosion Behaviour of Magnesium Alloys for Bone Implant Applications

by

Joyce Lam

A thesis
presented to the University of Waterloo
in fulfillment of the
thesis requirement for the degree of
Master of Applied Science
in
Mechanical Engineering

Waterloo, Ontario, Canada, 2013

AUTHOR'S DECLARATION

I hereby declare that I am the sole author of this thesis. This is a true copy of the thesis, including any required final revisions, as accepted by my examiners.

I understand that my thesis may be made electronically available to the public.

Abstract

Pure magnesium (Mg) and its alloys with calcium (Ca) and both Ca and zinc (Zn) have potential as bioresorbable bone implant materials provided the corrosion rate can be controlled. Thus, corrosion behaviour was investigated for pure Mg, Mg-2Ca, and Mg-2Ca-1Zn cast alloys subjected to either no heat treatment or to solutionizing and aging heat treatment. In addition, corrosion behaviour was investigated for surface modifications involving the deposition of silver (Ag) nanoparticles. These materials and constructs were all nominally biocompatible in that they would not elicit a strong and immediate adverse tissue reaction when implanted in bone.

Static immersion tests in Hanks' balanced salt solution were performed to evaluate the corrosion behaviour. The Mg-2Ca alloy exhibited the highest corrosion rate when compared with pure Mg and Mg-2Ca-1Zn for any length of immersion time. For short immersion times (48 hours), solutionizing followed by natural aging reduced the corrosion rate of Mg-2Ca alloy, but this heat treatment did not seem to have an effect on the corrosion rate of Mg-2Ca-1Zn alloy. As well, for short immersion times (48 hours), solutionizing and artificial aging also did not seem to have a large effect on corrosion rates for either Mg-2Ca or Mg-2Ca-1Zn, when compared to solutionizing and natural aging. Corrosion behaviour of surface-modified samples was sensitive to certain features of the Ag depositions. It was found that when the deposited Ag tracks were thick and wide, the corrosion rate of Ag-deposited samples increased significantly when compared to samples without any Ag deposition. However, when the Ag tracks were thinner and somewhat narrower, the corrosion rate did not appear to

be much higher than that of samples without Ag deposition. Therefore, controlled Ag deposition may not be too detrimental to the corrosion behaviour of Mg and Mg alloys.

The corrosion product morphology appeared to be similar for both the samples deposited with Ag and samples without any Ag. Needle-like formations were observed in small areas on the corroded surfaces. X-ray diffraction revealed $Mg(OH)_2$ as the main corrosion product. Because energy dispersive X-ray analysis consistently revealed multiple elements in the corrosion products (such as Mg, O, Ca, P, small amounts of C, and sometimes Cl), it was concluded that other compounds (possibly hydroxyapatite, magnesium chloride, and/or magnesium- and calcium-containing phosphates) may have formed in addition to the $Mg(OH)_2$.

Acknowledgements

First and foremost, I would like to acknowledge my supervisors, Dr. Shahrzad Esmaeili, Dr. John Medley, and Dr. Ehsan Toyserkani, for their endless guidance, support, and patience. I am very thankful to have had the opportunity to learn from them. What a tremendous learning experience!

I'd also like to acknowledge Dr. Hamidreza Alemohammad and Dr. Ehsan Foroozmehr for all of their help and guidance in using the M^3D machine. I'd like to thank Dr. Xiaogang Li for performing the XRD tests, Dr. Yuquan Ding for his assistance in operating the SEM/EDX, Dr. Panthea Sepehrband for the many hours she patiently spent helping me perform SEM/EDX on my numerous samples, and Brian Langelier for kindly offering advice and answering all my questions pertaining to Mg and Mg alloys. Teresa King is also thanked for her assistance with the Ag deposition during the early stages of sample fabrication. Dr. Daryoush Emadi and CANMET-MTL (AUAF program) are warmly thanked for casting and providing the alloys, and for related chemical analysis of the materials used in this work.

Finally, I would like to acknowledge my wonderful parents, Paul and Christina, for the never-ending love, support, and encouragement they have provided me over the years. As well, I'd like to acknowledge my brother, Gordon, for always believing in me and for being such an inspiration to me. Last but not least, I'd like to acknowledge Carl Chan for his constant motivation and support.

Dedication

To my wonderful family.

Table of Contents

List of Figures

List of Tables

List of Abbreviations

AC	As-cast
ANOVA	Analysis of variance
EDX	Energy dispersive X-ray (analysis)
M3D	(Optomec) Maskless Mesoscale Material Deposition (machine)
MAO	Microarc oxidation
RE	Rare earth (elements)
S&AA	Solutionized and artificially aged
S&NA	Solutionized and naturally aged
SEM	Scanning electron microscopy
XRD	X-ray diffraction

Chapter 1

Introduction

Metallic materials have commonly been used for bone implants, particularly for those requiring load-bearing capabilities. Metallic materials are selected for these applications because of their appropriate mechanical properties; such as high tensile and yield strength, and resistance to fatigue and creep [1]. Stainless steels, titanium alloys, and cobalt-chromium alloys are among the most common metallic materials used for implants and medical devices [1].

However, for implant applications such as bone fracture fixation plates, the use of these metals can be associated with several adverse effects, including stress-shielding in the surrounding bone and hypersensitivity to the metals [2]. Because of these effects, a second surgery is often required to remove the implant after the bone has healed [2]. Understandably, this second surgery would lead to increased patient morbidity as well as increased health care costs [3].

In most cases, it would be ideal if an implant could provide the necessary support needed to assist with bone healing, gradually resorb while the bone heals, and then 'disappear' after the bone tissue completely heals, thus eliminating the need for implant removal. Such a scenario could be achieved through the use of bioresorbable implants. Some ceramics have been used as bioresorbable implant materials, such hydroxyapatite and tricalcium phosphate [4]. Bioresorbable ceramics are attractive because of their ability to degrade in the body either slowly or rapidly, and also because they can be resorbed by osteoclasts due to their

similarity to bone's mineral components [4]. Several polymers have also been used as bioresorbable implant materials, such as polylactic acid and polyglycolic acid, and they have been used for sutures and in tissue engineering [4].

The main limitations in using polymers and ceramics as implant materials arise from their mechanical properties. Because of the relatively low strength and stiffness of most polymers, they are generally not used for load-bearing applications, and ceramics are limited by their brittleness as well as their low tensile strength [4]. Since metals appear to be advantageous as materials for load-bearing implants due to their superior mechanical properties, a bioresorbable metal would appear to fill the niche for a load-bearing implant that can also resorb into the body and eliminate the need for implant removal. Magnesium (Mg) and its alloys are metallic materials that have potential as bone implant materials. There are a number of reasons for this potential.

First, Mg is one of the major essential elements in the human body [5]. It is needed by the body for a number of important metabolic processes. An average adult human stores approximately 24 g of Mg in the body, with approximately 60-65% of that stored in bone [6]. Mg is obtained from a multitude of foods, with the recommended daily intake for average adults being 300-420 mg [6]. Some studies have shown that supplementary Mg may have beneficial effects on bone density, and thus, elevated levels of Mg may help reduce the risk of osteoporosis [6]. The upper level of serum Mg is controlled by the kidneys, which excretes excess Mg in the urine. Because of the body's ability to excrete excess Mg efficiently, complications of hyper-magnesium are rare [3] but can happen [7].

Second, the mechanical properties of Mg and its alloys are believed to be suitable for load-bearing bone implant applications. Their modulus of elasticity is much closer to that of cortical bone than other conventional metallic implant materials [8], such as stainless steels, titanium alloys, and cobalt-chromium alloys (Table 1). This reduces the possibility of stress shielding of the surrounding bone.

Table 1: Elastic moduli and tensile strength of various implant materials compared with that of cortical bone (data adapted from [8])

Material	Modulus of Elasticity (GPa)	Tensile Strength (MPa)
Cortical Bone	10-20	100-200
Magnesium	41-45	185-232
Stainless steels	193	480-834
Cobalt alloys	195-210	655-1400
Titanium alloys	100-105	550-985

Finally, Mg and its alloys have the ability to corrode in the physiological environment, making them suitable materials for bioresorbable implant applications. Unfortunately, Mg tends to corrode too rapidly in the human body. This may lead to the evolution of hydrogen gas with an accumulation of gas bubbles at the implant site which can lead to delayed healing along with necrosis of surrounding tissues [9] and a premature degradation of the implant with loss of support for the damaged bone.

The present thesis examines ways to control the corrosion behaviour of Mg and some of its alloys. The investigations include heat treatment, silver (Ag) nanoparticle deposition and alloy development. (Ag was chosen because it has been noted to have good antimicrobial

properties, and could lead to a reduced chance of bacterial colonization [10] at an implant site.) The findings of the present thesis will provide bone implant designers with supporting information to facilitate their application of Mg and its alloys.

There were three main objectives in this work. The first objective was to evaluate the corrosion behaviour of pure Mg and two biocompatible alloys with calcium (Ca) and both Ca and zinc (Zn) (Mg-2Ca and Mg-2Ca-1Zn) in as-cast and heat treated conditions. The second objective was to examine the effect of a surface modification strategy (involving the deposition of Ag nanoparticles in a particular pattern) on the corrosion behaviour of as-cast pure Mg, and as-cast and heat treated Mg-2Ca(-1Zn) alloys. The third objective was to identify the corrosion products that formed during the corrosion reaction.

In the chapters to follow, a review of the literature will first be presented, with discussions regarding early uses of Mg as orthopaedic implant materials, limitations surrounding the successful use of Mg, and current strategies used by researchers to overcome these limitations. The experimental procedures followed in this work will then be described in detail, followed by a presentation of results and discussion. Finally, concluding remarks will be given based on the findings in this work.

Chapter 2

Literature Review

The early uses and current limitations of Mg as a potential bioresorbable implant material (mainly, poor corrosion resistance) are presented. Several strategies have been employed by various researchers to help improve the corrosion resistance of Mg and these strategies are also described.

2.1 Magnesium as a Bioresorbable Implant Material

According to Staiger *et al*. [3], the application of Mg as a bioresorbable orthopaedic implant material began in the early 1900s, first by Lambotte in 1907, Troitskii and Tsitrin in 1944, and Znamenski in 1945. These early attempts at implants, such as plates and screws using pure Mg (Lambotte), Mg alloyed with cadmium (Troitskii and Tsitrin), and Mg alloyed with aluminum (Znamenski) were used to treat various bone fractures [3]. Some of these cases were not successful with rapid corrosion of the Mg and the production of hydrogen gas accumulating as subcutaneous bubbles. However, other cases demonstrated the potential of Mg as a bioresorbable implant material with fusing of fractures, no adverse inflammatory reactions to the implant, and no significant increases in serum magnesium levels [3]. Despite showing potential, the idea of Mg as an implant material was abandoned (likely due to the hydrogen gas formation) when stainless steels appeared as other potential implant materials [11].

Recently, perhaps because of a greater understanding of corrosion behaviour and strategies for improving corrosion resistance, interest in Mg as an implant material has been

regained. Surprisingly, Mg has so far seen the most application in blood vessel stents [12]. Bioresorbable Mg stents are often preferred over permanent stents that tend to interact with adjacent tissue leading to long-term endothelial dysfunction [13,14] and chronic inflammatory reactions [14]. The Mg stents, on the other hand, can provide the necessary support for the vessel while it heals/remodels and then resorb away, which reduces the risk of late restenosis [13]. Some animal studies, such as the one performed by Waksman *et al.* [15], in which stents made of magnesium, zirconium, yttrium, and rare earth elements were implanted into the coronary arteries of pigs, have demonstrated the safety of bioresorbable Mg stents. Clinical studies such as the one performed by Peeters *et al.* [13] (where 20 patients with critical limb ischemia received resorbable stents made of Mg and rare earth elements (Figure 1)) have further shown the potential and promise of Mg bioresorbable stents.

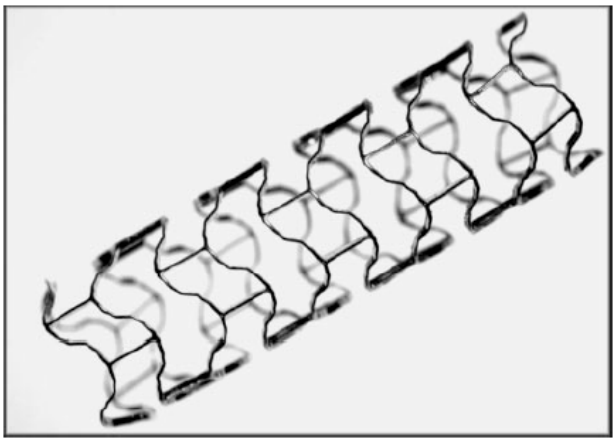

Figure 1: Bioresorbable Mg stent (Biotronik).

For bone implant applications, however, it is generally believed that Mg corrodes too rapidly in the physiological environment [16,17]. Because of this, improving the corrosion resistance of Mg and its alloys has become a prominent area of research, particularly for bone implant applications in orthopaedics.

2.2 Improving the Corrosion Resistance of Magnesium

Since rapid corrosion in the human body is currently one of the greatest limitations of Mg as a successful bone implant material [3,16,18], many researchers are focusing exclusively on modifying the *in vivo* corrosion properties. There have been several different strategies for improving the corrosion properties; two main strategies (alloying and surface modifications) are discussed in this section.

2.2.1 Alloying

In addition to the conditions of the environment, the corrosion behaviour is also affected by the alloy chemistry [19]. Therefore, proper alloying provides a way of controlling the corrosion rate of common Mg alloys. Several researchers have studied various alloys to determine which alloy systems have more desirable corrosion behaviour. Alloy systems that have been investigated for biomedical applications include aluminum (Al)-containing Mg alloys, alloys with rare earth (RE) elements, and alloys including manganese (Mn), zinc (Zn), and calcium (Ca). Elements such as Al, zirconium (Zr), yttrium (Y), and neodymium (Nd) have been understood to improve corrosion resistance [20]. Other elements have been shown to enhance the mechanical properties; for example, Mn enhances ductility, Ca can help grain refinement and enhance

precipitation strengthening, additions of Zn increase strength, and lithium (Li) improves ductility [19]. Although optimizing these changes in mechanical properties is not as important as controlling corrosion resistance, it does suggest that for a given application, it may be possible to reduce the surface area and mass of Mg alloy thus providing some indirect reduction of corrosion rate.

Many of the alloys being studied by researchers were "*mostly commercial alloys which have been developed for the needs in transportation industry*" [19], which may explain the prominence of biomedical studies in the literature using alloys containing elements that are thought to be not biocompatible or even having toxic effects on the human body. Such elements are Al (which has been linked to dementia [9] and Alzheimer's disease [21]), Zr (which has been associated with several types of cancer [9]), and several rare earth (RE) elements (such as praseodymium, cerium, and lutetium, which have been said to be toxic [9]).

Mg Alloys Containing Aluminum and/or Rare Earth Elements

As mentioned, several groups of researchers have investigated Al-containing Mg alloys [11,16,22]. Xin *et al.* [16] focused on the electrochemical behaviour of an Al-containing Mg alloy, AZ91 (9 wt. % Al, 1 wt. %Zn). They systematically investigated the electrochemical behaviour in the hopes of contributing to the understanding of the alloy's corrosion process. They observed the precipitation of magnesium and calcium phosphates, as well as magnesium oxide as corrosion products. They also commented on the marked effect that the secondary β-phase ($Mg_{17}Al_{12}$) had on corrosion; the β-phase

can act as a local cathode while the Mg matrix acts as the local anode, creating a micro-galvanic couple and thus accelerating the corrosion of the matrix.

Witte *et al*. [11] carried out an investigation with two aluminum-containing alloys (AZ31 and AZ91) as well as two alloys containing RE elements (WE43 and LAE442). In this study, their approach focused on investigating the degradation mechanism *in vivo* and, in particular, observing the bone-implant interface to reveal the effects of the corroding alloys on the bone [11]. They implanted these alloys into the femora of guinea pigs, and found that the LAE442 implant corroded more slowly than the AZ31, AZ91, and WE43 alloy implants [11].

Other researchers have performed investigations with other alloys containing rare earth elements as well. Zhang *et al.* [23] investigated an Mg-Zn-Y alloy with relatively low Zn content. They tested these alloy samples for their mechanical and corrosion properties, and performed microstructure characterization. Their findings indicated Y additions played a strong role in the grain refinement of the alloy and could have a beneficial effect on the alloy's tensile strength and elongation. They identified the presence of the secondary 'I-phase' (Mg_3Zn_6Y) which they observed to have a strengthening effect on the alloy [23]. In addition, they noted that the corrosion resistance was better when only a single secondary phase was present rather than having both secondary phases present (i.e., the I-phase and W-phase). In particular, the alloy which exhibited the lowest corrosion rate had only the I-phase as the secondary phase present [23].

Wu *et al.* [24] investigated fourteen different alloys based on the AZ91D alloy to determine the effect of Ca and RE additions on the mechanical properties, microstructure, and corrosion properties. They added various amounts of Ca to the AZ91D alloy (AZ91D-*x*Ca), various amounts of RE to the AZ91D (AZ91D-*x*RE), and then various amounts of Ca to an AZ91D alloy with 1 wt. % RE (AZ91D-1RE-*x*Ca). They compared results from these alloys with those of the base AZ91D alloy. This systematic approach yielded results which very clearly showed the individual effects of the Ca additions, RE additions, or both on the resultant properties. The results from the immersion tests, electrochemical polarization tests, tensile tests, and microstructural characterization revealed several key results. The addition of up to 1 wt. % Ca caused an increase in the ultimate tensile strength and elongation (compared to the base AZ91D) due to the resultant fine grained structure and presence of the $Mg_{17}Al_{12}$ phase [24]. As well, the corrosion resistance of the AZ91D-*x*Ca alloys improved with Ca additions of up to 2 wt. %. Furthermore, the additions of RE elements resulted in an improvement in the ultimate tensile strength and a decrease in the elongation. The corrosion rate also decreased with RE additions up to 1 wt. %. The effects of the Ca and RE additions on corrosion resistance were illustrated in detail (Figure 2). In general, when considering additions of both RE and Ca, Wu *et al.* found that the additions of both improved the ultimate tensile strength as well as corrosion resistance of the alloys; the improved corrosion resistance was said to be attributed to the formation and presence of the Al_2Ca phase.

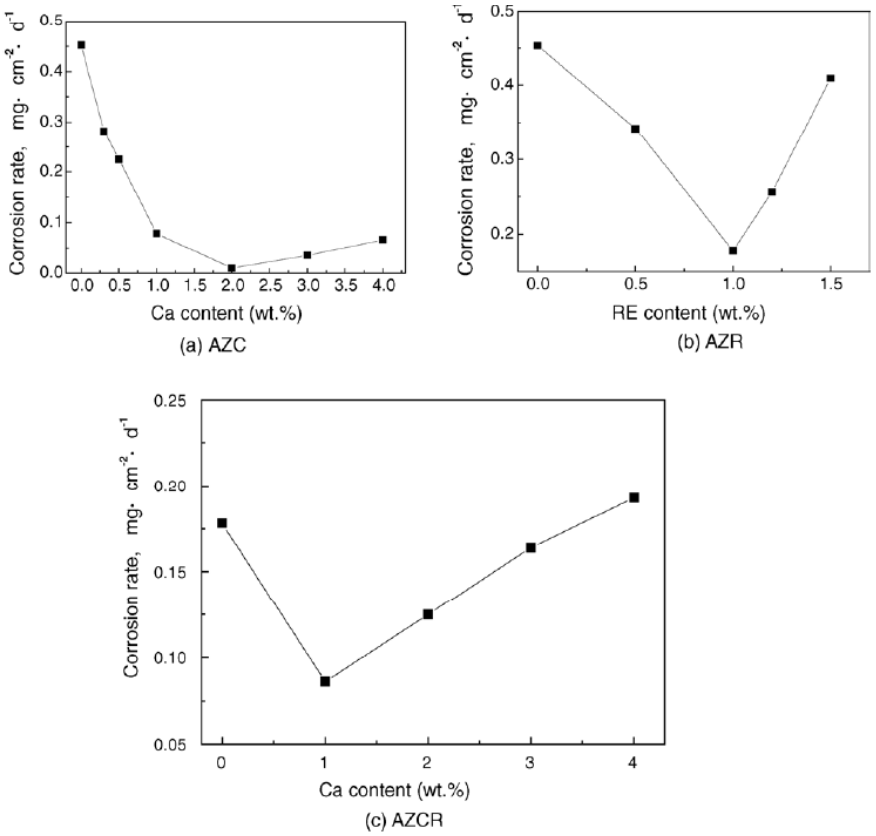

Figure 2: Corrosion results as functions of Ca and RE additions to AZ91D alloy [24]

Reprinted from Materials Science and Engineering A, 408, Wu, G., Fan, Y., Gao, H., Zhai, C., Zhu, Y.P., The effect of Ca and rare earth elements on the microstructure, mechanical properties and corrosion behavior of AZ91D, Pages 255-263, Copyright (2005), with permission from Elsevier.

In another study, Quach *et al.* [18] investigated an Mg-Y-RE alloy, which consisted of Y, Nd, Zr, and trace amounts of other elements, in two different corrosive media (simulated body fluid and artificial plasma). In this investigation, the focus was on the effects of the different media as well as possible corrosion protection through anodizing.

It is reasonable to contend that the investigation of alloys containing potentially harmful elements is useful in contributing to the general understanding of Mg corrosion mechanisms and, as such, studies involving these types of alloys have some value.

However, it is not advisable for clinical use as bioresorbable implants, as the elements in such implants are meant to dissolve into the body without causing adverse (long- or short-term) reactions or effects. Therefore, when choosing elements to create a suitable Mg alloy for bioresorbable implant applications, it would be sensible to consider only alloys containing biocompatible and non-toxic elements. Zn, Ca, and Mn are a few elements that are thought to be biocompatible and well-tolerated in the human body [9].

Mg Alloys Containing Calcium, Zinc, and Manganese

Indeed, many researchers have focused on Mg alloys containing some of the elements that have been thought to be biocompatible and non-toxic (Mn, Zn, and Ca). For example, Zhang *et al.* [25] investigated the Mg-Zn-Mn-Ca alloy system. Through mechanical testing and electrochemical measurements, they obtained several important results. First, it was noted that Ca (up to 0.5 wt. %) acted as a grain refiner [25] (consistent with other reports that Ca played a role in grain refinement [19]). Second, the ratio of Zn to Ca played a key role in determining the type of phases that would form in the alloy. These phases could be primary Mg (α-Mg) plus lamellar eutectic ($Ca_2Mg_6Zn_3$) or primary Mg (α-Mg) plus divorced eutectic (Mg_2Ca + $Ca_2Mg_6Zn_3$) [25]. Electrochemical tests were performed in Hanks' balanced salt solution (Figure 3) and revealed that the Mg-1.5Zn-1.1Mn-1.0Ca alloy (Alloy III) had a higher corrosion resistance than either Mg-2.0Zn-1.2Mn-0.5Ca (Alloy II) or Mg-1.8Zn-1.1Mn-0.3Ca (Alloy I) [25]. The authors believed that the presence of the Mg_2Ca phase led to decreased mechanical properties (tensile strength and ductility) but increased corrosion resistance [25].

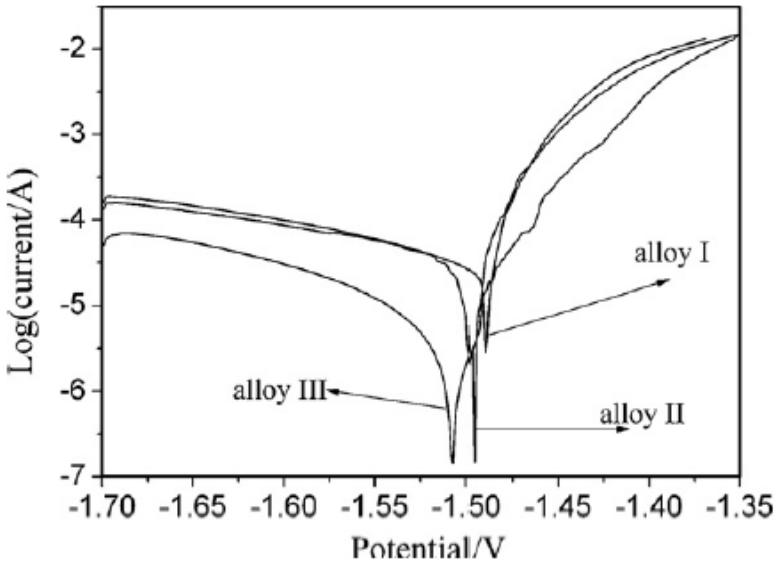

Figure 3: Electrochemical polarization curves showing higher corrosion resistance for the alloy with highest Ca content ("Alloy III") [25]

Reprinted from Materials Science and Engineering A, 497, Zhang, E., Yang, L., Microstructure, mechanical properties and bio-corrosion properties of Mg-Zn-Mn-Ca alloy for biomedical application, Pages 111-118, Copyright (2008), with permission from Elsevier.

Binary Magnesium-Calcium Alloys

The binary alloy system Mg-Ca has been of interest to several researchers, and many studies have focused on different Mg-Ca alloys [26-30]. Good resistance to high temperature oxidation (compared with pure Mg) [31] and an ability to age harden attracted some interest to these alloys [26]. As well, it was suggested that the Ca ions released from a degrading Mg-Ca implant may be beneficial to the bone healing process [32]. Wan *et al.* [26] investigated binary Mg-Ca alloys with varying Ca contents (0.6, 1.2, 1.6, and 2.0 wt. %). X-ray diffraction (XRD) analysis performed on their solutionized and artificially aged samples revealed the presence of pure (α) Mg and Mg_2Ca phases (Figure

4) as would be predicted by the Mg-Ca phase diagram [26]. Their study involved microstructure characterization (Figure 5), three-point bending and compression tests, and corrosion testing in simulated body fluid involving electrochemical measurements.

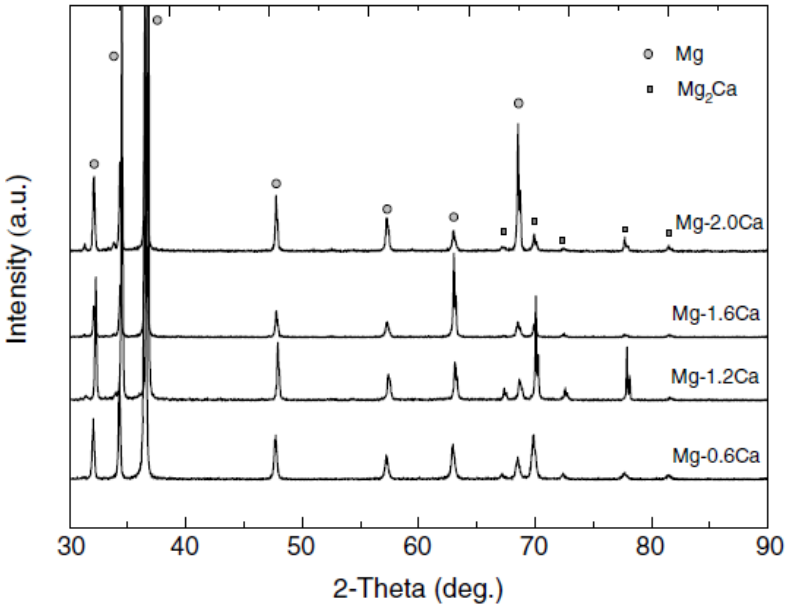

Figure 4: XRD patterns for various Mg-Ca alloys [26]

Reprinted from Materials and Design, 29, Wan, Y., Xiong, G., Luo, H., He, F., Huang, Y., Zhou, X., Preparation and characterization of a new biomedical magnesium-calcium alloy, Pages 2034-2037, Copyright (2008), with permission from Elsevier.

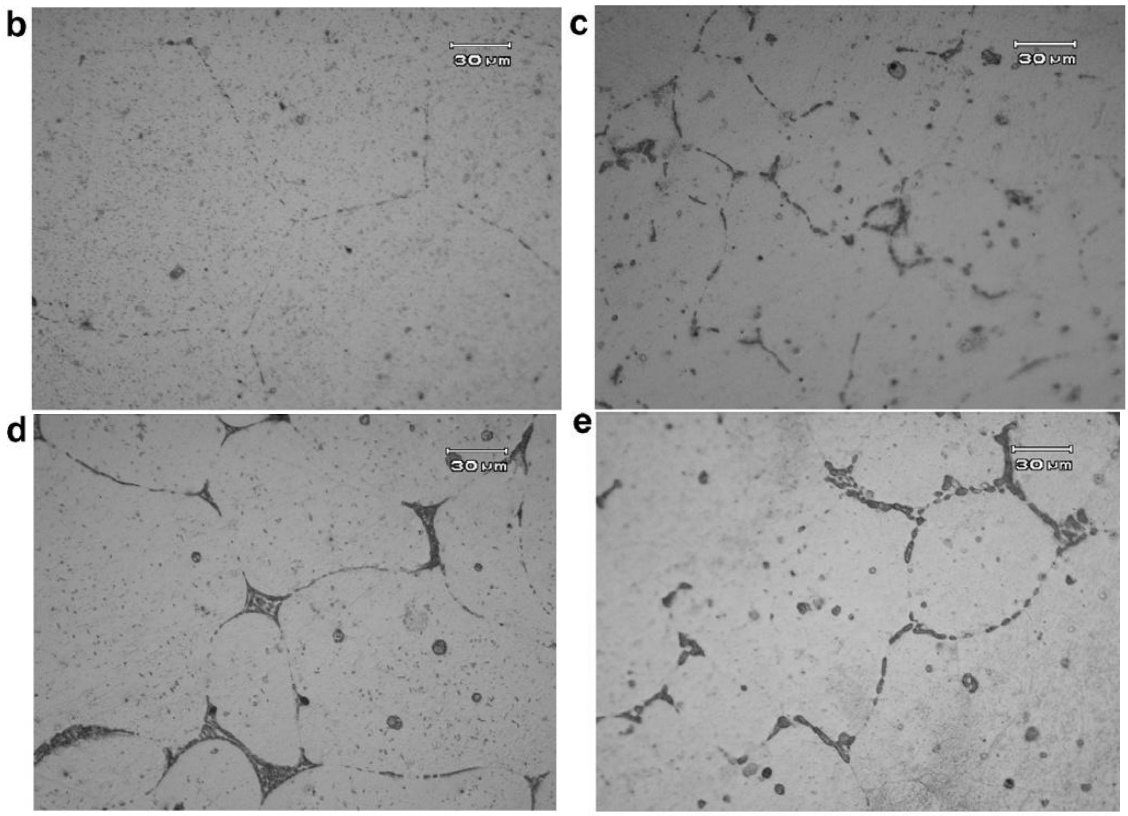

Figure 5: Microstructure of solutionized and artificially aged Mg-0.6Ca (top left), Mg-1.2Ca (top right), Mg-1.6Ca (bottom left), and Mg-2.0Ca (bottom right) [26]

Reprinted from Materials and Design, 29, Wan, Y., Xiong, G., Luo, H., He, F., Huang, Y., Zhou, X., Preparation and characterization of a new biomedical magnesium-calcium alloy, Pages 2034-2037, Copyright (2008), with permission from Elsevier.

Wan *et al.* [26] found that the Mg-0.6Ca alloy had the highest polarization resistance (Figure 6), which was projected to mean that this alloy had the highest corrosion resistance of those tested [26]. They related this corrosion resistance of the alloy to the presence (and amount) of the Mg_2Ca phase present, stating that "*the decline of corrosion resistance with excessive calcium is likely to be attributed to the large amount of* Mg_2Ca" [26]. In addition to influencing corrosion behaviour, the mechanical properties also

appeared to be influenced by the Mg_2Ca phase since the bending strength decreased with increasing Ca content [26]. Overall, the authors indicated that the Mg-0.6Ca alloy seemed to be the best of the alloys tested [26].

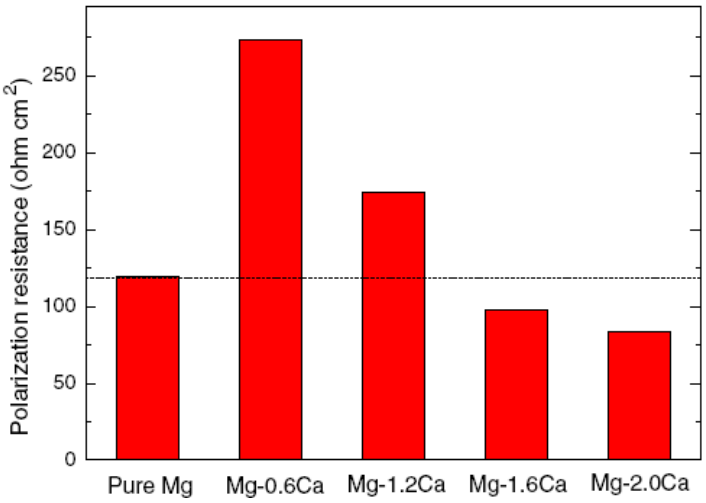

Figure 6: Electrochemical test results showing polarization resistance of the various Mg-Ca alloys tested compared with pure Mg [26]

Li *et al*. [27] also studied various binary Mg-Ca alloys (Mg-1Ca, Mg-2Ca, and Mg-3Ca). Their study involved the characterization of microstructure, tensile tests, *in vitro* corrosion tests, cytotoxicity tests, and finally, animal tests (in which 18 rabbits received the Mg-Ca alloy implants in their femoral shafts). In characterizing the microstructures, as in the work by Wan *et al.* [26], they identified two phases present in the alloys: α-Mg and Mg_2Ca (Figure 7).

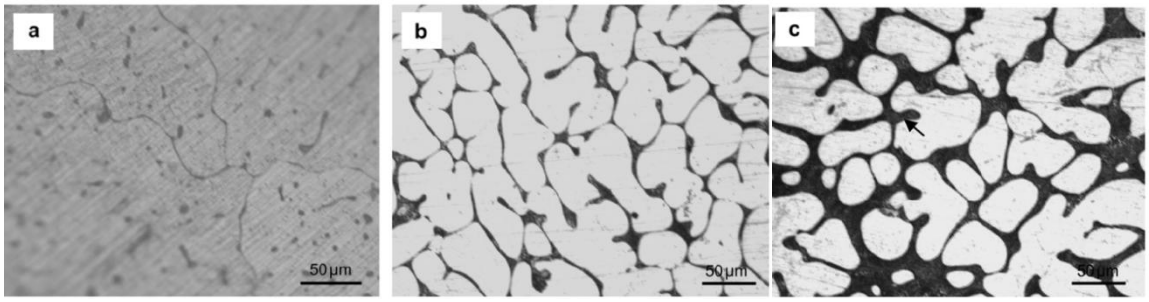

Figure 7: Microstructure of as-cast (a) Mg-1Ca, (b) Mg-2Ca, and (c) Mg-3Ca [27]

Reprinted from Biomaterials, 29, Li, Z., Gu, X., Lou, S., Zheng, Y., The development of binary Mg-Ca alloys for use as biodegradable materials within bone, Pages 1329-1344, Copyright (2008), with permission from Elsevier.

Li *et al.* [27] found that the yield strength, ultimate tensile strength, and elongation all decreased with increasing Ca content. Also, *in vitro* corrosion tests (static immersion tests and electrochemical measurements) revealed that the microstructure of the alloys had significant influences on corrosion behaviour. They found that corrosion rate was higher when more of the Mg_2Ca phase was present (12.56 mm/year for as-cast Mg-1Ca, 12.98 mm/year for as-cast Mg-2Ca, and 25.00 mm/year for as-cast Mg-3Ca, as calculated from the results of their electrochemical tests). The results from the electrochemical measurements indicated that the surface films on the Mg-1Ca offered more corrosion protection than surface films on the Mg-2Ca and Mg-3Ca alloy samples, suggesting that the Ca content of 1% was optimal. Li *et al.* [27] also suggested that processing via hot rolling and hot extrusion may also increase corrosion resistance. For example, their Mg-1Ca alloy, that had been processed via hot extrusion, exhibited a much slower rate of hydrogen evolution (and thus, a slower corrosion rate) than as-cast Mg-1Ca (Figure 8).

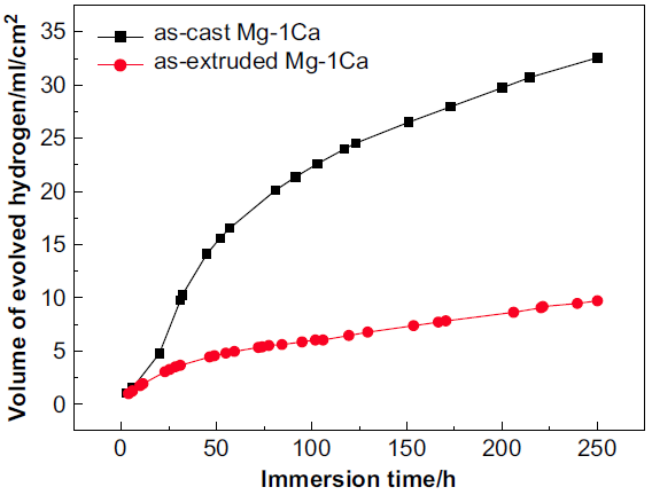

Figure 8: Hydrogen evolution during immersion of as-cast Mg-1Ca and hot extruded Mg-1Ca [27]

Reprinted from Biomaterials, 29, Li, Z., Gu, X., Lou, S., Zheng, Y., The development of binary Mg-Ca alloys for use as biodegradable materials within bone, Pages 1329-1344, Copyright (2008), with permission from Elsevier.

Ternary Magnesium-Calcium-Zinc Alloys

Recently, studies involving the ternary Mg-Ca-Zn alloy system have emerged [32-38]. Mg-Ca-Zn alloys would be favourable for use as bioresorbable implant materials not only because of the inclusion of alloying elements thought to be biocompatible, but also because the precipitation hardening ability of binary Mg-Ca alloys could be significantly enhanced with Zn additions (Figure 9) [39]. The age hardening response of these ternary alloys was attributed to the formation of the $Ca_2Mg_6Zn_3$ phase by Bamberger *et al.* [40], who studied the precipitation hardening in several Mg-Ca-Zn alloys with Ca content ranging from 0.3-1.2 wt. % and Zn content ranging from 0.2-1.9 wt. %. However, in a study by Langelier *et al.* [41], the $Mg_6Ca_2Zn_3$ phase was not detected during non-isothermal heat treatments of the Mg-2.1Ca-0.9Zn alloy. Instead, Guinier-Preston (GP)

zones were formed and were said to be responsible for the hardening of the alloy up to peak-aged condition [41].

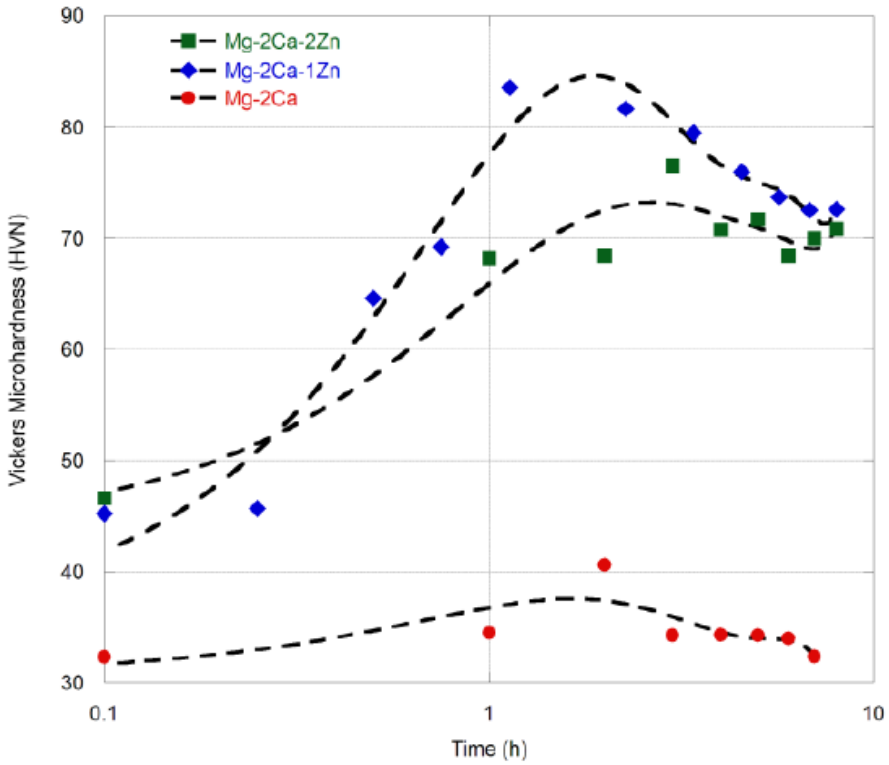

Figure 9: Microhardness results versus aging time for Mg-2Ca, Mg-2Ca-1Zn, and Mg-2Ca-2Zn [39]

Reprinted from Proceedings from 2010 TMS Annual Meeting & Exhibition, Agnew, S., Neelameggham, N.R., Nyberg, E.A., Sillekens, W., The effect of Zn Additions on Precipitation Hardening of Mg-Ca Alloys, Copyright (2010), with permission from Wiley.

Geng *et al.* proposed the Mg-4.0Zn-0.5Ca alloy as a "*high performance structure material as well as a biomaterial*" [42]. The mechanical properties of the Mg-4.0Zn-0.5Ca alloy (in both the as-cast and hot extruded conditions) were determined. Geng *et al.* found that the as-cast alloy exhibited good tensile strength and ductility (211 MPa and 17% elongation respectively), and that hot extrusion further improved both tensile

strength and ductility (273 MPa and 34% elongation). Resultant stress-strain curves from their tensile tests performed at room temperature are shown in Figure 10.

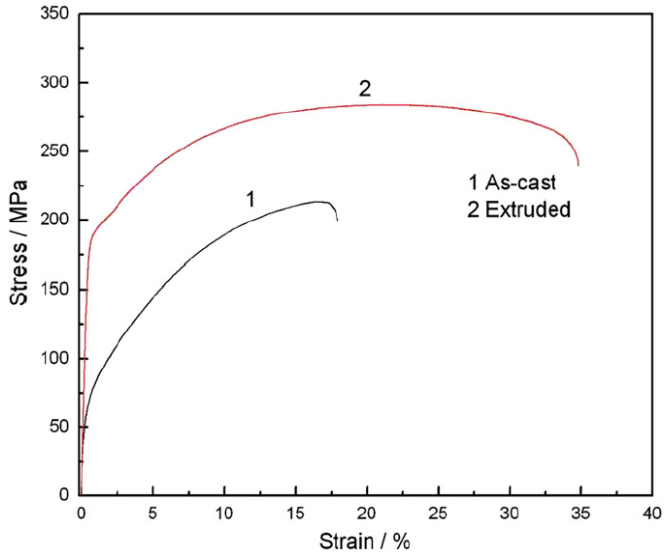

Figure 10: Resultant stress/strain curves of the Mg-4.0Zn-0.5Ca alloy [42]

Reprinted from Materials Letters, 63, Geng, L., Zhang, B.P., Li, A.B., Dong, C.C., Microstructure and mechanical properties of Mg-4.0Zn-0.5Ca alloy, Pages 557-559, Copyright (2009), with permission from Elsevier.

As well, Geng *et al.* [42] found that the average grain size of the α-Mg phase decreased dramatically from 120-150 μm for the as-cast alloy to 8-12 μm after hot extrusion. They also observed the refinement of a second phase (thought to be $Ca_2Mg_6Zn_3$) after hot extrusion. These microstructural changes were attributed to dynamic recrystallization in the alloy during the hot extrusion process. Geng *et al.* demonstrated that this alloy had very good mechanical properties that could be improved by hot extrusion thus indicating that it had the potential to serve as load-bearing implant materials. Although the authors asserted that this alloy could be used as a biomaterial, their study did not include corrosion testing or even any mention of how this alloy might fare in the corrosive

physiological environment. However, there have been several other research groups that have investigated the corrosion behaviour of similar Mg-Zn-Ca alloys.

Du *et al.* [32] investigated the effects of the addition of 2 wt. % Zn on the mechanical properties and corrosion resistance of Mg-3Ca alloys. They observed an increase in the ultimate tensile strength (from 118 ± 5 MPa to 145 ± 5 MPa) as well as elongation (from 0.26 ± 0.04 % to 0.57 ± 0.04 %). Through corrosion tests (immersion tests and electrochemical measurements) performed in Hanks' solution, it was revealed that the corrosion resistance of the Mg-3Ca-2Zn alloy was significantly better than the binary Mg-3Ca alloy. The improved corrosion resistance was attributed to the formation and presence of the $Ca_2Mg_6Zn_3$ phase in the ternary alloy, which was thought to be cathodic to both α-Mg and Mg_2Ca. As shown in Figure 11, the Mg-3Ca alloy samples were completely destroyed after immersion in Hanks' solution for only 24 hours, while the Mg-3Ca-2Zn alloy samples stayed intact.

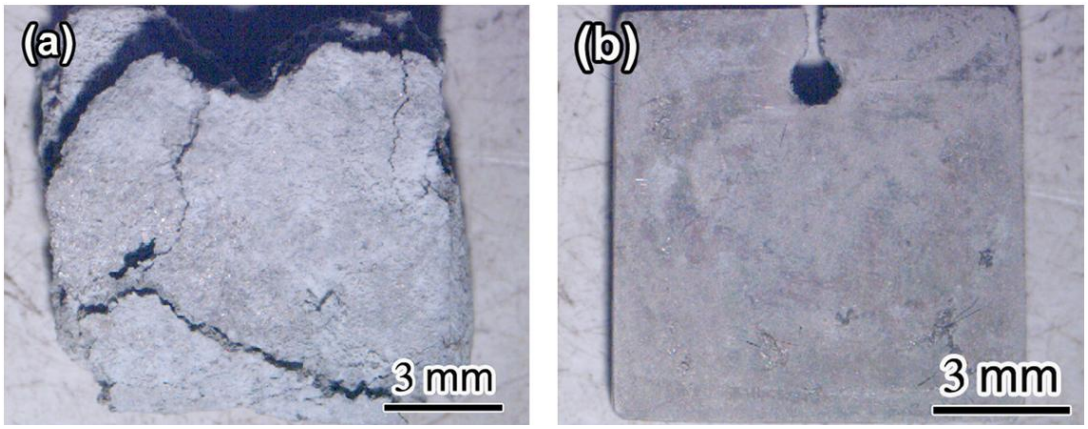

Figure 11: Samples after 24 hours of immersion in Hanks' solution: (a) Mg-3Ca and (b) Mg-3Ca-2Zn [32]

Reprinted from Materials Chemistry and Physics, 125, Du, H., Wei, Z., Liu, X., Zhang, E., Effects of Zn on the microstructure, mechanical property and bio-corrosion property of Mg-3Ca alloys for biomedical application, Pages 568-575, Copyright (2011), with permission from Elsevier.

Zhang *et al.* [35] studied the mechanical and corrosion properties of various Mg-*x*Zn-1.0Ca alloys, with varying Zn content (x = 0, 1.0, 2.0, 3.0, 4.0, 5.0, and 6.0). It was found that the amount of Zn had a marked effect on the mechanical properties of the ternary alloy. The Zn content of 4 wt. % resulted in the highest ultimate tensile strength and percent elongation (182 ± 5 MPa and 9.1 ± 2.5 % respectively). Immersion in Hanks' solution with electrochemical measurements revealed that the alloys with lower Zn content had higher corrosion resistance than the ternary alloys with the highest Zn content as well as the binary Mg-1.0Ca alloy, indicating that some small amount of Zn is beneficial for corrosion resistance.

Brar *et al*. [8] studied the corrosion behaviour of the Mg-15Zn-2Ca (ZX152) alloy. In their static immersion corrosion tests, this alloy was compared with commercially pure Mg (99.95%) in Hanks' solution. They also compared their results with those obtained by Xin *et al.* [16] for the AZ91 alloy. The authors showed that their ZX152 alloy had a lower corrosion rate than pure Mg and AZ91 (Figure 12).

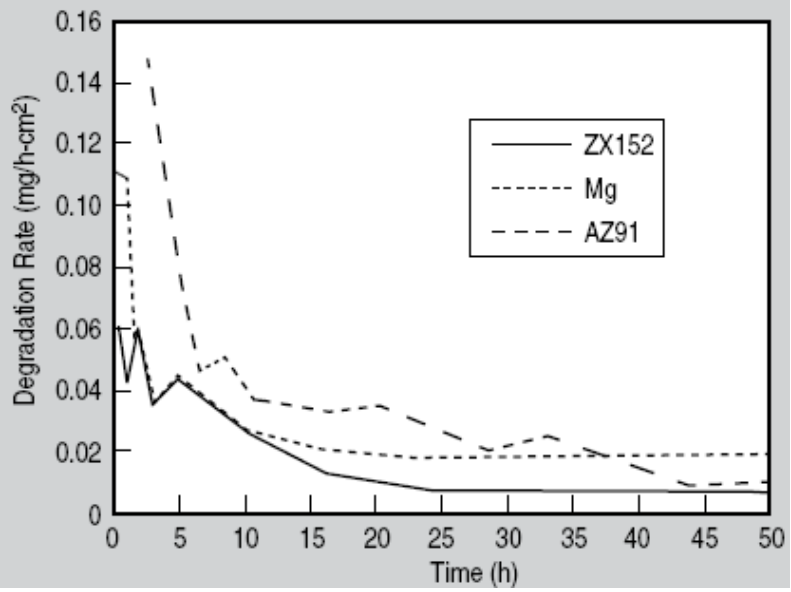

Figure 12: Corrosion rates of Mg-15Zn-2Ca, pure Mg, and Mg-9Al-1Zn [8]

Reprinted from JOM, 61, Brar, H.S., Platt, M.O., Sarntinoranont, M., Martin, P.I., Manuel, M.V., Magnesium as a biodegradable and bioabsorbable material for medical implants, Pages 31-34, Copyright (2009), with kind permission from Springer Science and Business Media.

Brar *et al.* [8] also compared corrosion layer features of their ZX152 and pure Mg samples. They found that the pure Mg sample showed a more uniform corrosion mechanism while the ZX152 displayed more of a pitting type of corrosion behaviour (Figure 13). It was suggested that the eutectic phase present in ZX152 may have been more corrosion resistant than the Mg-rich matrix, thus explaining why ZX152 showed "preferential" pitting corrosion behaviour rather than uniform corrosion as in the pure Mg sample.

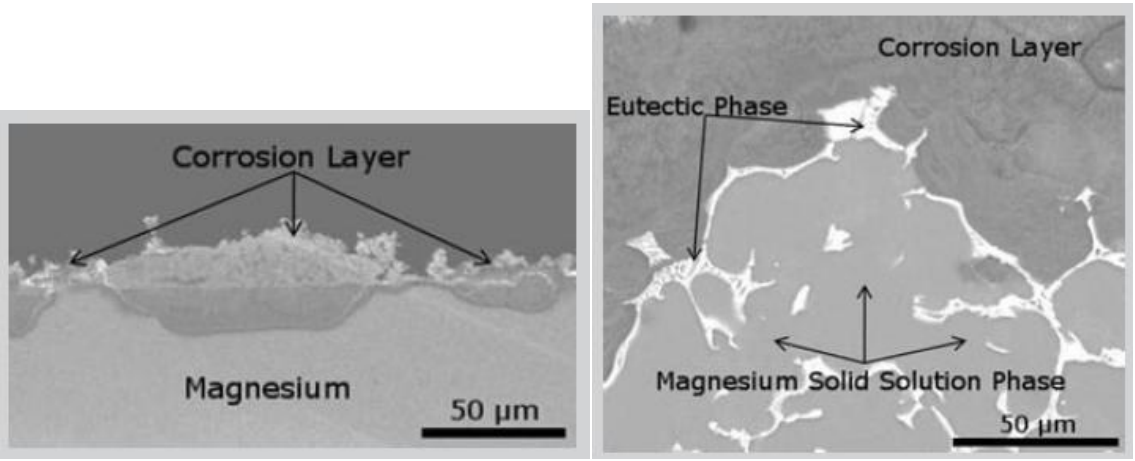

Figure 13: Corrosion morphology at the surface of (a) pure Mg and (b) ZX152 after immersion in Hanks' solution [8]

Because the presence of second phases in the alloy seemed to result in preferential corrosion, and because this type of non-uniform corrosion may lead to quick losses in strength [43], Gu *et al.* [43] asserted that it would be important to investigate other Mg-based materials that could corrode in a more uniform manner (as well as continuing to have good mechanical properties and low corrosion rates). Gu *et al.* proposed that Mg-based bulk metallic glasses may be more suitable because such materials, in addition to possibly having improved mechanical and corrosion properties, would likely exhibit more uniform corrosion behaviour due to the nature of the "*single-phase, chemically homogenous alloy system*" [43]. The Mg-based bulk metallic glass Mg-Zn-Ca (Mg66Zn30Ca4 and Mg70Zn25Ca5) were investigated and found to exhibit more

uniform corrosion morphologies than the pure Mg. The Mg66Zn30Ca4 alloy exhibited the most uniform corrosion.

2.2.2 Surface Modifications

Modifying the surface of the implant is another strategy to delay the onset of corrosion of a material. Many different coatings and surface modification treatments for Mg have been used in industry for the purposes of improving wear and corrosion resistance, such as electrochemical plating, ion implantation, conversion and hydride coatings, organic and polymer coatings, painting, and polymer plating [44]. However, many of such strategies are used for industrial applications and thus the resultant surfaces may contain elements or compounds that are not biocompatible.

The modification of Mg implant surfaces is an important area of research, not only because corrosion resistance needs to be improved, but also because it is the surface of the implant that initially interacts with the surrounding body fluids and tissues. It is therefore reasonable to say that the implant surface and accompanying properties are likely to influence the cellular reactions at the implant site, and ultimately, influence the success of the implant, particularly in terms of tissue integration [1] and consequent ability to achieve implant fixation. This seems sensible, as the atoms on the surface of a material can be viewed as lacking "*near neighbour atoms on one side of the surface*" [4]. The atoms on a surface have a higher free energy than atoms inside the material, and in an attempt to reduce their free energy (and thereby reach a more favourable energy state),

the atoms on the surface tend to bond with reactive atoms/molecules available [4] at the implant-tissue interface.

According to Paital *et al.* [1], surface modifications of implants can be classed into categories depending on what surface properties are adjusted or modified; two such categories are physiochemical and morphological.

Physiochemical modifications are considered first and involve changing surface properties such as energy, charge and composition to modify the material and/or biological responses [1]. Many surface modification strategies fall into this category, including surface coatings and ion implantation.

Surface coatings have been investigated for biomedical Mg alloys, with many focusing on calcium phosphate coatings, which are hoped to enhance bone cell activity and tissue integration. Techniques for coating calcium phosphates onto titanium alloys have been documented, such as ion beam assisted deposition, plasma spray deposition, sol-gel derived coatings, and microarc oxidation [1].

While it is widely recognized that calcium phosphate coatings can enhance an implant's biocompatibility and have positive effects on bone growth [45], Cui *et al.* [46] sought to determine if such calcium phosphate coatings could also alter the degradation behaviour of Mg alloys. In their investigation, calcium phosphate coatings were created on AZ31 alloy samples by immersion of the samples in supersaturated calcification solution (the solutions were composed of Ca_2^+, $H_2PO_4^-$, HCO_3^-, Na^+, NO_3^-) [46]. Three solutions, with varying ratios of Ca to phosphate ($H_2PO_4^-$), were used to create coatings with slightly different compositions and properties. In the degradation behaviour test,

coated samples (as well as the non-coated samples for comparison) were immersed in a solution of sodium chloride (NaCl) for up to 15 days, while refreshing the solution every three days. While characterization of the coatings revealed slightly different compositions and phase structures, Cui *et al.* found that the corrosion behaviour of all the coated samples was similar. Figure 14 illustrates the corrosion behaviour of two sample types: one with and one without a coating. Figure 15 shows a comparison of the mass loss due to corrosion versus time for all the coated and uncoated samples.

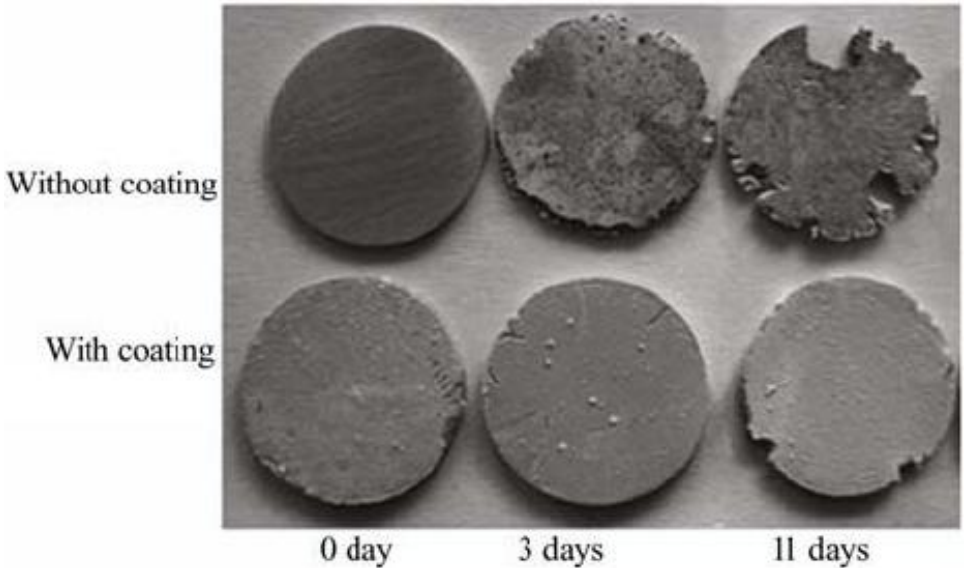

Figure 14: Corroded samples after immersion in NaCl solution [46]

Reprinted from Frontiers of Materials Science in China, 2, Cui, F.Z., Yang, J.X., Jiao, Y.P., Yin, Q.S., Zhang, Y., Lee, I.S., Calcium phosphate coating on magnesium alloy for modification of degradation behavior, Pages 143-148, Copyright (2008), with kind permission from Springer Science and Business Media.

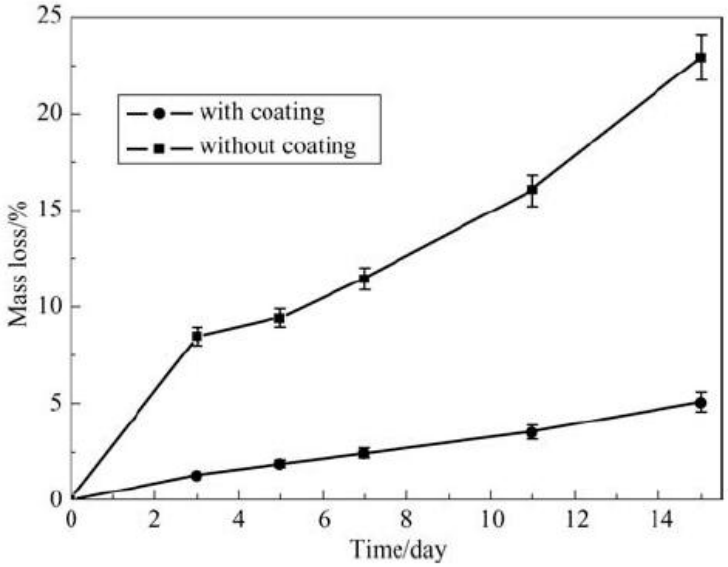

Figure 15: Mass loss results comparing coated and uncoated samples after immersion in NaCl solution [46]

The authors estimated that, after 15 days of immersion, the mass loss of the uncoated samples was approximately five times greater than the coated samples, indicating that coating with calcium phosphate can significantly improve the degradation behaviour of the AZ31 alloy [46].

Anodizing is another surface modification process that can improve corrosion resistance. This electrolytic process results in the formation of a thick and stable oxide film [44]. The resultant oxide film formed during anodization is porous. To attain better corrosion resistance, sealing of this film is often necessary; this can be done in several ways (such as boiling in water) [44]. Anodizing is typically used to improve wear and

corrosion resistance of aluminum and magnesium alloys, as well to improve paint adhesion for dyeing/colouring treatments [44].

Several research groups have utilized the anodizing process on Mg and Mg alloys for improving the corrosion resistance for biomedical applications [9,18,47,48]. Song [9] investigated the effect of anodizing on commercially pure Mg samples. The samples were anodized in a bath containing 1.6 wt.% K_2SiO_3 + 1 wt.% KOH. The resultant anodized coating showed to contain magnesium oxides/hydroxides as well as silicon oxides/hydroxides (less than 30%) [9]. The thickness of the coating was approximately 4μm [9]. The hydrogen evolution during immersion tests (lasting 1 month) was monitored, as hydrogen evolution rate is said to be proportional to corrosion rate [9]. As the evolution of hydrogen gas was not detected during the immersion tests, the author concluded that the coating was successful in delaying the degradation of the pure Mg substrates [9].

Similarly, Quach *et al.* [18] sought to provide temporary corrosion protection for a Mg-Y-RE alloy, creating a thin hydroxide film via a galvanostatic anodizing treatment. The anodizing bath used in this process was a solution of 0.1 M NaOH + 0.05 M Na_3PO_4 [18]. The resultant hydroxide film was approximately 350-400 nm thick, consisting of mainly magnesium and oxygen [18]. Immersion tests in both simulated body fluid and artificial plasma indicated an increase in initial corrosion resistance of the alloy for both corrosive solutions [18].

In addition to increasing the initial corrosion resistance of Mg alloys, anodizing can also play a role in controlling the precipitation of corrosion products on the implant

surface. A study by Hiromoto *et al.* [49] showed that by varying the voltage during anodizing in a NaOH bath, both rough and smooth anodized films were produced on their pure Mg samples. Consequently, it was demonstrated that more calcium phosphate precipitated on the rough, porous anodized film than the smooth film during immersion in artificial plasma [49].

Similar to anodizing, microarc oxidation (MAO) is a process in which oxide ceramic coatings are produced on the surface of metals by a "*plasma-chemical and electrochemical process*" [1]. This technique is used on metals such as Mg, Al, and Ti alloys, improving the wear and corrosion resistance of the metals [50]. As such, some researchers have investigated the effect of MAO on the corrosion resistance of Mg alloys for biomedical applications [50,51].

Zhang *et al*. (2007) were interested in the effect MAO has on the corrosion and wear resistance of the AZ91D alloy, particularly from the biomedical standpoint, as they state that there was not much literature on the "*corrosion and wear resistance of AZ91D magnesium alloy with and without MAO coating in simulation body fluid*" [50]. As such, they test for the effect of MAO on corrosion and wear resistance of this AZ91D alloy through immersion, electrochemical and wear testing. Figure 16 shows an image of the oxide coating on their samples.

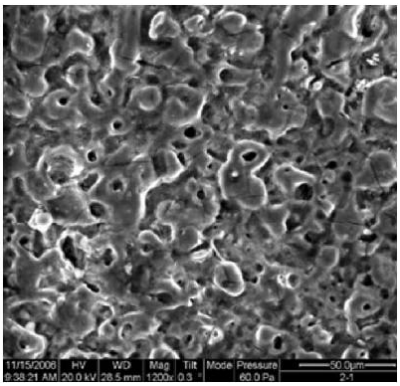

Figure 16: The coating on the AZ91D samples processed by MAO [50]

Reprinted from Journal of Materials Science, 42, Zhang, X.P., Zhao, Z.P., Wu, F.M., Wang, Y.L., Corrosion and wear resistance of AZ91D magnesium alloy with and without microarc oxidation coating in Hank's solution, Pages 8523-8528, Copyright (2007), with kind permission from Springer Science and Business Media.

Their results indicated that the corrosion resistance of the AZ91D alloy improved as a result of the MAO coating, compared with untreated AZ91D; from the immersion tests, the mass loss of the MAO treated samples was 15 times less than the mass loss of the untreated samples after 21 days of immersion in Hanks' solution (Figure 17) [50]. Other results indicated that the wear resistance of the MAO treated samples improved as well, compared to the untreated samples [50].

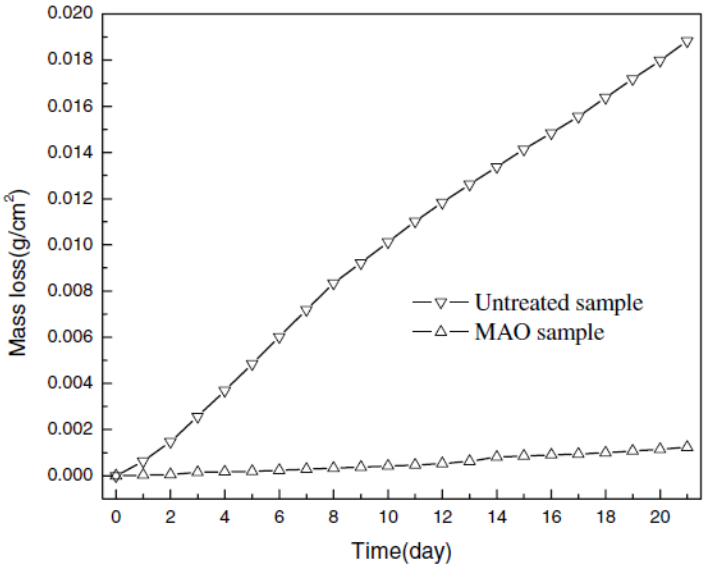

Figure 17: Mass loss results of MAO treated and untreated AZ91D alloy immersed in Hanks' solution [50]

Reprinted from Journal of Materials Science, 42, Zhang, X.P., Zhao, Z.P., Wu, F.M., Wang, Y.L., Corrosion and wear resistance of AZ91D magnesium alloy with and without microarc oxidation coating in Hank's solution, Pages 8523-8528, Copyright (2007), with kind permission from Springer Science and Business Media.

In an effort to further improve the corrosion resistance of Mg, Shi *et al.* [51] implemented a two-step process, involving first the coating of pure Mg by MAO, and then the sealing of pores of the resultant oxide layer with a TiO_2 sol-gel coating. Their two-step process resulted in a composite coating that was determined to be approximately 12 μm thick [51]. Images of the MAO coating (before TiO_2 sealing) and the TiO_2 sealed coating are shown in Figure 18. Characterization of the coating by thin-film XRD revealed that the porous MAO layer of the coating contained MgO and MgF_2 [51].

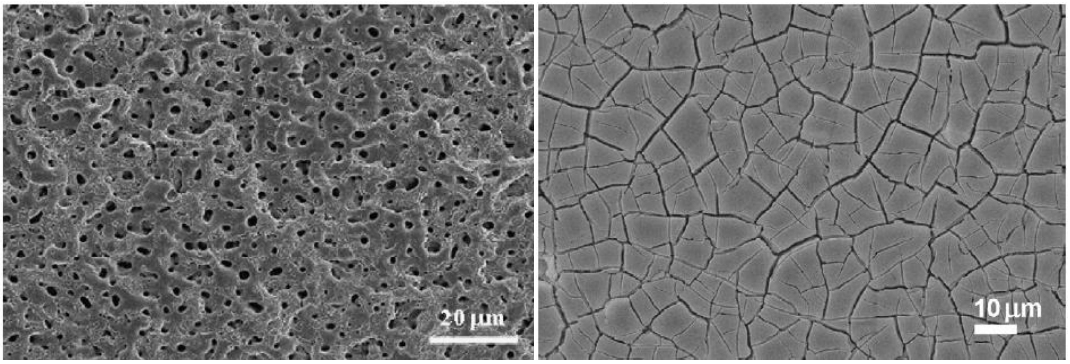

(a) (b)

Figure 18: Coating by MAO on pure Mg samples: (a) without sealing and (b) with sealing [51]

Reprinted from Journal of Alloys and Compounds, 469, Shi, P., Ng, W.F., Wong, M.H., Cheng, F.T., Improvement of corrosion resistance of pure magnesium in Hanks' solution by microarc oxidation with sol-gel TiO2 sealing, Pages 286-292, Copyright (2009), with permission from Elsevier.

The results of the electrochemical tests by Shi *et al.* [51] revealed that, after 12 hours of immersion in Hanks' solution, the corrosion resistance of the MAO-TiO_2 coated Mg samples was approximately 30 times higher than that of bare samples. It was therefore concluded that this coating significantly enhanced the corrosion resistance of pure Mg [51].

Ion implantation is another surface modification method that has been experimented with in the past. Ion implantation of iridium into Ti-6Al-4V has been reported to improve the corrosion resistance [52]. It has also been said that implantation of Ca ions into titanium implants may help improve the bone conductivity of the Ti implants [52]. Hanawa [52] also noted that the precipitation of calcium phosphates on Ti surfaces is accelerated with implanted Ca ions, and it has been observed that "*large amounts of new bones are formed early on calcium-ion-implanted titanium, compared to un-implanted*

titanium" [52]. For biomedical Mg alloys, Wan *et al*. [53] performed a study to investigate the effect of zinc ion implantation on the mechanical and corrosion properties of Mg-Ca alloys. They noted that, while the implantation of zinc ions improved the surface hardness and modulus of the Mg-Ca alloys, the implanted Zn ions also decreased the corrosion resistance of the Mg-Ca alloys [53]. The authors therefore indicated that "*zinc is not a favourable element for the ion implantation of biomedical Mg-Ca alloys*" [53].

Another group of researchers also utilized the ion implantation technique to observe the effect on corrosion resistance of biomedical Mg alloys. Mao *et al.* [54] prepared Mg-1.0Ca-0.3Zn alloys and implanted Ag ions into the surface. Ag was chosen for this effort because Ag was believed to have the ability to reduce the adhesion of bacteria on the surface [54]. The Ag-ion implanted Mg-1.0Ca-0.3Zn was characterized for mechanical properties; it was found that both the hardness and the elastic modulus at the surface of the samples were improved in the Ag-ion implanted samples (versus samples without Ag-ion implantation) [54]. Corrosion properties were also investigated by corrosion tests performed in simulated body fluid. Electrochemical measurements indicated that the polarization resistance of the Ag-ion implanted samples was higher than that of un-implanted samples, indicating a higher corrosion resistance for the samples with Ag-ion implantation [54]. The increased corrosion resistance of the Ag-ion implanted samples was partly attributed to the Ag ions 'dissolving' into the alloy's surface, potentially reducing the electrochemical potential difference between the matrix and second phases [54].

Ag has long been regarded as having antibacterial properties [55]. The use of Ag as some type of coating on potential implant materials for antibacterial purposes is not new. For example, in a study by Colmano *et al.* [56], the effects of Ag on the behaviour of the bacteria *staphylococcus aureus* on stainless steel pins implanted into the femurs of rabbits were investigated [56]. Indeed, there have been various studies involving the incorporation of Ag onto the surfaces of various materials in efforts to reduce bacterial complications associated with implants [57,58]. Hydroxyapatite coatings containing Ag deposited onto Ti substrates have been investigated by Chen *et al.* [57] as well as Bai *et al.* [58], with Chen *et al.* [57] reporting reduced amounts of the bacteria *staphylococcus epidermidis* and *staphylococcus aureus* on the Ti surfaces with Ag (compared with the Ti surfaces without Ag) in their bacterial adhesion study [57]. To the best of the author's knowledge at the present time, there were not many studies in the literature involving the use of Ag on biomedical Mg alloys other than that presented by Mao *et al*. [54].

Other types of surface modifications are often of interest when the success of a potential implant depends on the interaction with surrounding cells. Morphological modifications involve altering the features on a surface from a *mechanical* viewpoint, such as by creating pores, pits, and adjusting surface roughness [1]. Figure 19 shows different types of nano-patterns created by Choi *et al.* to investigate "*the exclusive effect of the nanotopographical three-dimensionality to cell behaviours*" [59]. Based on their observations, Choi *et al.* commented on the new possibilities for biomaterial design that can be opened based on the observed ability to control cell interactions (e.g., adhesion and growth) simply by altering the nano-scale surface topographies [59].

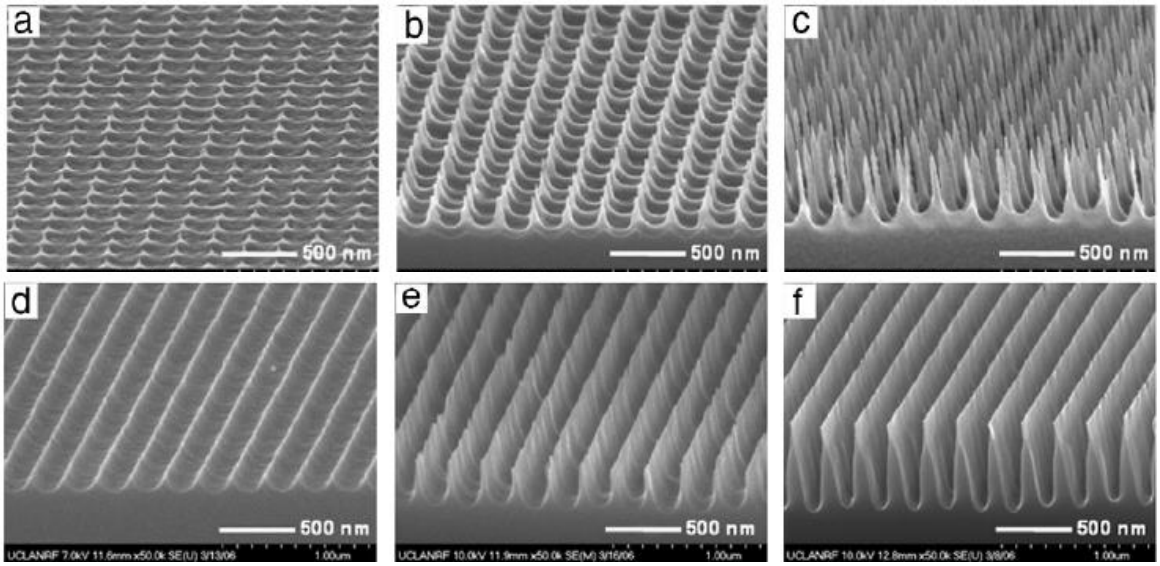

Figure 19: Different types of nano-patterns created by Choi *et al.* [59]

Reprinted from Biomaterials, 28, Choi, C.H., Hagvall, S.H., Wu, B.M., Dunn, J.C.Y., Beygui, R.E., Kim, C.J., Cell interaction with three-dimensional sharp-tip nanotopography, Pages 1672-1679, Copyright (2007), with permission from Elsevier.

Indeed, it has been shown that the responses of cells can be altered depending on the topographic features of the substrates [60]. For example, Teixeira *et al*. [60] demonstrated that epithelial cells cultured on different substrates responded differently when exposed to substrates with different topographic features (which can be very easily seen in Figure 20) [60].

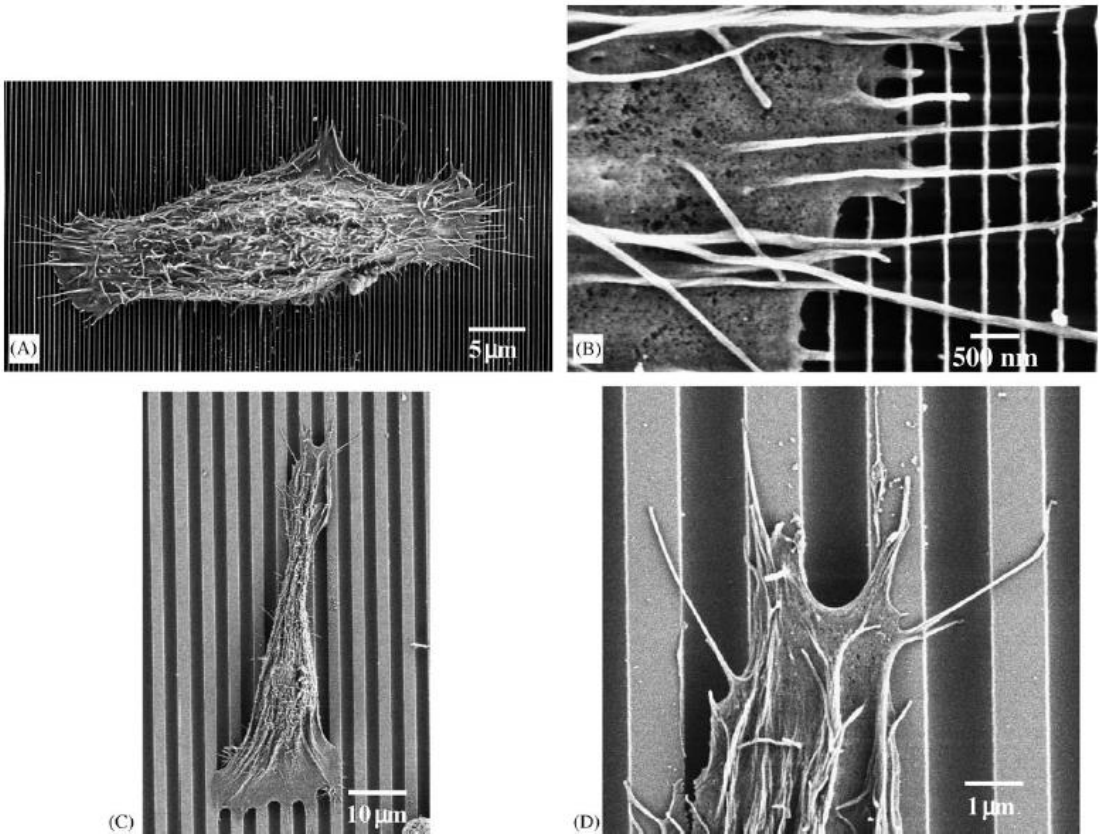

Figure 20: Different responses of epithelial cells on substrates with varying topographic features [60]

Reprinted from Biomaterials, 27, Teixeira, A.I., McKie, G.A., Foley, J.D., Bertics, P.J., Nealey, P.F., Murphy, C.J., The effect of environmental factors on the response of human corneal epithelial cells to nanoscale substrate topography, Pages 3945-3954, Copyright (2006), with permission from Elsevier.

As in the case of the epithelial cells studied by Teixeira *et al.* [60], it has been shown that the response of human osteoblast-like cells were influenced by the features of a hydroxyapatite surface [61]. *In vitro* cell cultures revealed that the size of the hydroxyapatite particles could influence the proliferation and apoptosis of the osteoblast-like cells [61]. The concept of cells being influenced by the topographic features of the substrate or implant on which they are exposed to bears importance when designing bone

implants, as the different topographic features may well affect the integration of an implant to the surrounding bone.

2.3 Concluding Remarks

Review of the literature revealed much research involving the use of different alloys and surface modification techniques. The same approach was used for the present research. Ag was chosen for the surface modification technique because of its antibacterial properties. Ag was deposited onto substrates in a particular pattern based on the concept of altered cell responses to topographical patterns as discussed in the literature. Only one variation of Ag deposition pattern was used in this work (i.e., the deposition of Ag nanoparticles was done in only one pattern for all of the samples tested). Three different materials were chosen based on the inclusion of elements believed to be biocompatible: pure Mg, Mg-2Ca, and Mg-2Ca-1Zn. Static immersion testing was chosen as the main evaluation method for use in the present research. Mass loss measurements were used to measure and assess corrosion behaviour, and pH testing was conducted to compare corrosion behaviour among different materials. Corrosion in the physiological environment was of interest; therefore, testing was performed in a solution that mimics body fluids. However, proteins were not included in these tests. In the interest of time, immersion tests were only performed for up to 14 days.

Chapter 3

Fabrication and Experimental Procedures

This chapter outlines the procedure followed for the fabrication of samples. Because a number of samples were created for a variety of conditions, a list of all the samples that were fabricated is provided. Finally, the experimental procedures for the immersion tests (along with immersion conditions) are described.

3.1 Materials and Sample Preparation

Cast pure Mg plates (from Timminco Ltd., Toronto, ON) and gravity cast Mg-2Ca and Mg-2Ca-1Zn alloys (cast at CANMET-MTL, Hamilton, ON) were used in this work. The composition of these materials is given in Table 2.

Table 2: Elemental composition of the materials used

	Element (Wt. %)									
Material	Mg	Ca	Zn	Fe	Ni	Cu	Si	Al	Sn	Cd
Pure Mg	99.95	0.001	0.003	0.001	0.0002	0.0002	0.001	0.001	0.001	0.0001
Mg-2Ca	Bal.	2.3	< 0.05	-	-	-	-	-	-	-
Mg-2Ca-1Zn	Bal.	2.1	0.9	-	-	-	-	-	-	-

Samples of pure Mg were cut from the cast plates into pieces with approximate dimensions of 10 mm x 10 mm x 3 mm using a hand saw. Alloy samples were cut from cast (25.4 mm diameter) rods into discs using a band saw. The band saw was then used to cut each disc into four pieces, making quarter-circle shapes with an approximate thickness of 3 mm.

Samples remaining in the as-cast condition were then ground and polished. Alloy samples to be heat treated (described in the following section) were done so first, and then followed by grinding and polishing, to allow for the removal of oxides formed on the surfaces during the heat treatment. The surfaces of the samples were ground with waterproof SiC paper, using water during the initial grinding steps and then an alcohol-based lubricant (Struers DP-Lubricant Yellow) for the final grinding step, which was done with 1200 Fine Grit SiC paper from Leco. Following grinding, the samples were washed with ethanol and then polished with diamond abrasive from Leco (up to 1 μm), again using the alcohol-based lubricant. In between each polishing step (and after final polishing), the samples were washed with ethanol in an ultrasonic cleaner. Microstructures of the samples were observed using optical microscopy after polishing. Figure 21 shows the polished (a) pure Mg and (b) alloy samples as an example.

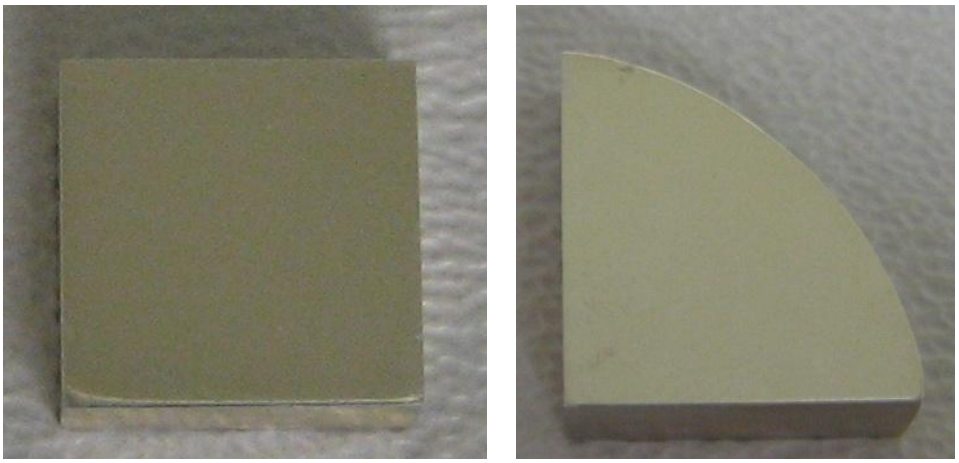

(a) (b)

Figure 21: Cut and polished samples: (a) pure Mg and (b) Mg-2Ca and Mg-2Ca-1Zn

3.2 Heat Treatments

Sets of Mg-2Ca and Mg-2Ca-1Zn samples were heat treated to observe the effect of solutionizing and artificial aging (S&AA) or solutionizing and natural aging (S&NA) on corrosion, compared to samples in the as-cast (AC) condition. The alloy samples were first solutionized at 480°C for 24 hours and quenched in water at room temperature. Some samples were then immediately artificially aged to near peak-aged condition (at 200°C for 1.5 hours [39], followed by a water quench). Other samples were stored at room temperature for 72 hours after solutionizing; these samples are identified as naturally aged. The heat treatments were done in air, with the samples packed in magnesium oxide powders in an attempt to minimize high-temperature oxidation of the sample surfaces during the heat treatment. Following the heat treatment, the samples were ground and polished, as mentioned in Section 3.1.

The surface modification involving the deposition of Ag nanoparticles was carried out after polishing. After deposition of Ag nanoparticles, the samples underwent a heat treatment (herein referred to as the ‘sintering treatment’) to allow for sintering of the Ag nanoparticles. (The surface modification and sintering treatment are described in more detail in Section 4.3.) Samples not undergoing Ag deposition, as well as those remaining in the as-cast condition, were also subjected to the sintering treatment to ensure consistent thermal history among all samples.

For the alloys, it should be noted that the Ag deposition was only done on the samples that were solutionized and naturally aged. In an effort to not be wasteful of resources, corrosion tests were initially performed on S&AA and S&NA alloy samples without any Ag

deposition (for both Mg-2Ca and Mg-2Ca-1Zn) to observe which heat treatment yielded better corrosion resistance. Details and results of this corrosion test are described in later sections, but to summarize here, significant differences in corrosion results between S&AA and S&NA samples after 48 hours of corrosion were not detected for either Mg-2Ca or Mg-2Ca-1Zn. Therefore, solutionizing and natural aging was the chosen heat treatment for alloy samples to be deposited with Ag, with two advantages in mind. The first was the elimination of a processing step (or potential manufacturing step) (i.e., artificial aging), saving time and energy. The second advantage was the idea that the sintering treatment itself could be utilized for precipitation hardening of the solutionized material, and could produce material in the peak-aged condition if implemented appropriately. In contrast, if an alloy piece were solutionized, artificially aged, *and then* subjected to the sintering treatment, the material would be over-aged and would possess inferior mechanical properties.

Table 3 summarizes all of the samples made for subsequent corrosion testing. The left column lists the samples fabricated without any surface modification (herein referred to as 'uncoated' for simplicity). At least 7 samples were made for *each* of the conditions listed in the left column, with at least 4 being allotted for mass loss testing, and at least 3 being allotted for pH testing (these tests are explained in a later section). The column on the right lists the samples that were made with Ag. At least 4 samples (for mass loss testing) were made for each of these conditions. The Ag deposition process used to make these samples is described in the next section.

Table 3: Summary of fabricated samples

Uncoated Samples (No Ag)	Ag-Deposited Samples
As-cast pure Mg	As-cast pure Mg
As-cast Mg-2Ca	As-cast Mg-2Ca
As-cast Mg-2Ca-1Zn	As-cast Mg-2Ca-1Zn
S&NA Mg-2Ca	S&NA Mg-2Ca
S&NA Mg-2Ca-1Zn	S&NA Mg-2Ca-1Zn
S&AA Mg-2Ca	
S&AA Mg-2Ca-1Zn	

3.3 Surface Modification

Ag nanoparticles were deposited onto the surfaces of polished samples using the Optomec Maskless Mesoscale Material Deposition (M^3D) machine. In this process, an Ag ink (a mixture of Ag nanoparticles in suspension, purchased from Cabot) was used. The Ag nanoparticles (approximately 20 nanometers in diameter) were suspended in an ethylene glycol carrier; this suspension was mixed with deionized water to achieve the appropriate viscosity before being used in the M^3D machine. Figure 22 shows the set-up of the machine and Figure 23 shows a close-up view of the deposition head and nozzle above the substrate.

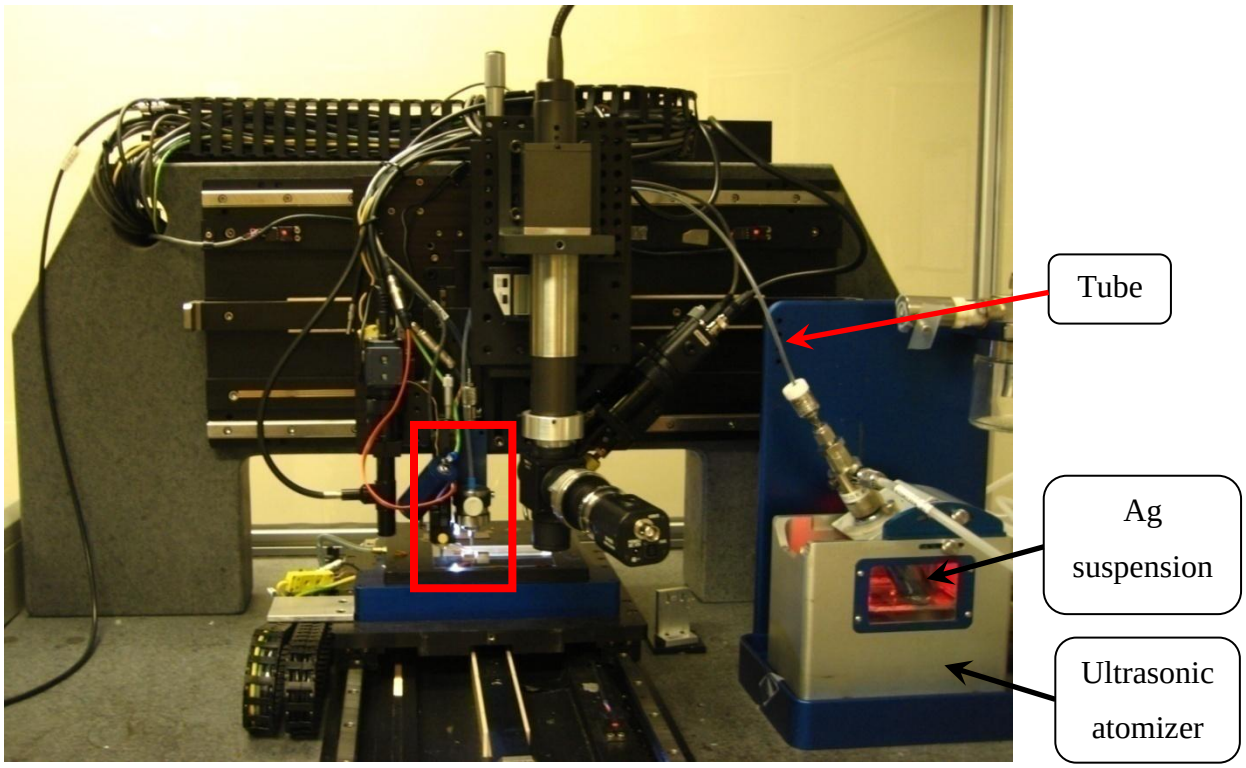

Figure 22: M^{3}D machine

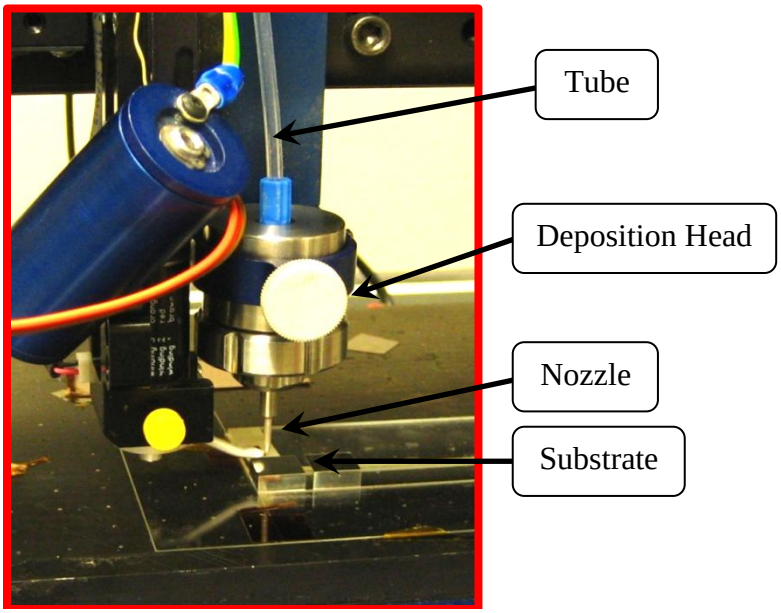

Figure 23: Close-up view of the deposition head and nozzle over the substrate

The ultrasonic atomizer was used for the fabrication of the samples in this work. As seen in Figure 22, a vial containing the Ag nanoparticle suspension is placed in the ultrasonic atomizer. Ultrasonic waves generated by the atomizer are transferred to the vial (and thus, the Ag nanoparticle suspension); this causes the suspension to aerosolize [62]. Tiny droplets containing the Ag nanoparticles form a dense mist in the vial [62]. The generated mist is carried through the tube and toward the deposition head by flowing N_2 gas. Inside the deposition head, a sheath gas (N_2) focuses the flowing stream (Figure 24) and directs it through the nozzle and onto the substrate below [62].

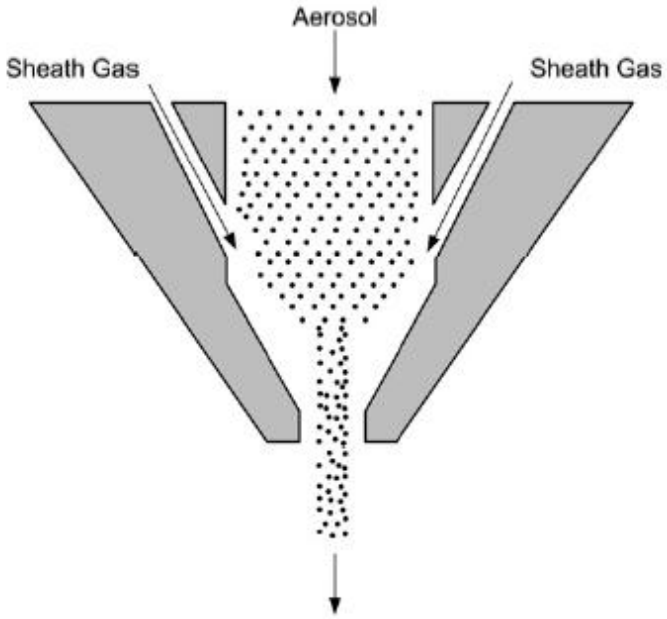

Figure 24: Inside the deposition head: Sheath gas focuses flowing stream of Ag nanoparticle suspension droplets [62]

Reprinted from Journal of Micromechanics and Microengineering, 18, Alemohammad, H., Aminfar, O., Toyserkani, E., Morphology and microstructure analysis of nano-silver thin films deposited by laser-assisted maskless microdeposition, Pages 1-12, Copyright (2008), with permission from IOP Publishing Ltd. doi:10.1088/0960-1317/18/11/115015

The diameter of the nozzle that was used in this work was 150 μm. The process parameters that were used are listed in Table 4 below.

Table 4: Process parameters used for Ag deposition

	Pure Mg	Mg2Ca	Mg2Ca1Zn
Process Velocity [mm/s]	2-3	3	3
Platen (Substrate) Temperature [°C]	70	60	70
Flow Controller: Sheath [ccm]	50	50	50
Flow Controller: Atomizer [ccm]	10-12	15-16	10
Atomizer Power [V]	50	48	50

Ag nanoparticles were deposited onto the polished substrates in a cross-hatch pattern, with a line spacing of 120 μm (as shown in Figure 25). One layer of Ag was deposited in this pattern on each sample.

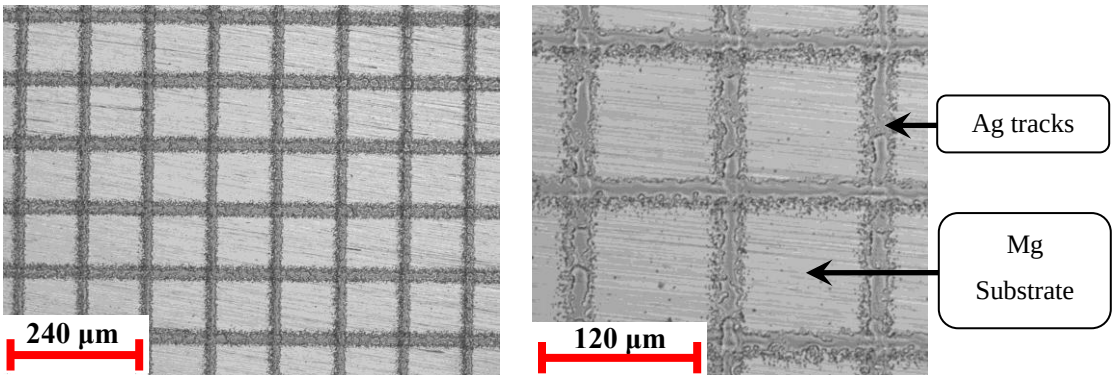

Figure 25: Cross-hatch pattern of Ag nanoparticles deposited onto substrates

After the deposition process, samples were subjected to a heat treatment ('sintering treatment') to allow for sintering of the Ag nanoparticles and complete evaporation of the liquid carrier. This sintering treatment was done in a tube furnace (MTI High Temperature Tube Furnace (GSL—1500X-50, Richmond, CA)), under argon atmosphere to prevent

oxidation of the polished and Ag-deposited surfaces. Following recommendations from the manufacturer of the Ag ink (which proposed appropriate time and temperature ranges for satisfactory sintering of the nanoparticles), the samples were sintered at 190°C for 30 minutes. In this process, Ag-deposited samples were placed in the furnace and the temperature was set to ramp up to 190°C in 10 minutes, held at 190°C for 30 minutes, and then finally furnace cooled.

3.4 Summary of the Fabrication Process

To summarize the fabrication process, Figure 26 shows the steps taken to create both (a) the uncoated samples and (b) the samples deposited with Ag.

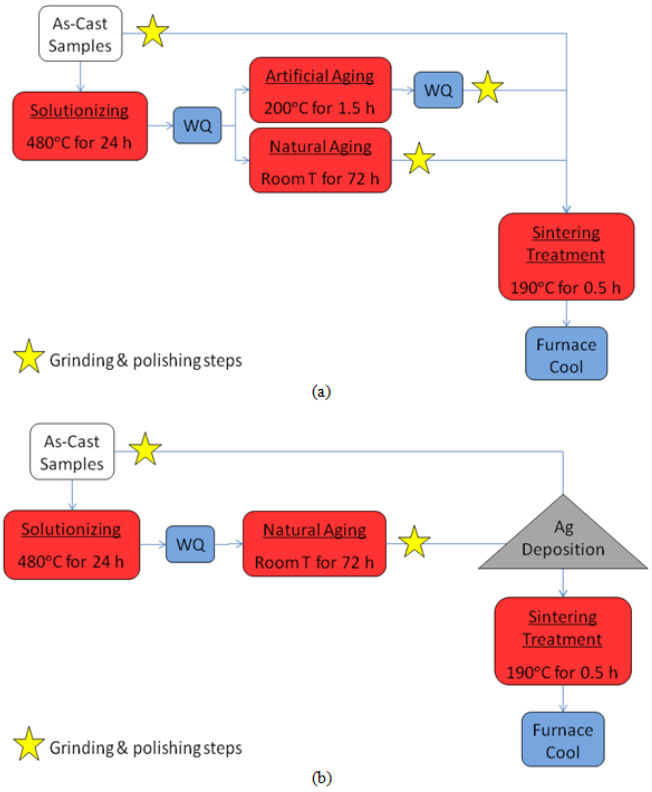

Figure 26: Fabrication process of samples (a) without Ag deposition and (b) with Ag deposition

Prior to corrosion testing, the deposited Ag tracks were characterized for width and thickness. Prepared samples were viewed under an optical microscope (Olympus), and image analysis software (Image-Pro 6.3) was used to measure the width of the deposited Ag tracks. Optical profilometry (WYKO NT 1100 optical profiling system, manufactured by Veeco) was used to measure the thickness of the Ag tracks. Table 5 lists the parameters used for optical profilometry.

Table 5: Optical profilometry parameters

	Parameter	Option
Measurement Options	Measurement Type	VSI (Infinite Scan)
	Resolution	Full
	Objective	20x
	Field Of View	1.0x
VSI Options	Scan Options	1x Speed
		Single Scan
Primary Scan	Backscan	2 µm
	Length	4 µm
	Modulation Threshold	1%

3.5 Immersion Corrosion Testing

Corrosion testing was performed on all the fabricated samples listed in Table 3. The objective of the corrosion testing was to examine the effects of alloying, heat treatment, and Ag deposition on corrosion behaviour. These observations were made by comparing a particular group of samples with another. For example, the corrosion results of as-cast pure Mg, as-cast Mg-2Ca, and as-cast Mg-2Ca-1Zn could be compared with each other to evaluate the effect of the alloying elements Ca and Zn on the corrosion behaviour. Figure 27 summarizes all of the comparisons of interest in this work.

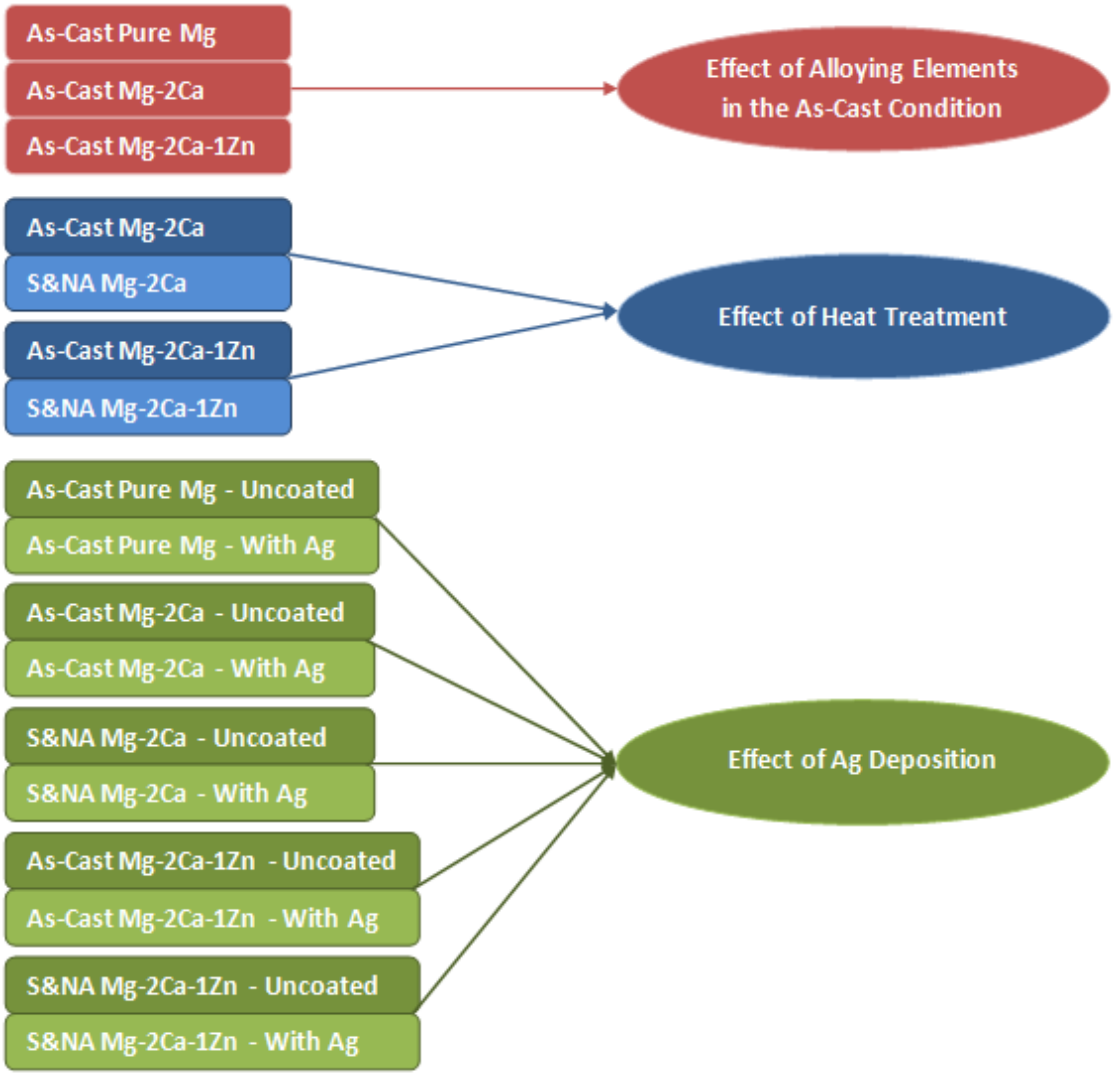

Figure 27: Comparisons of sample groups (left side) and observed effects (right side). For all sample groups, n=4 for mass loss tests and n=3 for pH tests.

Samples were tested using static immersion tests; this type of testing has been referred to as the most commonly used method of testing orthopaedic implant materials [45]. In this type of testing, samples are placed into stationary containers of a corrosive medium for specified amounts of time. In this work, two different immersion tests were performed: mass loss tests and pH tests.

3.5.1 Immersion Testing Conditions for Mass Loss Tests and pH Tests

Prior to any corrosion testing, all samples were cleaned with ethanol in an ultrasonic cleaner. All but one of the immersion conditions were common to both the mass loss tests and the pH tests. These conditions are described in this section.

Test Solution

The corrosion medium used in all immersion tests was Hanks' balanced salt solution (purchased from Lonza). Hanks' solution was chosen because of its similarity in concentrations of inorganic components (salts) to those in human blood plasma. Table 6 lists the concentration of components in the Hanks' solution that used in this work. Hanks' solution had been used by other researchers for *in vitro* corrosion studies [8,9,32,35,63,64**].** Using Hanks' solution in the present research would have allowed comparisons with those previous studies.

Table 6: Composition of Hanks' solution used for immersion tests

Components	Concentration [mg/L]
$CaCl_2 \cdot 2H_2O$	186
KCl	400
KH_2PO_4	60
$MgSO_4 \cdot 7H_2O$	200
NaCl	8000
$NaHCO_3$	350
$Na_2HPO_4 \cdot 7H_2O$	90
Glucose	1000

Test Temperature

It has been shown that corrosion rate of Mg is affected by the temperature at which corrosion takes place [65]. Because of this, and to mimic the physiological environment,

the test solution was held at 37°C (body temperature) using a water bath (Fisher Scientific Isotemp Economy Analog-Control) for the duration of the immersion tests.

Ratio of Exposed Surface Area to Volume of Test Solution

An important factor during immersion testing is the ratio of exposed surface area of a sample to the volume of test solution (herein referred to as *surface-area*-to-*solution-volume* ratio (SA:SV ratio)). It has previously been shown that the corrosion rates of Mg can be greatly affected by the SA:SV ratio [63]; Yang *et al*. [63] measured the mass loss of Mg-1Mn-1Zn samples in Hanks' solution with different SA:SV ratios and showed much different mass loss results when the ratio was changed (Figure 28).

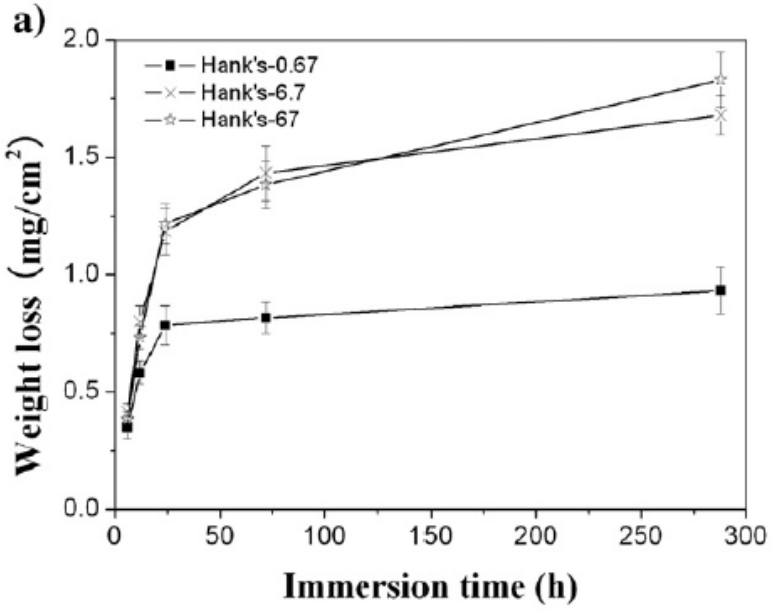

Figure 28: Effect of SA:SV ratio on mass loss measurements. [63]

Reprinted from Materials Science and Engineering C, 29, Yang, L., Zhang, E., Biocorrosion behavior of magnesium alloy in different simulated fluids for biomedical application, Pages 1691-1696, Copyright (2009), with permission from Elsevier.

Because of this, it was important that the SA:SV ratio be kept consistent among all samples for all immersion tests performed. In this work, a ratio of $1mm^2$:1mL was chosen. To measure the surface area, an image of a sample placed directly beside calipers (open to 10 mm) was taken. Image analysis software (Image-Pro 6.3) was used to measure the surface area of the sample in pixels, which was then converted to mm^2.

3.5.2 Immersion Testing for pH Measurement

During static immersion testing in which the test solution is never changed, a rise in pH accompanies the corrosion reaction of Mg, as OH^- ions are released into the solution as corrosion proceeds [29]. Thus, monitoring the change in pH levels during corrosion is a good indicator of how quickly the corrosion reaction happens, and can be a good tool for comparing the corrosion behavior of different materials. Indeed, pH tests have often been performed by researchers in the past when carrying out immersion tests [27,43,54].

In an effort to determine the extent to which the pH level evolves during the corrosion reaction of different samples, samples were placed in beakers of Hanks' solution for 336 hours. In order to measure pH evolution, the Hanks' solution remained unchanged throughout the duration of the test. pH values were measured at various time points using a bench-top pH meter (Omega PHB-550R pH/mV/Temp Meter) with an accuracy of ± 0.02. The pH meter was calibrated every few days using buffer solutions of pH 7 and 10. At least 3 samples per alloy/condition were tested. The result reported for a certain alloy/condition at a given time point was the average of the tested samples within that group, plus or minus the standard deviation.

3.5.3 Immersion Testing for Mass Loss Measurements

As noted before, in a confined corrosion environment, the release of OH^- ions results in the consequent rise in pH level, which causes the corrosion rate to decrease as the corrosion reaction proceeds [29]. However, in the human body, homeostasis maintains a pH level of around 7.4 [5]. It would therefore be inaccurate to attempt to predict *in vivo* mass loss (and thus, corrosion rates) by way of *in vitro* immersion tests if the pH of the test solution was not controlled. In fact, it has been said that "*corrosion rates measured* in vitro *are of little relevance to the physiological condition if the* in vivo *pH levels are not maintained*" [29]. Therefore, for the mass loss tests in this work, efforts to maintain physiological pH throughout the duration of immersion testing were made by replacing the Hanks' solution every 24 hours, a practice that has been done by several other researchers in the past [32,45]. It may be worthy to mention that while the mass loss tests would indeed be more physiologically relevant (since the test solution was replenished every day), the pH tests (in which the test solution was *not* changed) can still provide some insight into the corrosion reaction, particularly when comparing different alloys or samples.

Because Ag was only deposited on the top surface of each sample, the sides and bottom of the samples were masked off using 3M high adhesion tape, leaving only the top (Ag-deposited) surface exposed. The samples were then placed in beakers containing appropriate amounts of Hanks' solution and immersed for 48, 168, and 336 hours. For a given alloy/condition, at least 4 samples *of that particular alloy/condition* were tested *for each time point*.

In order to obtain mass loss data from the immersion tests, the samples were weighed prior to immersion using a scale with an accuracy of ± 0.5 mg. After immersion for the specified duration (i.e., 48, 168, or 336 hours), the samples were taken from the Hanks' solution, rinsed gently with distilled water, and dried with a light stream of air at room temperature. The corrosion products that formed during the corrosion reaction were chemically removed by submersing the corroded sample into a solution of CrO_3 (200 g/L) + $AgNO_3$ (10 g/L), a step that has been done by many other researchers in the past [48,50]. After corrosion product removal, the samples were weighed again for the final mass. The mass loss of a particular sample was simply the difference between the initial mass and final mass. Because the samples were not all exactly the same size with identical surface area prior to corrosion (since samples were cut and polished by hand), the calculated mass loss value after immersion was divided by the initial surface area to normalize the mass loss values across all samples (Equation 1).

$$\text{Mass Loss} = \frac{\left(\begin{matrix}\text{Mass before}\\ \text{immersion}\end{matrix}\right) - \left(\begin{matrix}\text{Mass after corrosion}\\ \text{product removal}\end{matrix}\right)}{\left(\begin{matrix}\text{Surface area exposed}\\ \text{to test solution}\end{matrix}\right)} \qquad (1)$$

The mass loss (average ± standard deviation) was reported for each material/condition at a given time point. When comparing mass loss values of one material/condition type with another (e.g., comparing uncoated as-cast Mg-2Ca with uncoated S&NA Mg-2Ca) for a given immersion time, p-values were calculated to determine if any differences observed were statistically significantly different. To do so, an F-test was first performed on the two data sets of interest to determine equality of

variance within the data sets. The t-test (either assuming equal or unequal variance) was then performed on the same sets of data according to the results of the prior F-test. As is commonly done, t-test results yielding $p < 0.05$ was considered to be statistically significantly different. In cases where three different conditions were compared (e.g., mass loss values of Mg-2Ca in the as-cast, solutionized and naturally aged, and solutionized and artificially aged conditions), single-factor analysis of variance (ANOVA) was used to determine if any significant difference existed among the three values. Again, a p-value of less than 0.05 was considered significant. All statistical tests were performed using Microsoft Excel 2007 statistics (http://office.microsoft.com/en-ca/excel-help/about-statistical-analysis-tools-HP005203873.aspx).

3.6 Characterization of the Corrosion Products and Corrosion Product Morphology

To observe the morphology of the corrosion products on the samples' surfaces, corroded samples were viewed under the scanning electron microscope (SEM) (using both secondary electron and back-scattered electron modes) before the removal of the corrosion products. To identify the corrosion products formed during immersion, the corrosion products (while still intact on the samples) were analyzed using energy dispersive x-ray (EDX) analysis.

X-ray diffraction (XRD) analysis (Rigaku, AFC-8 generator, Cu target, wavelength 0.1542 nm, 2 kW, 50 kV, 40 mA) was used to determine the phases of the corrosion products. Initial attempts to examine the corrosion products directly on corroded samples

(i.e., before corrosion product removal, while the corrosion products were still adhered to the sample) were unsuccessful, as strong, distinct signals could not be obtained. Instead, extra samples of particular conditions (e.g., as-cast Mg-2Ca with Ag deposition) were fabricated and subjected to immersion for extended periods of time (approximately 30 days) to allow as much corrosion product to form as possible. During this time, much of the corrosion products that formed flaked off of the sample and settled at the bottom of the beaker, away from the sample itself. After immersion, this excess corrosion product was carefully collected and packed onto sticky tape on a mount to be placed in the XRD unit. Care was taken to place enough corrosion products onto the mount so that the thickness of the corrosion products placed on each mount (approximately 1 mm) was consistent among samples.

Chapter 4

Results and Discussion

The results of all of the immersion tests are presented in this chapter, and the effects of the alloying elements, heat treatments, and Ag deposition on corrosion are discussed. As well, the morphology of the corrosion products after immersion is shown, and the identification of the corrosion products is discussed.

4.1 Immersion Corrosion Tests

Immersion corrosion results in this section are presented according to Figure 27 (i.e., a material/condition type compared with another to observe the effect of alloying, heat treatment, or Ag deposition). Mass loss results (mg/cm^2) are presented in conjunction with the results of corresponding pH tests for uncoated samples, which can, in some ways, act as confirmation of mass loss results.

4.1.1 Effect of Alloying Elements on Corrosion in the As-Cast Condition

Mass loss results of as-cast pure Mg and as-cast Mg-2Ca samples were compared to observe the effects of the addition of 2 wt. % Ca to pure Mg (Figure 29). Table 7 lists the p-values calculated to compare pure Mg with Mg-2Ca at the three different time points.

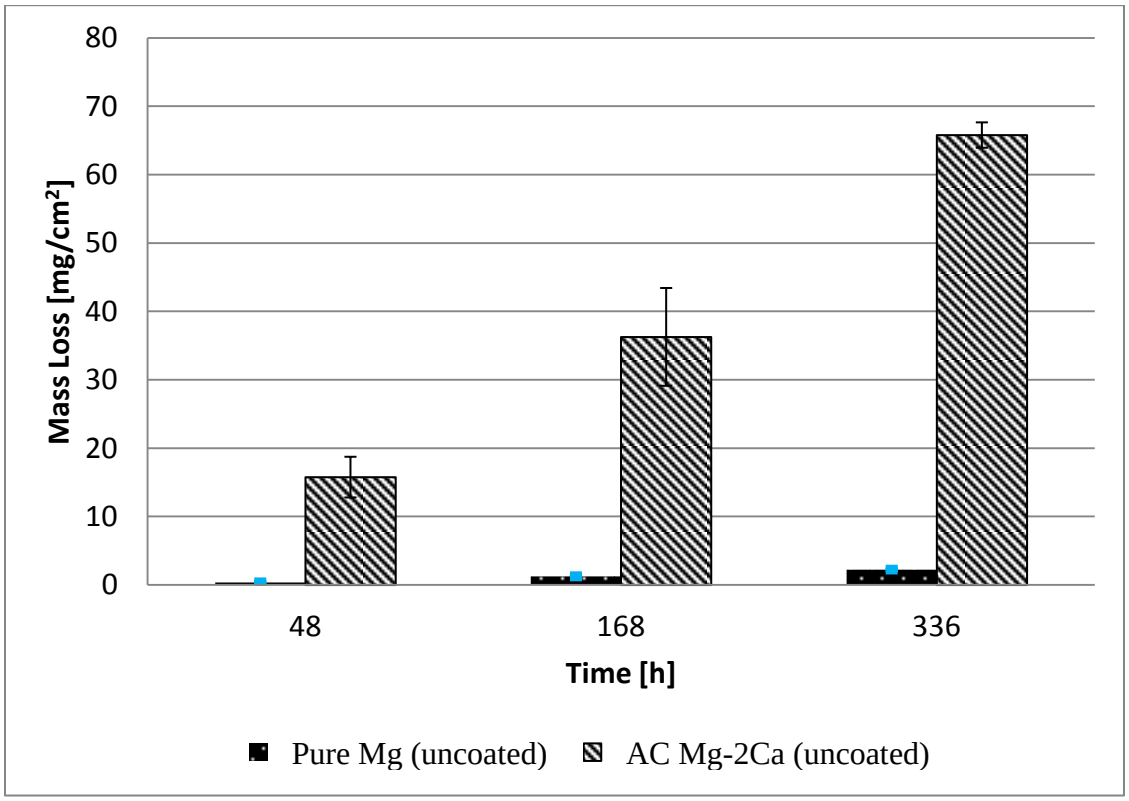

Figure 29: Mass loss results for as-cast pure Mg and as-cast Mg-2Ca (without Ag deposition) at three different immersion times

Table 7: p-values comparing mass loss results of as-cast pure Mg and as-cast Mg-2Ca at three immersion time points (without Ag deposition)

As-cast Pure Mg vs. As-cast Mg-2Ca		
Time [h]	**p-value (t-test)**	**Conclusion**
48	0.00032	Statistically significant difference
168	0.00227	Statistically significant difference
336	0.00029	Statistically significant difference

Statistically significant differences were detected between as-cast pure Mg and as-cast Mg-2Ca samples for all three time points, with the Mg-2Ca samples corroding much more rapidly than pure Mg, revealing that the addition of 2 wt. % Ca severely worsens the corrosion rate of Mg. This result corresponds well with other results in the literature; for example, Wan *et al*. [26] showed that Mg-2Ca alloy had lower corrosion resistance

than pure Mg (Figure 6) in their electrochemical tests on pure Mg and various binary Mg-Ca alloys. The fast corrosion rate of Mg-Ca alloys has been attributed to the presence of the Mg_2Ca phase [26]; the Mg_2Ca phase can clearly be seen in the microstructure of the tested Mg-2Ca samples (Figure 30).

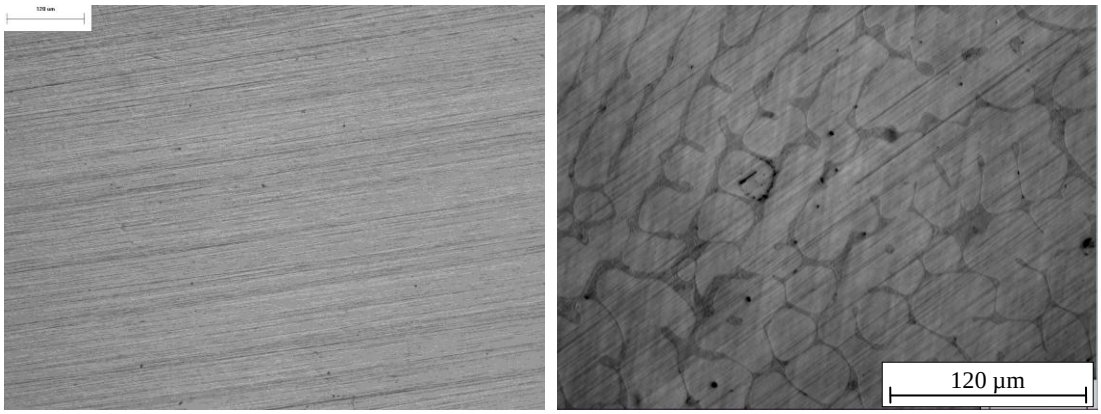

(a) (b)

Figure 30: Microstructures of (a) pure Mg and (b) as-cast Mg-2Ca prior to immersion testing

The presence of the second phases (Mg_2Ca) within the α-Mg matrix resulted in micro-galvanic couples within the microstructure. Microelectrochemical testing has identified the Mg_2Ca phase to be more anodic than α-Mg [29,66] (which is atypical as many common intermetallics present in Mg alloys have been shown to be cathodic to α-Mg [66]). Because the network of the Mg_2Ca phase (which is distributed around the grain boundaries) serves as local anodes to the surrounding α-Mg matrix, the Mg_2Ca phases would corrode preferentially, creating a corrosion channel, and thus leading to serious corrosion at the grain boundaries [32].

The results from the pH tests further confirm that the Mg-2Ca samples corroded more rapidly than pure Mg. The evolution of pH during immersion for pure Mg and Mg-2Ca is

shown in Figure 31. The pH rises rapidly at the start of immersion for both pure Mg and Mg-2Ca and plateaus after approximately 50 hours of immersion. However, the corrosion of Mg-2Ca causes the pH level to rise to a value much higher than that of pure Mg (due to the release of more OH^- ions), which indicates that much more corrosion has occurred with the Mg-2Ca samples than pure Mg.

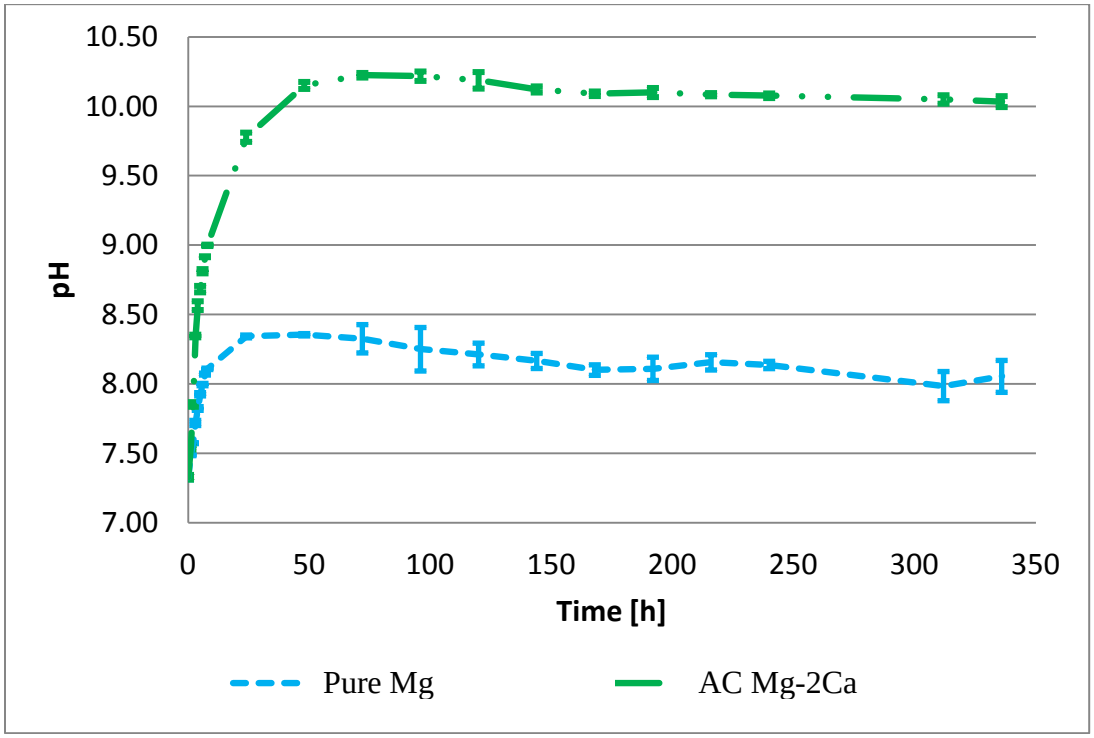

Figure 31: pH test results for as-cast pure Mg and as-cast Mg-2Ca

The mass loss results of as-cast Mg-2Ca and as-cast Mg-2Ca-1Zn samples were then compared to observe the effects of the addition of 1 wt. % Zn to the Mg-2Ca alloy. These results are seen in Figure 32. Table 8 lists the p-values calculated to compare Mg-2Ca with Mg-2Ca-1Zn at the different time points.

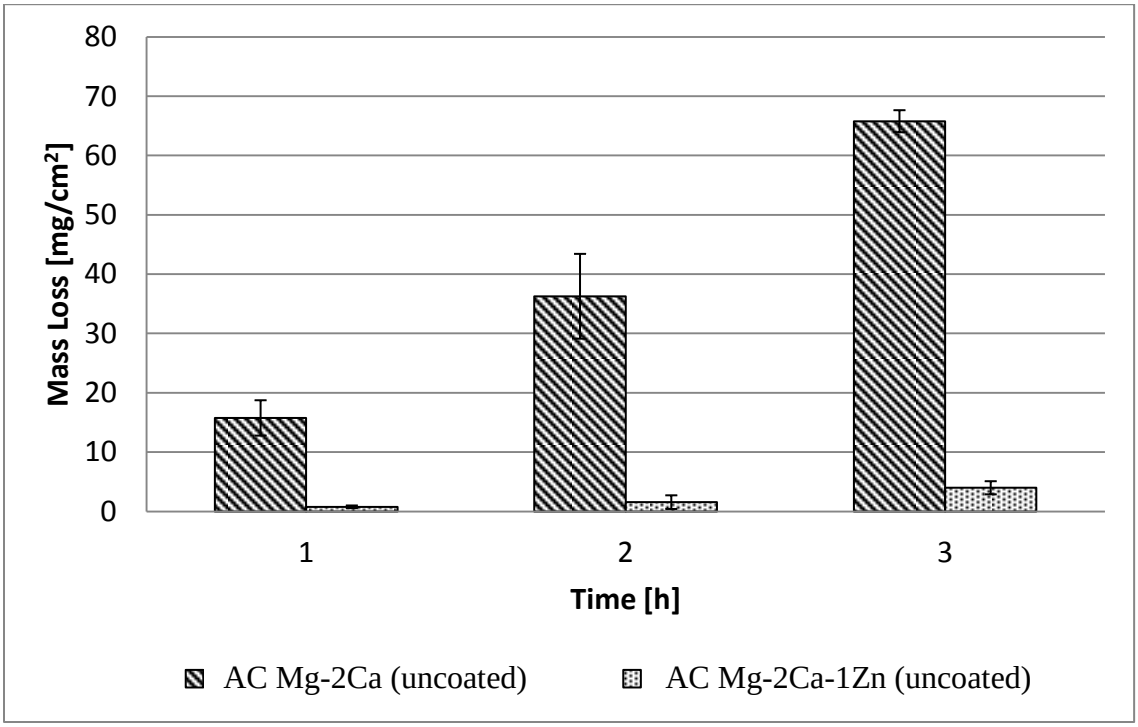

Figure 32: Mass loss results for as-cast Mg-2Ca and as-cast Mg-2Ca-1Zn (without Ag deposition) at three different immersion times

Table 8: p-values comparing mass loss results of as-cast Mg-2Ca and as-cast Mg-2Ca-1Zn at three immersion time points (without Ag deposition)

As-cast Mg-2Ca vs. As-cast Mg-2Ca-1Zn		
Time [h]	**p-value (t-test)**	**Conclusion**
48	0.00036	Statistically significant difference
168	0.00249	Statistically significant difference
336	3.5213×10^{-8}	Statistically significant difference

Again, statistically significant differences were detected between as-cast Mg-2Ca and as-cast Mg-2Ca-1Zn samples for all three time points, with the Mg-2Ca-1Zn samples corroding much more slowly than Mg-2Ca. This reveals that the addition of just 1 wt. % Zn to Mg-2Ca alloy dramatically improves the corrosion rate. This result corresponds well with other results in the literature; a study by Du *et al.* (2011) revealed that the

corrosion resistance of the Mg-3Ca alloy is improved after the addition of 2 wt. % Zn to the alloy [32]. The improved corrosion properties were attributed to the formation and presence of the $Ca_2Mg_6Zn_3$ phase in the Mg-3Ca-2Zn alloy [32], as seen in Figure 33. The $Ca_2Mg_6Zn_3$ phase was believed to contribute to the improved corrosion properties by reducing the volume fraction of the Mg_2Ca phase as well as interrupting the Mg_2Ca network, thus preventing the fast dissolution of the anodic Mg_2Ca [32].

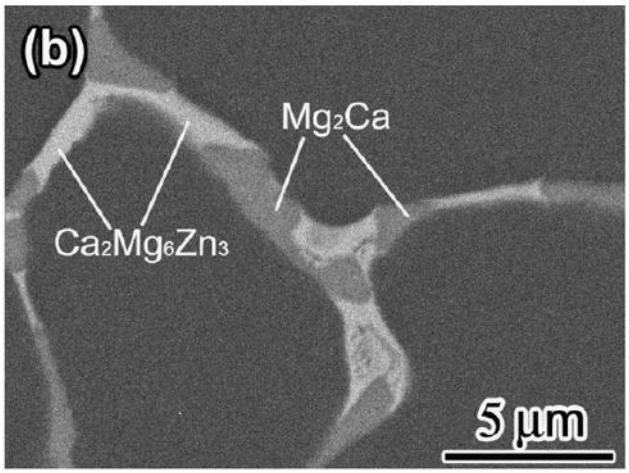

Figure 33: SEM image of the eutectic structure in as-cast Mg-3Ca-2Zn alloy [32]

Reprinted from Materials Chemistry and Physics, 125, Du, H., Wei, Z., Liu, X., Zhang, E., Effects of Zn on the microstructure, mechanical property and bio-corrosion property of Mg-3Ca alloys for biomedical application, Pages 568-575, Copyright (2011), with permission from Elsevier.

Examination of the as-cast Mg-2Ca-1Zn samples (tested in this work) under SEM revealed a microstructure similar to that found by Du *et al.* [32] (Figure 33), and EDX analysis performed on the phases revealed that the 'white' (brighter) phase was rich in Zn (Spectrum 1 in Figure 34). Those brighter areas in the microstructure shown in Figure 34 (indicated by black arrows) are thus thought to be the $Ca_2Mg_6Zn_3$ phase as well, and it

was believed that the presence of this phase in the samples tested contributed to the improved corrosion performance of the Mg-2Ca-1Zn alloys.

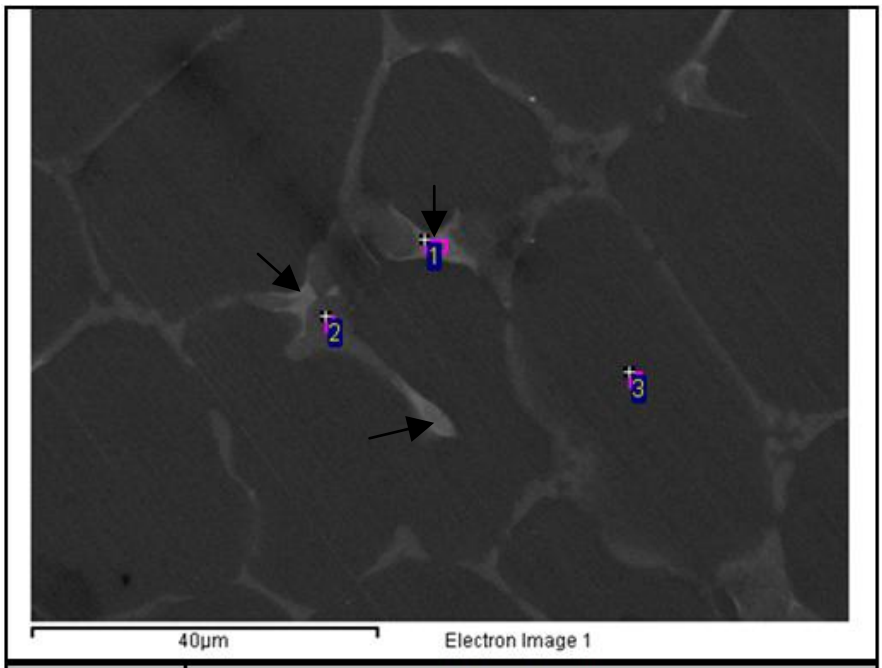

	Weight %		
Element	Spectrum 1	Spectrum 2	Spectrum 3
Mg	69.25	63.33	99.07
Ca	9.84	31.38	0.49
Zn	20.92	5.29	0.45

Figure 34: EDX results of the three phases in Mg-2Ca-1Zn alloy.

Once again, the results from the pH tests confirm that the Mg-2Ca-1Zn samples corroded more slowly than Mg-2Ca. The evolution of pH during immersion for Mg-2Ca and Mg-2Ca-1Zn is shown in Figure 35, showing much higher pH values for the Mg-2Ca samples when compared with Mg-2Ca-1Zn throughout the duration of the test.

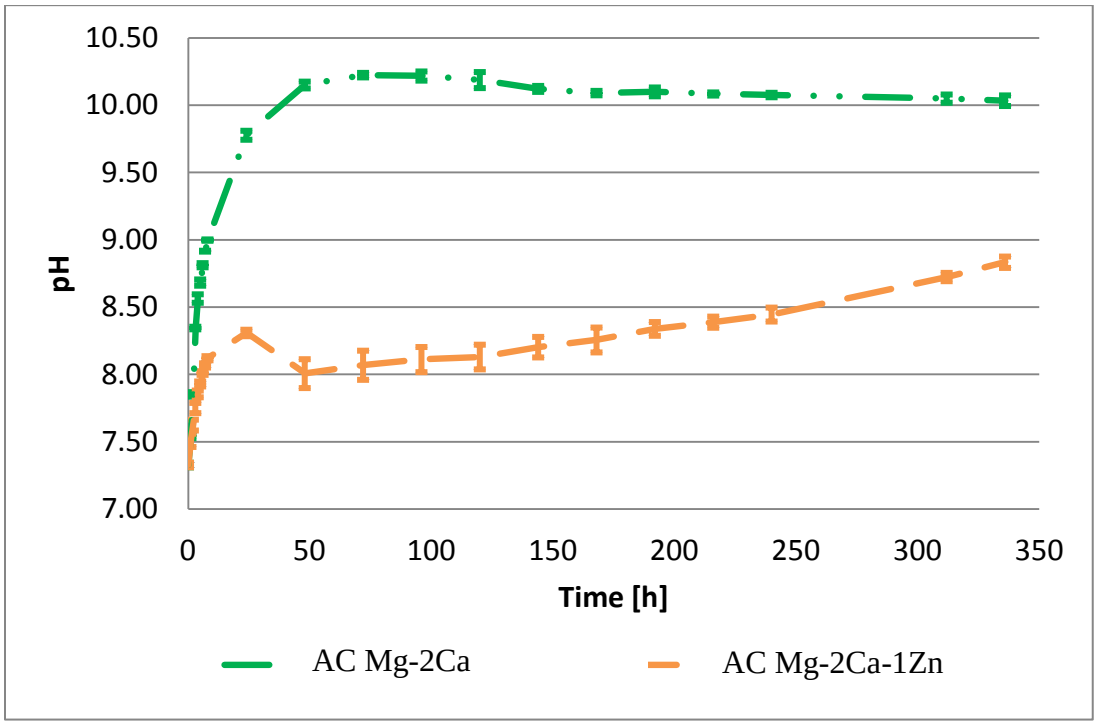

Figure 35: pH test results for as-cast Mg-2Ca and as-cast Mg-2Ca-1Zn

The mass loss results of as-cast pure Mg and as-cast Mg-2Ca-1Zn samples were then compared (Figure 36). Table 9 lists the p-values calculated to compare pure Mg with Mg-2Ca-1Zn at the three time points.

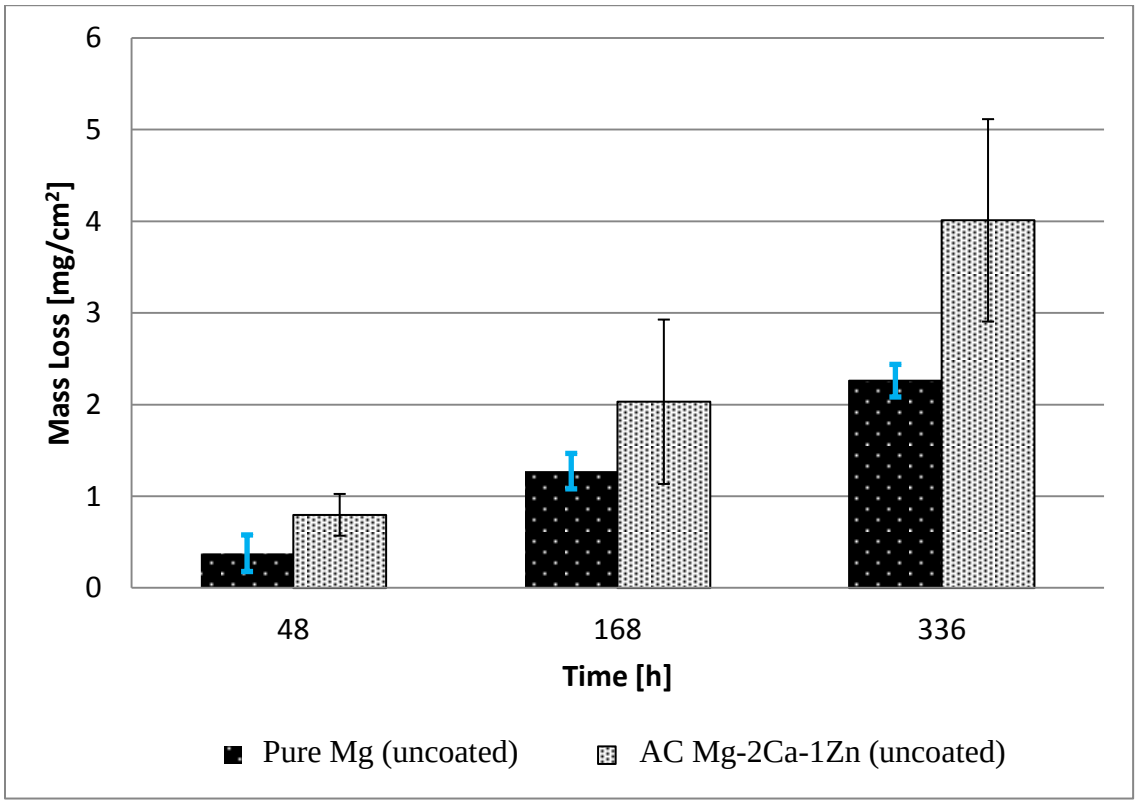

Figure 36: Mass loss results for as-cast pure Mg and as-cast Mg-2Ca-1Zn (without Ag deposition) at three different immersion times

Table 9: p-values comparing mass loss results of as-cast pure Mg and as-cast Mg-2Ca-1Zn at three immersion time points (without Ag deposition)

As-cast Pure Mg vs. As-cast Mg-2Ca-1Zn		
Time [h]	**p-value (t-test)**	**Conclusion**
48	0.03266	Statistically significant difference
168	0.28724	No significant difference detected
336	0.05216	No significant difference detected

Although it appears in Figure 36 that Mg-2Ca-1Zn exhibited slightly more mass loss than pure Mg over all time points, a statistically significant difference was only detected for the samples immersed for 48 hours. After 48 hours, statistically significant differences could not be detected. This might suggest that the addition of Zn to the binary Mg-2Ca alloy improved the corrosion performance so much so that it was relatively comparable to

the corrosion performance of pure Mg. However, further testing with larger sample sizes would be necessary to prove (or disprove) this, as it was difficult to confidently draw a conclusion from Figure 36 and Table 9 alone.

4.1.2 Effect of Heat Treatments on Corrosion of Alloy Samples

As described in Chapter 4, a preliminary immersion corrosion test was performed to determine which heat treatment (solutionizing and naturally aging *or* solutionizing and artificially aging) to select for fabrication of heat treated samples to be deposited with Ag. Sets of (uncoated) samples were heat treated via both heat treatments, then subjected to immersion corrosion for 48 hours. Figure 37 shows the mass loss measurements of Mg-2Ca samples (in the as-cast, S&NA, and S&AA conditions) after 48 hours of immersion.

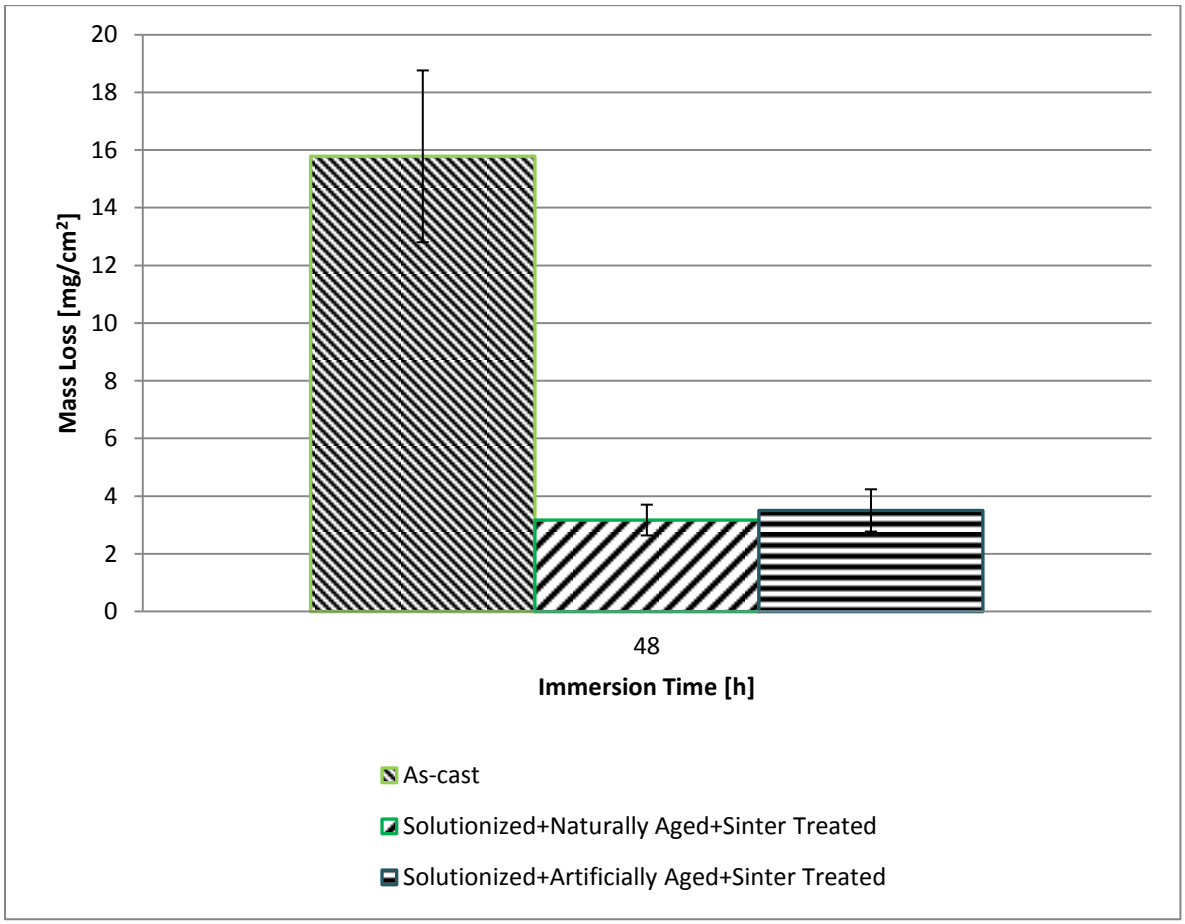

Figure 37: Mass loss measurements for Mg-2Ca alloy (as-cast, S&NA, S&AA) after 48 hours of immersion

Single-factor ANOVA was used to determine if any significant difference among the three conditions could be detected. A p-value of 1.16E-07 was calculated, indicating a significant difference of at least one of the conditions ($p < 0.05$). From Figure 37, it was clear that the mass loss of the as-cast Mg-2Ca was significantly higher than that of both heat treated groups. This might be explained by considering the microstructures of the un-corroded Mg-2Ca samples. The Mg_2Ca phase was apparent in both the as-cast sample

and the S&NA sample (Figure 38), but it was clear that the as-cast sample had a greater volume fraction of the Mg_2Ca phase than the S&NA sample had.

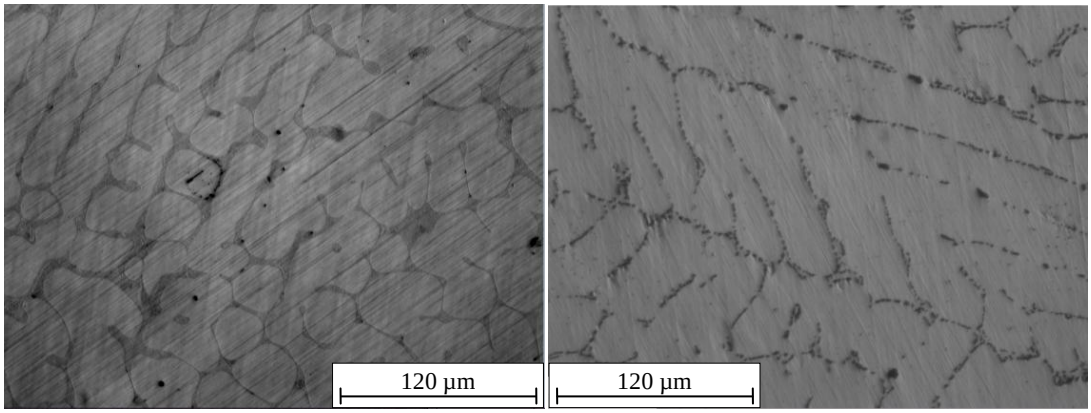

(a) (b)

Figure 38: Microstructure of un-corroded Mg-2Ca: (a) as-cast and (b) S&NA

The difference in the amount of Mg_2Ca phase present in these samples was due to the solutionizing heat treatment, during which a large proportion of the Mg_2Ca phase dissolves into the matrix. The amount of second phases present at equilibrium in Mg-2Ca (and ternary Mg-Ca-Zn alloys) as a function of temperature has previously been calculated using FactSage (Figure 39) by Langelier *et al.* [39]. The amount of the Mg_2Ca phase is clearly shown to decrease with increasing temperature. The samples in this work were solutionized at 480°C for 24 hours; according to Figure 39, a large proportion of the Mg_2Ca phase would have dissolved into the matrix at such a temperature (as compared with the as-cast Mg-2Ca).

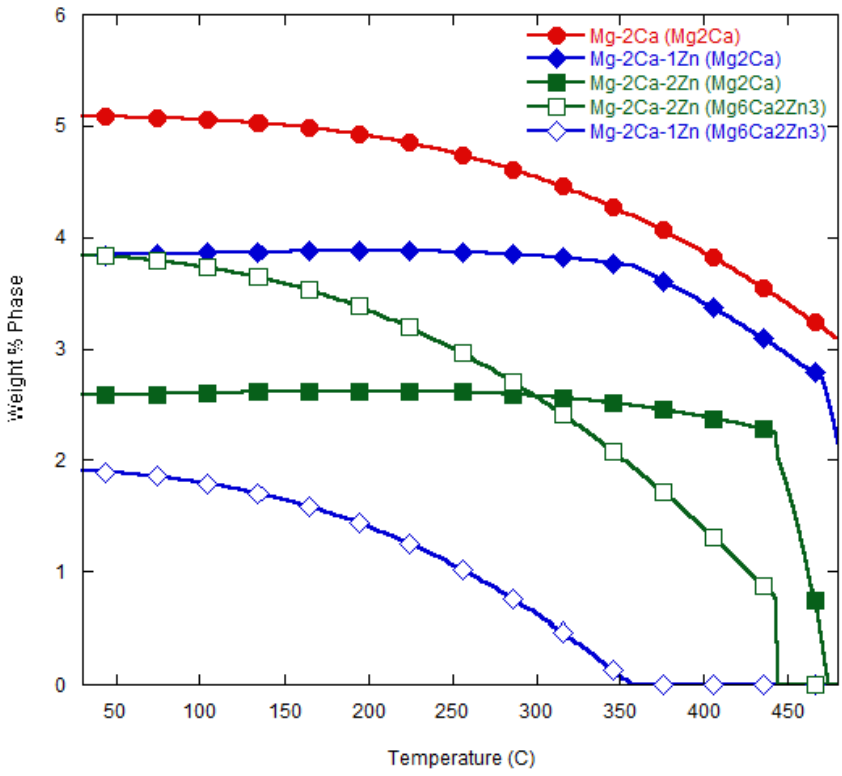

Figure 39: Equilibrium second phases for Mg-2Ca, Mg-2Ca-1Zn, and Mg-2Ca-2Zn as calculated by FactSage [39]

Reprinted from Proceedings from 2010 TMS Annual Meeting & Exhibition, Agnew, S., Neelameggham, N.R., Nyberg, E.A., Sillekens, W., The effect of Zn Additions on Precipitation Hardening of Mg-Ca Alloys, Copyright (2010), with permission from Wiley.

Since the as-cast samples had more Mg_2Ca than the S&NA samples, it was reasonable that the as-cast samples corroded faster than the S&NA samples after 48 hours, since the Mg_2Ca phase, as the local anodes, corroded preferentially. With a higher surface area of the anode (versus surface area of the cathode), more corrosion would indeed be expected to occur. This was supported by the results of Li *et al.* [27], in which as-cast Mg-1Ca, Mg-2Ca, and Mg-3Ca were tested (Figure 7), with the authors reporting that "*an increasing content of Mg_2Ca phase led to a higher corrosion rate*" [27]. This notion that

the presence (and amount) of the Mg_2Ca phase has deleterious effects on the corrosion behaviour of Mg alloys has been supported by many different researchers [27,32,37].

Because the mass loss between the S&NA samples and S&AA samples did not appear to be statistically significantly different, solutionizing and natural aging was the heat treatment chosen for the remainder of the Mg-2Ca samples to be immersion tested. Figure 40 shows the mass loss test results for as-cast Mg-2Ca compared to S&NA Mg-2Ca after 48, 168, and 336 hours of immersion. Table 10 lists the p-values calculated to compare the mass loss results at the three different time points. Statistically significant differences were observed after 48 hours and 168 hours of immersion. However, the difference did not appear to be significantly different after 336 hours.

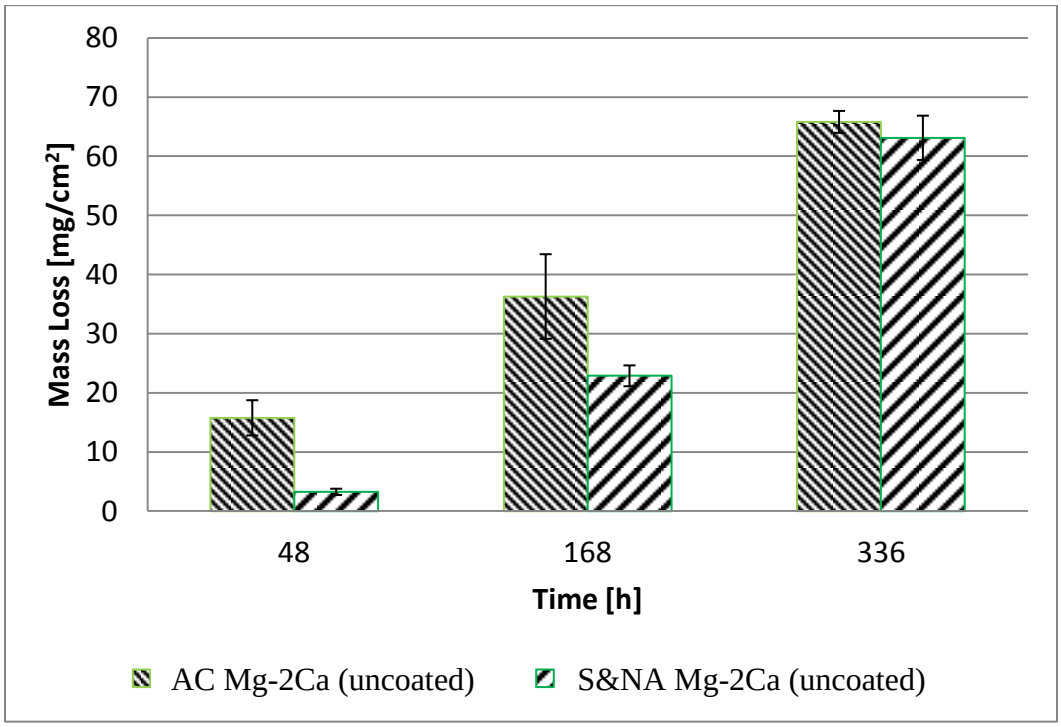

Figure 40: Mass loss results for as-cast Mg-2Ca and S&NA Mg-2Ca (without Ag deposition) at three different immersion times

Table 10: p-values comparing mass loss results of as-cast Mg-2Ca and S&NA Mg-2Ca at three immersion time points (without Ag deposition)

As-cast Mg-2Ca vs. Solutionized and Naturally Aged Mg-2Ca		
Time [h]	**p-value (t-test)**	**Conclusion**
48	0.00075	Statistically significant difference
168	0.03573	Statistically significant difference
336	0.31139	No significant difference

The results from the pH tests of the same materials (Figure 41) indicated a similar result. The pH increased significantly more rapidly for the as-cast samples than the S&NA samples for the first (approximately) 100 hours, but both plateau to about the same value towards the end of the test.

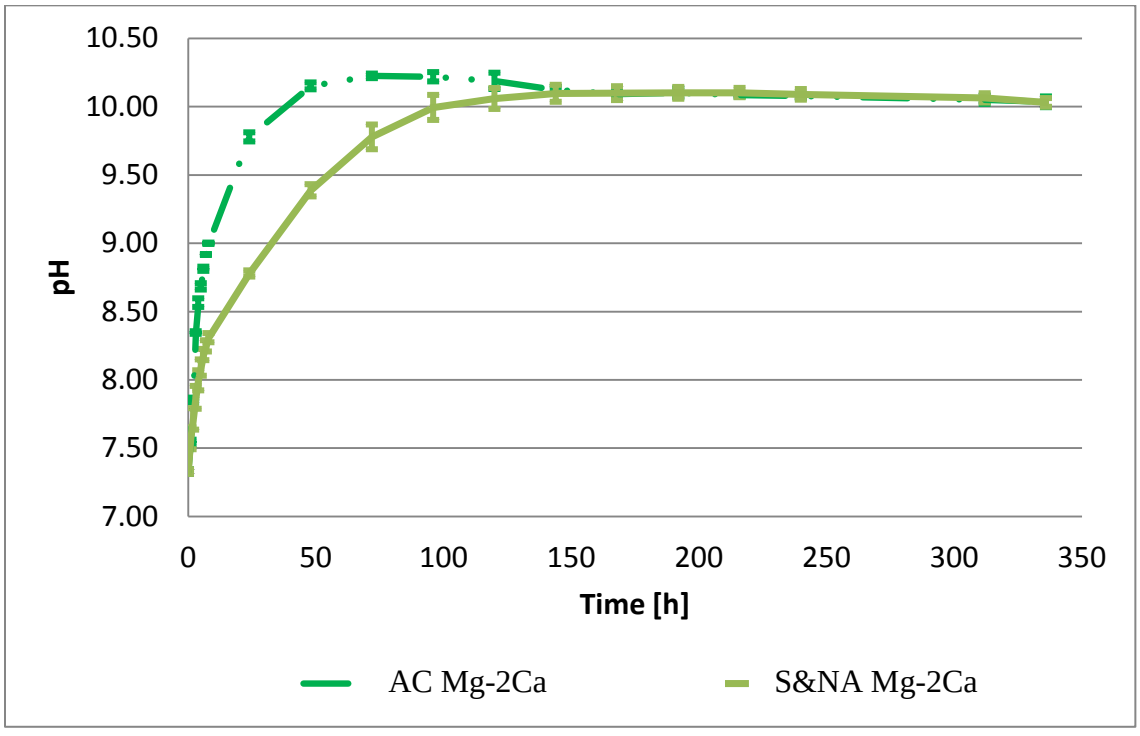

Figure 41: pH test results for as-cast Mg-2Ca and S&NA Mg-2Ca

These pH results correspond well with the mass loss results, in which the difference in mass loss no longer appeared significant after 336 hours of immersion. As explained earlier, the difference in corrosion performance near the beginning of the immersion test could be explained by considering the difference in the microstructure of Mg-2Ca before and after heat treatment (Figure 38); the as-cast samples corroded more quickly than the S&NA samples because of the higher amount of the Mg_2Ca phase. Because the Mg_2Ca phase is more electrochemically active than the α-Mg matrix, the Mg_2Ca phase would have corroded preferentially in the early stages of the corrosion reaction, which could explain why the as-cast samples corroded more quickly than the heat treated samples (as was noted before). However, the mass loss did not appear to be significantly different after longer immersion times; it was speculated that a partially protective layer had formed on the surfaces of the samples after a certain period of time, thus slowing down the corrosion process for both sample types.

Figure 42 shows the mass loss measurements of Mg-2Ca-1Zn samples (in the as-cast, S&NA, and S&AA conditions) after 48 hours of immersion.

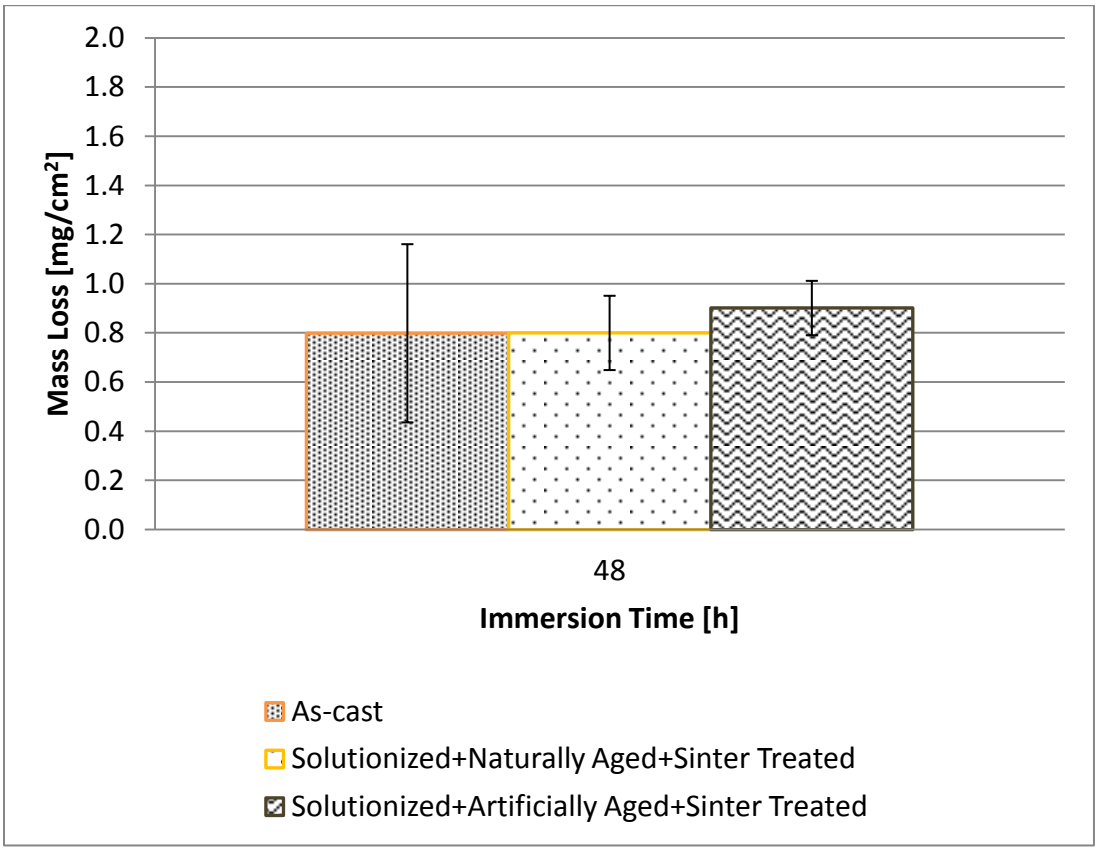

Figure 42: Mass loss measurements for Mg-2Ca-1Zn alloy (as-cast, S&NA, S&AA) after 48 hours of immersion

Again, single-factor ANOVA was used to determine if any significant difference existed among the three conditions. A p-value of 0.498 was calculated, indicating that a significant difference could not be detected among these three conditions ($p > 0.05$). This might be explained by, again, considering the microstructure of Mg-2Ca-1Zn before and after heat treatment. When observing the microstructures of as-cast Mg-2Ca-1Zn and S&NA Mg-2Ca-1Zn prior to immersion (Figure 43), it was noted that, while the second phases were present in both types of samples (and thus, the existence of micro-galvanic couples), there did not appear to be very much difference in terms of the amount of the

phases within the matrices between the sample types. Because of this, it seemed reasonable that the mass loss rates of these sample types did not appear to be significantly different.

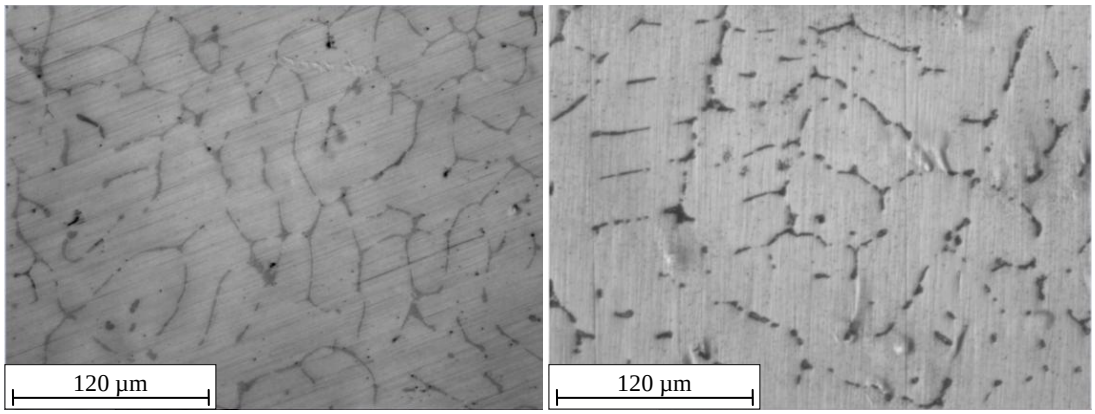

(a) (b)

Figure 43: Microstructure of un-corroded Mg-2Ca-1Zn: (a) as-cast and (b) S&NA

Because the mass loss between the S&NA samples and S&AA samples did not appear to be significantly different, solutionizing and natural aging was the heat treatment chosen for the remainder of the Mg-2Ca-1Zn samples to be immersion tested (again, for reasons described in Chapter 4). Figure 44 shows the mass loss results for as-cast Mg-2Ca-1Zn compared to S&NA Mg-2Ca-1Zn after 48, 168, and 336 hours of immersion. Table 11 lists the p-values calculated to compare the mass loss results at the three different time points. Statistically significant differences were not detectable for all three time points. The fact that the difference between as-cast and heat treated Mg-2Ca-1Zn samples was not as apparent as the Mg-2Ca samples may be explained by the FactSage calculations as displayed in Figure 39. The decrease in volume fraction of the Mg_2Ca phase with increasing temperature for the Mg-2Ca-1Zn alloy is not as pronounced as that

of the Mg-2Ca alloy. In other words, in the Mg-2Ca-1Zn alloy, less Mg_2Ca phase dissolves into the matrix with heat treatment as compared to the Mg-2Ca alloy, thus a fair amount of the anodic Mg_2Ca phase remains in the microstructure of the Mg-2Ca-1Zn alloy after heat treatment. Therefore, it was reasonable that the difference in corrosion behaviour was not as pronounced (i.e., no significant difference was detected) in the Mg-2Ca-1Zn alloy after heat treatment.

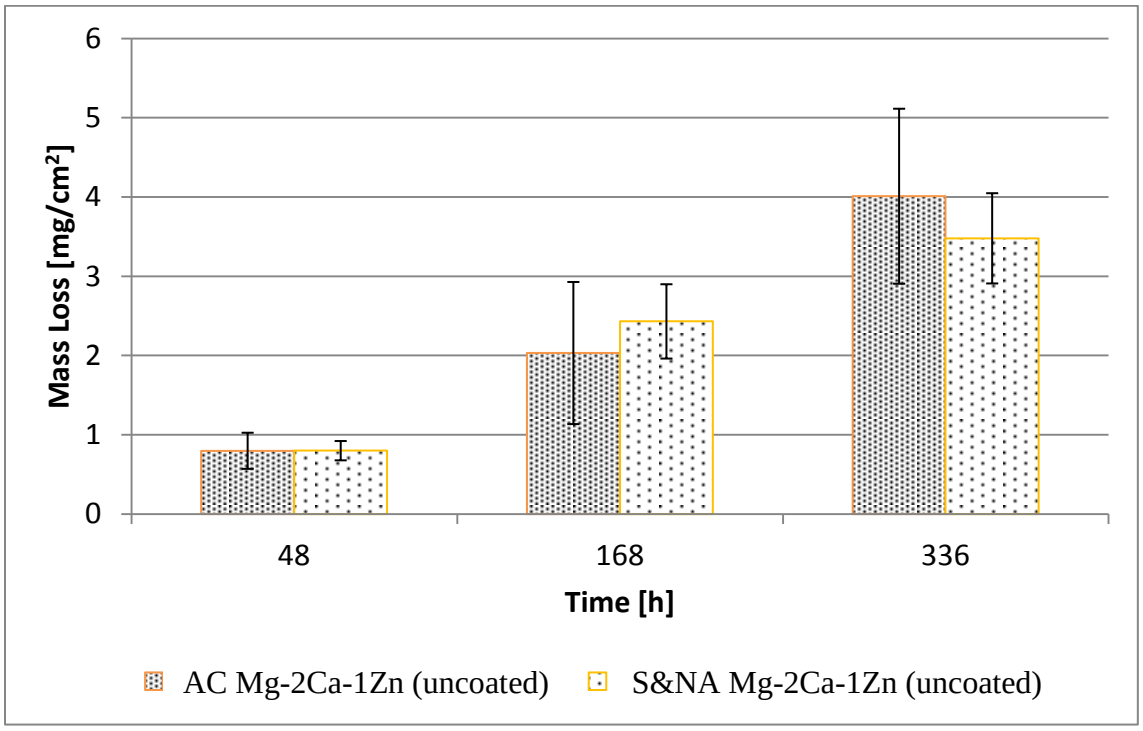

Figure 44: Mass loss results for as-cast Mg-2Ca-1Zn and S&NA Mg-2Ca-1Zn (without Ag deposition) at three different immersion times

Table 11: p-values comparing mass loss results of as-cast Mg-2Ca-1Zn and S&NA Mg-2Ca-1Zn at three immersion time points (without Ag deposition)

As-cast Mg-2Ca-1Zn vs. Solutionized and Naturally Aged Mg-2Ca-1Zn		
Time [h]	**p-value (t-test)**	**Conclusion**
48	0.99029	No significant difference
168	0.22358	No significant difference
336	0.42521	No significant difference

The results from the pH tests (Figure 45) seemed to confirm this observation. No significant difference in pH values between as-cast and S&NA Mg-2Ca-1Zn was observed throughout the duration of the test.

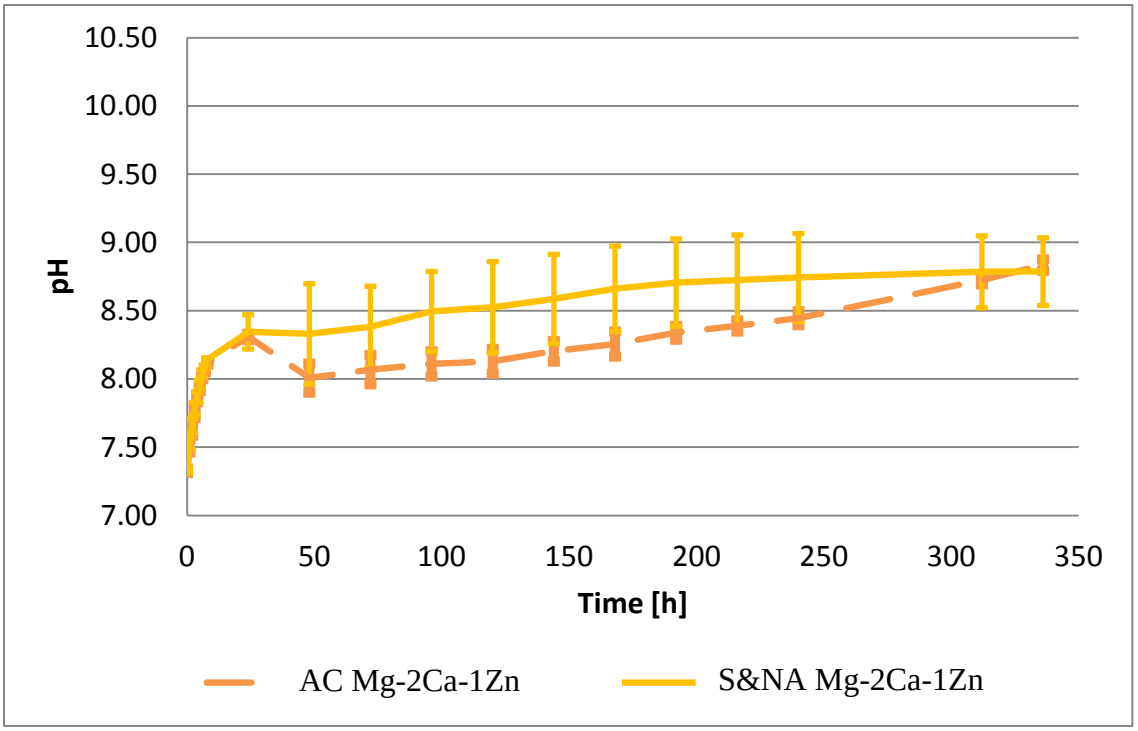

Figure 45: pH test results for as-cast Mg-2Ca-1Zn and S&NA Mg-2Ca-1Zn

4.1.3 Effect of Ag Deposition on Corrosion

To observe the effect of Ag deposition on corrosion behaviour, the mass loss results of a particular type of sample was compared to the mass loss results of the same sample type with Ag deposition. In this section, general observations will first be made, and discussions incorporating all observations will be presented.

First, uncoated pure Mg samples were compared with pure Mg samples with Ag deposition. These results are shown in Figure 46, and Table 12 lists the calculated p-values used to compare the samples at the different time points. Statistically significant differences between the uncoated samples and Ag-deposited samples were not detected for all three time points.

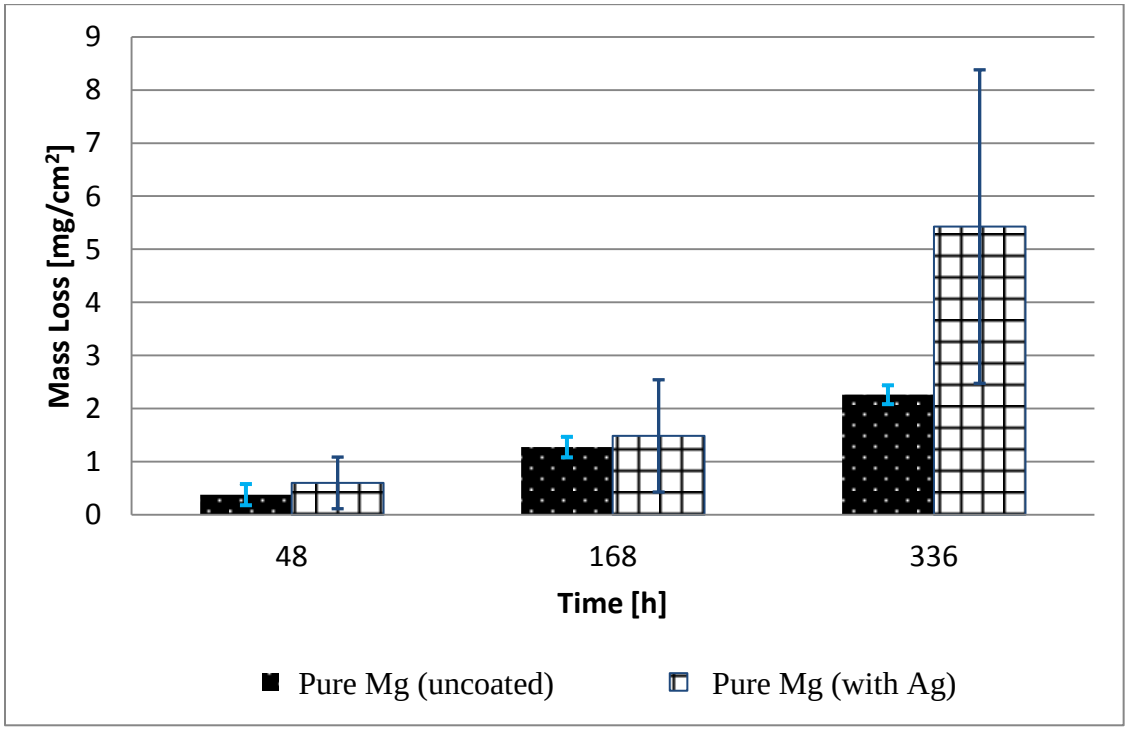

Figure 46: Mass loss results for as-cast pure Mg (with and without Ag deposition) at three different immersion times

Table 12: p-values comparing mass loss results of as-cast pure Mg (with and without Ag deposition) at three immersion time points

As-cast Pure Mg: Uncoated vs. With Ag Deposition		
Time [h]	**p-value (t-test)**	**Conclusion**
48	0.43271	No significant difference
168	0.72110	No significant difference
336	0.12169	No significant difference

Uncoated as-cast Mg-2Ca samples were then compared to as-cast Mg-2Ca samples with Ag deposition. The mass loss results for these samples are shown in Figure 47. Table 13 lists the calculated p-values. Again, statistically significant differences between the uncoated samples and Ag-deposited samples were not detected for all three time points.

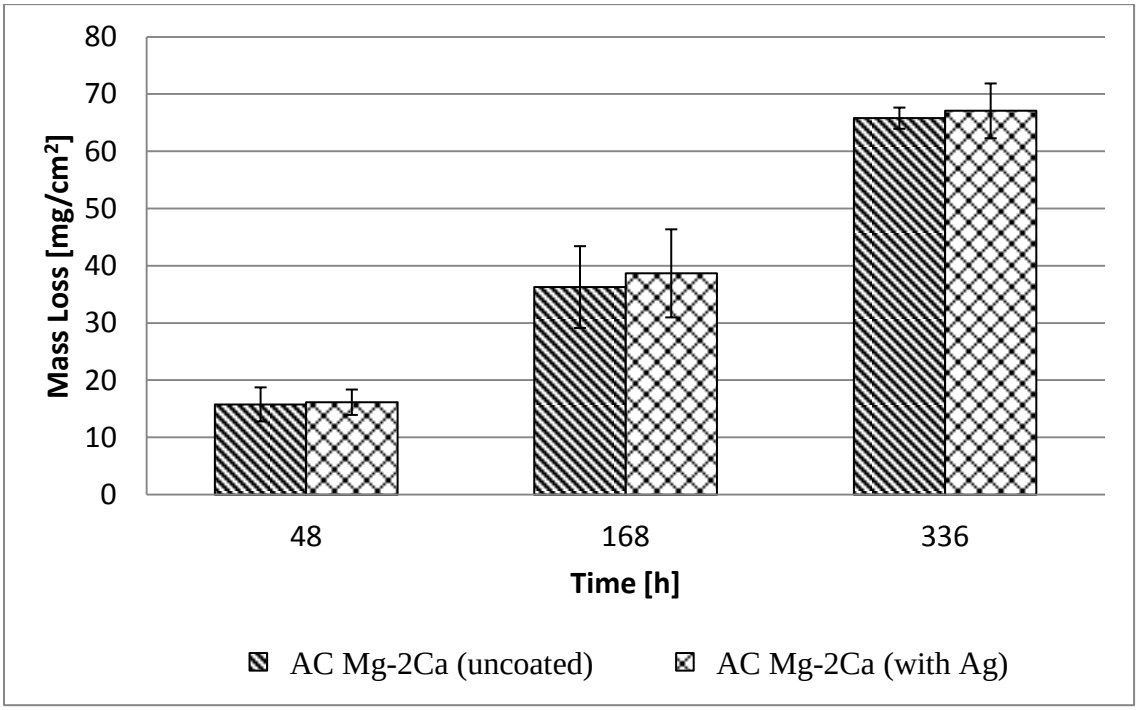

Figure 47: Mass loss results for as-cast Mg-2Ca (with and without Ag deposition) at three different immersion times

Table 13: p-values comparing mass loss results of as-cast Mg-2Ca (with and without Ag deposition) at three immersion time points

As-cast Mg-2Ca: Uncoated vs. With Ag Deposition		
Time [h]	**p-value (t-test)**	**Conclusion**
48	0.83691	No significant difference
168	0.66388	No significant difference
336	0.68406	No significant difference

Uncoated Mg-2Ca samples (in the S&NA condition) were then compared to those with Ag deposition. The mass loss results for these samples are shown in Figure 48. Table 14 lists the calculated p-values. In this case, there appeared to be a significant difference between the uncoated samples and Ag-deposited samples after 48 hours of immersion. However, significant differences were not detected for samples immersed for 168 and 336 hours.

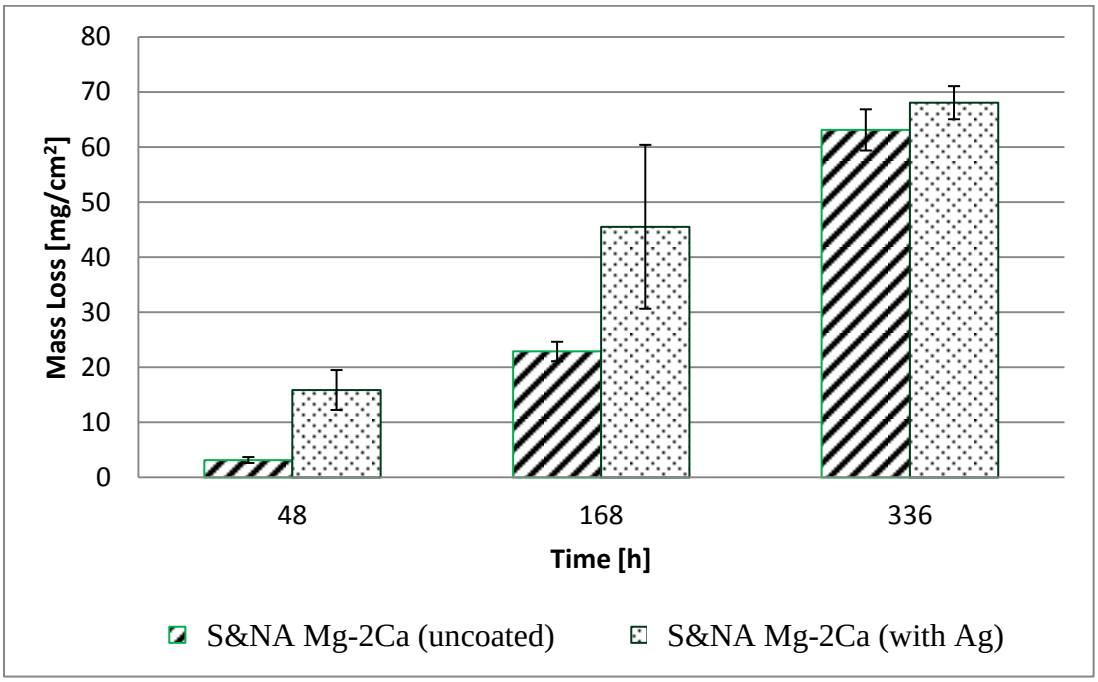

Figure 48: Mass loss results for S&NA Mg-2Ca (with and without Ag deposition) at three different immersion times

Table 14: p-values comparing mass loss results of S&NA Mg-2Ca (with and without Ag deposition) at three immersion time points

As-cast Mg-2Ca: Uncoated vs. With Ag Deposition		
Time [h]	**p-value (t-test)**	**Conclusion**
48	0.00618	Statistically significant difference
168	0.05670	No significant difference
336	0.08499	No significant difference

Uncoated as-cast Mg-2Ca-1Zn samples were compared to as-cast Mg-2Ca-1Zn samples with Ag deposition. These mass loss results are shown in Figure 49, and Table 15 lists the calculated p-values. A statistically significant difference appeared for the samples immersed for 336 hours, but significant differences could not be detected between sample immersed for 48 and 168 hours.

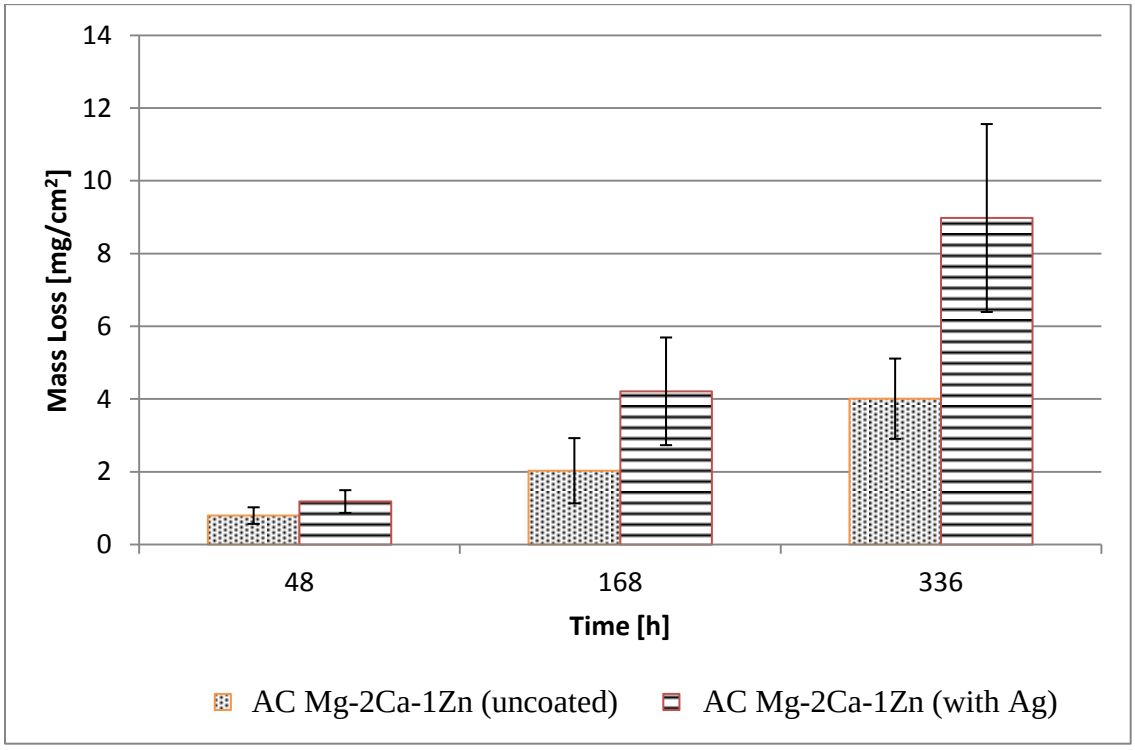

Figure 49: Mass loss results for as-cast Mg-2Ca-1Zn (with and without Ag deposition) at three different immersion times

Table 15: p-values comparing mass loss results of as-cast Mg-2Ca-1Zn (with and without Ag deposition) at three immersion time points

As-cast Mg-2Ca: Uncoated vs. With Ag Deposition		
Time [h]	**p-value (t-test)**	**Conclusion**
48	0.09372	No significant difference
168	0.07575	No significant difference
336	0.01227	Statistically significant difference

Finally, uncoated Mg-2Ca-1Zn samples (in the S&NA condition) were compared to S&NA Mg-2Ca-1Zn samples with Ag deposition. These results are shown in Figure 50, with Table 16 listing the calculated p-values. In this case, a significant difference was observed between the uncoated samples and Ag-deposited samples after 168 and 336 hours of immersion, but a significant difference was not detected for samples immersed for 48 hours.

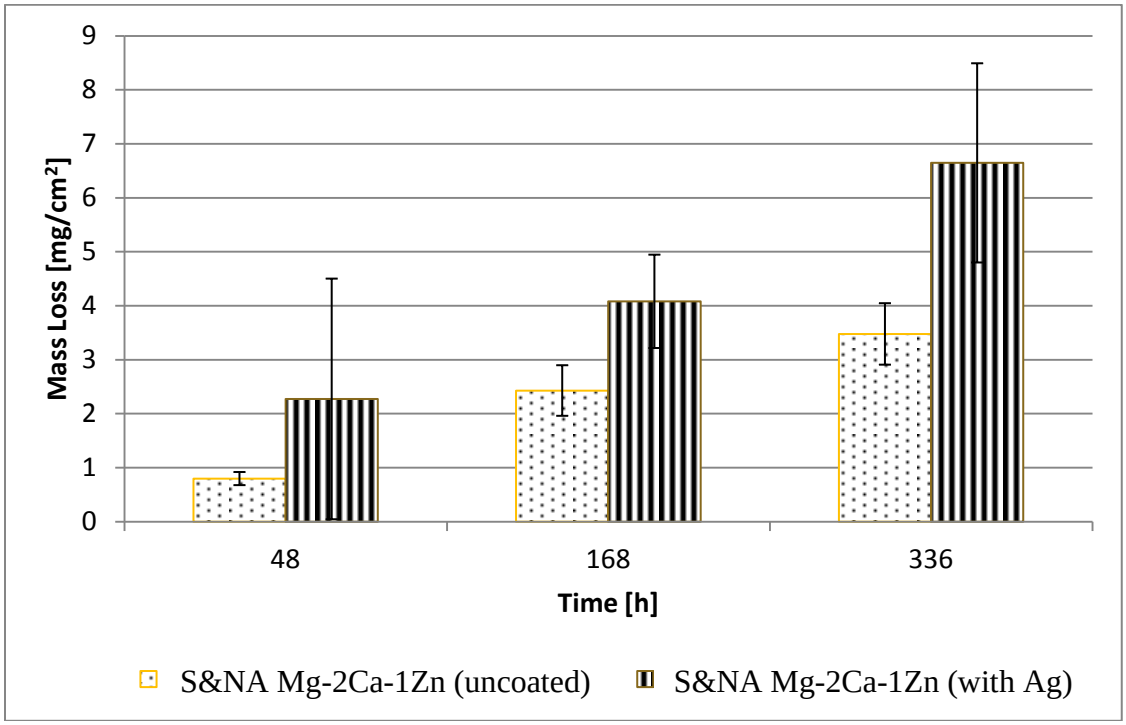

Figure 50: Mass loss results for S&NA Mg-2Ca-1Zn (with and without Ag deposition) at three different immersion times

Table 16: p-values comparing mass loss results of S&NA Mg-2Ca-1Zn (with and without Ag deposition) at three immersion time points

As-cast Mg-2Ca: Uncoated vs. With Ag Deposition		
Time [h]	**p-value (t-test)**	**Conclusion**
48	0.27792	No significant difference
168	0.01522	Statistically significant difference
336	0.03045	Statistically significant difference

Overall, the fact that significant differences between uncoated samples and samples deposited with Ag were detected in some comparisons (e.g., S&NA Mg-2Ca immersed for 48 hours) but not others (e.g., S&NA Mg-2Ca immersed for 168 and 336 hours) points to the possibility that Ag may indeed have had an effect on the corrosion behaviour, but this effect may depend on the Ag depositions themselves (i.e., the individual characteristics of the Ag tracks). Further analysis of the mass loss results and re-examination of all of the samples tested provided more insight on the possible effect of Ag deposition on corrosion behaviour.

4.1.4 Variations Within Sample Groups

In reviewing all of the mass loss results when comparing uncoated samples with samples with Ag-deposition (Figure 46 through Figure 50), an observation was made regarding the size of the error bars associated with the mass loss results: in general, the error bars tended to be quite large for the groups of Ag-deposited samples, and in almost all cases, they were larger than those associated with the uncoated samples. This observation suggested that the corrosion behaviour of the substrates was likely very sensitive to the Ag deposition.

Whether or not Ag deposition affected corrosion behaviour seemed to depend heavily on the characteristics of the Ag tracks themselves. In many comparisons, no significant difference was detected between a group of uncoated samples and the corresponding group of Ag-deposited samples. However, if each Ag-deposited sample within that group was examined, differences in the characteristics of the Ag tracks were found among the

different samples. These differences in Ag track characteristics were due to inconsistencies from the M^3D machine during the Ag deposition process. Although efforts were made during this process to produce consistent Ag tracks among all samples (e.g., using the same processing parameters, checking the Ag tracks of the first few samples produced each session under an optical microscope, rejecting bad samples, etc.), it was very difficult to produce numerous samples with exactly identical Ag tracks. Because of this, the variation of mass loss results within a given group of Ag-deposited samples was partly attributed to the fact that inconsistencies in Ag track characteristics among samples existed. Relating the mass loss result of an individual sample to the characteristics of the Ag tracks *on that same sample* (and doing so for every single sample tested), it was found that, in general, corrosion was more severe for samples on which the Ag tracks were thicker, denser, and more 'solid' in appearance compared to samples on which the Ag tracks were thinner and sparser.

To illustrate, the pure Mg samples immersed for 168 hours were examined (refer to Figure 46). The mass loss of each individual (Ag-deposited) sample was plotted and shown in Figure 51. Examining the samples immersed for 168 hours, it was obvious that one sample in this group (called Sample 7A) exhibited a much higher mass loss than the other samples in that group.

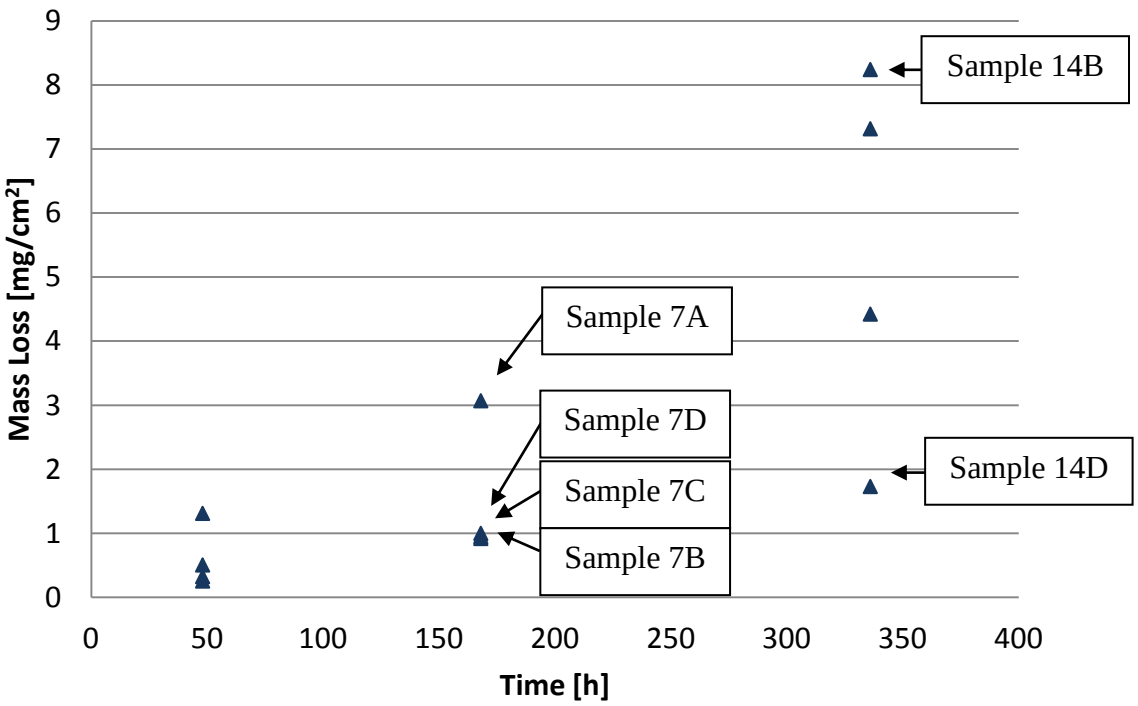

Figure 51: Individual mass loss results of pure Mg samples with Ag deposition

As mentioned prior, the characteristics of the Ag tracks on each individual sample had been examined using optical microscopy and optical profilometry. Figure 52 shows the optical microscopy images of the Ag tracks on the pure Mg samples prior to being subjected to 168 hours of immersion. It was observed that the Ag tracks on Sample 7A (the sample with the highest mass loss) were thicker and more solid than the tracks on the other three samples within that group (that exhibited less mass loss).

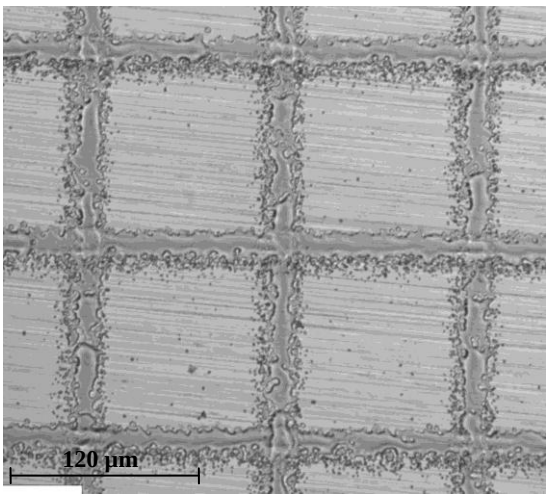

Pure Mg Sample 7A
Highest Mass Loss
Mass Loss: 3.0719 mg/cm^2

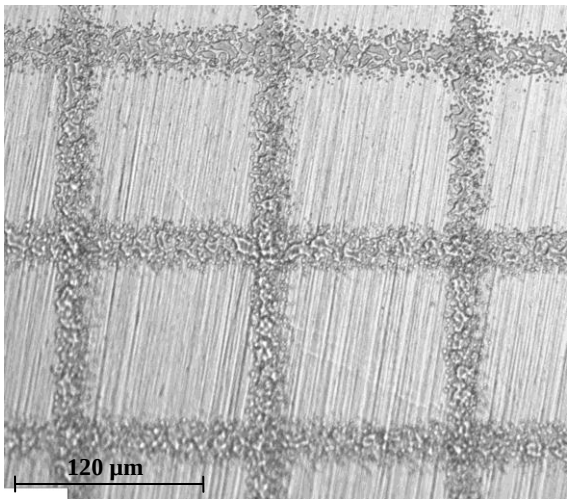

Pure Mg Sample 7B
Lowest Mass Loss
Mass Loss: 0.9214 mg/cm^2

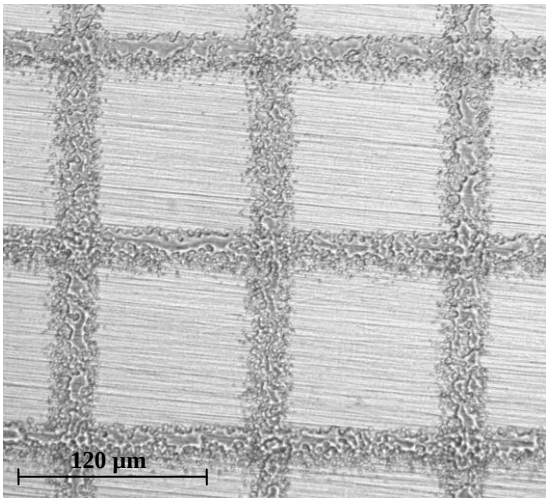

Pure Mg Sample 7C
Mass Loss: 0.9510 mg/cm^2

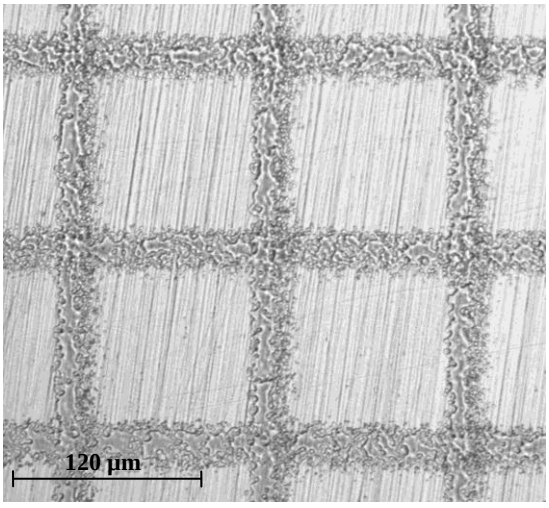

Pure Mg Sample 7D
Mass Loss: 1.0019 mg/cm^2

Figure 52: Optical microscope images of the Ag tracks on the pure Mg samples prior to immersion for 168 hours

Optical profilometry allowed for the thickness of the Ag tracks to be measured. X and Y profile plots were obtained, which essentially showed the cross-section of the observed Ag tracks on a particular sample. For illustration purposes, Figure 53 shows the X and Y

profile plots of Sample 7A and Sample 7B to compare the thickness and width characteristics of the samples that exhibited the highest and lowest mass loss, respectively. The peaks on the profile plots represent the Ag tracks on the samples, with the y-axis representing the thickness (or height) of the tracks and the x-axis representing the width. Observing these profile plots, it was clear that the Ag tracks on Sample 7A were generally both thicker and wider than the tracks on Sample 7B.

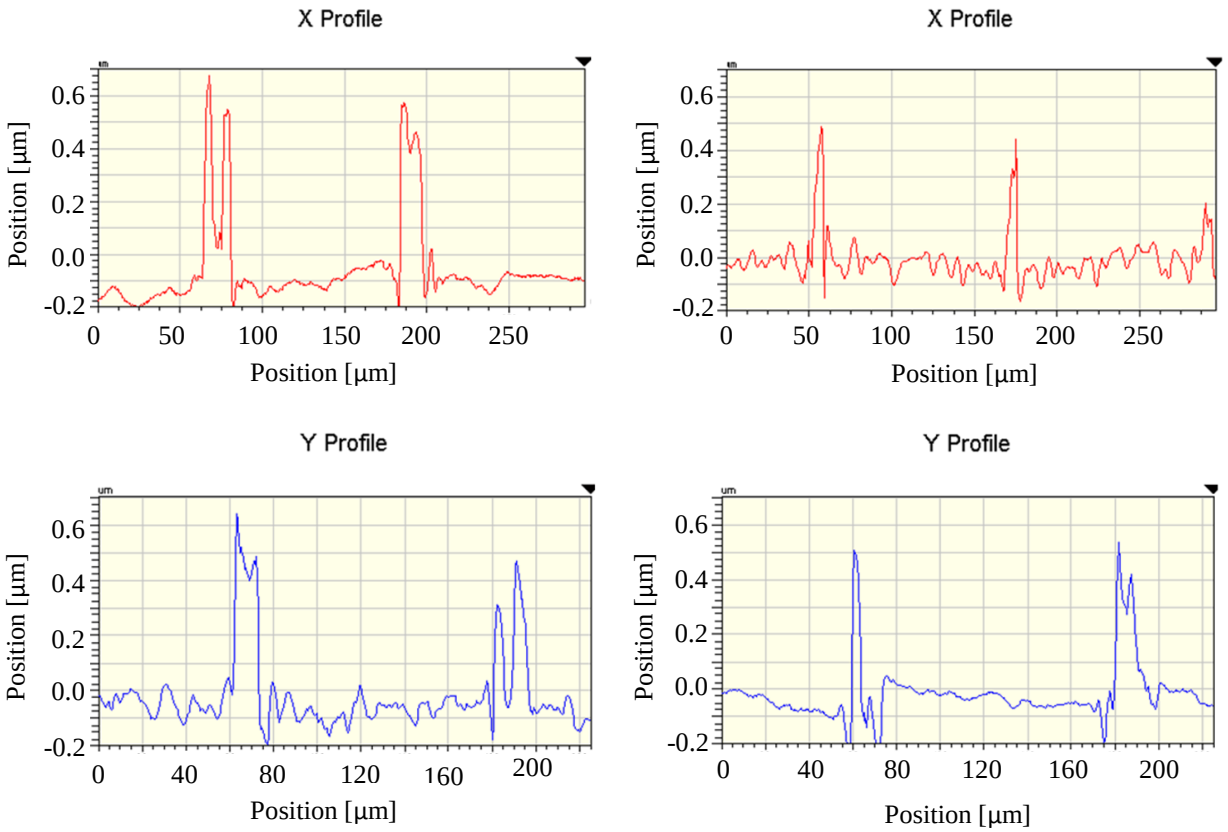

Pure Mg Sample 7A
(Highest Mass Loss)
Mass Loss: 3.0719 mg/cm^2

500-600 nm Thickness
15-20 µm Width

Pure Mg Sample 7B
(Lowest Mass Loss)
Mass Loss: 0.9214 mg/cm^2

400-500 nm Thickness
5-10 µm Width

Figure 53: X and Y profile plots of the Ag tracks on two pure Mg samples immersed for 168 hours

To further illustrate how much of an effect the characteristics of the Ag tracks can have on corrosion behaviour, the group of pure Mg samples immersed for 336 hours was examined next. From Figure 51, it was clear that Sample 14B exhibited the highest mass loss and Sample 14D exhibited a much lower mass loss. The optical microscope images of the Ag tracks on these samples are shown in Figure 54. In this case, it was extremely obvious that the Ag tracks on Sample 14B were much thicker, denser, and more solid than the tracks on Sample 14D, which had a more 'splattered' appearance. In terms of mass loss, Sample 14B indeed exhibited much more mass loss than Sample 14D.

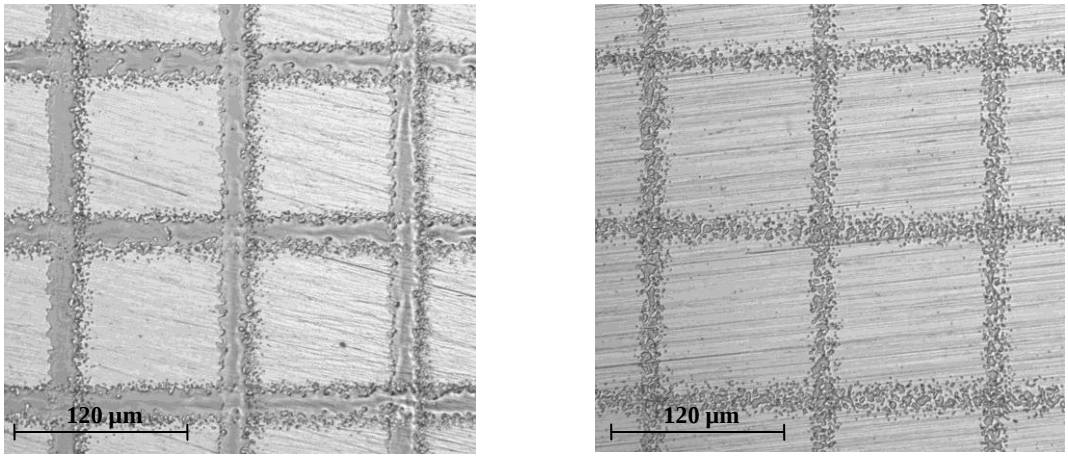

Pure Mg Sample 14B
Highest Mass Loss
Mass Loss: 8.2430 mg/cm^2

Pure Mg Sample 14D
Lowest Mass Loss
Mass Loss: 1.7328 mg/cm^2

Figure 54: Optical microscope images of the Ag tracks on two of the pure Mg samples prior to immersion for 336 hours

After analyzing other samples in addition to these pure Mg samples shown above, it was observed that, generally, samples with very thick, dense, and solid Ag tracks exhibited more mass loss (i.e., more severe corrosion) than samples with thinner, less

dense tracks. In fact, the mass losses exhibited by samples with thinner, less dense tracks were often quite close to those of samples without any Ag deposition at all. The set of S&NA Mg-2Ca samples immersed for 168 hours was taken as an example to illustrate this observation. Figure 55 shows the individual mass loss results of the uncoated samples (U7A, U7B, U7C, and U7D) and samples with Ag deposition (7A, 7B, 7C, and 7D) that were immersed for 168 hours. While samples 7A, 7B, and 7C (with Ag deposition) had mass loss values that were much higher than the uncoated samples, Sample 7D (with Ag deposition) had a mass loss value within the range of those exhibited by the uncoated samples. Again, the difference in mass loss results within the group of Ag-deposited samples was attributed to the differences in the characteristics of the Ag tracks (Figure 56); the Ag tracks on Samples 7A, 7C, and 7B (highest mass loss) were thicker and more solid than the Ag tracks on Sample 7D (lowest mass loss), which had a slightly splattered, non-solid appearance.

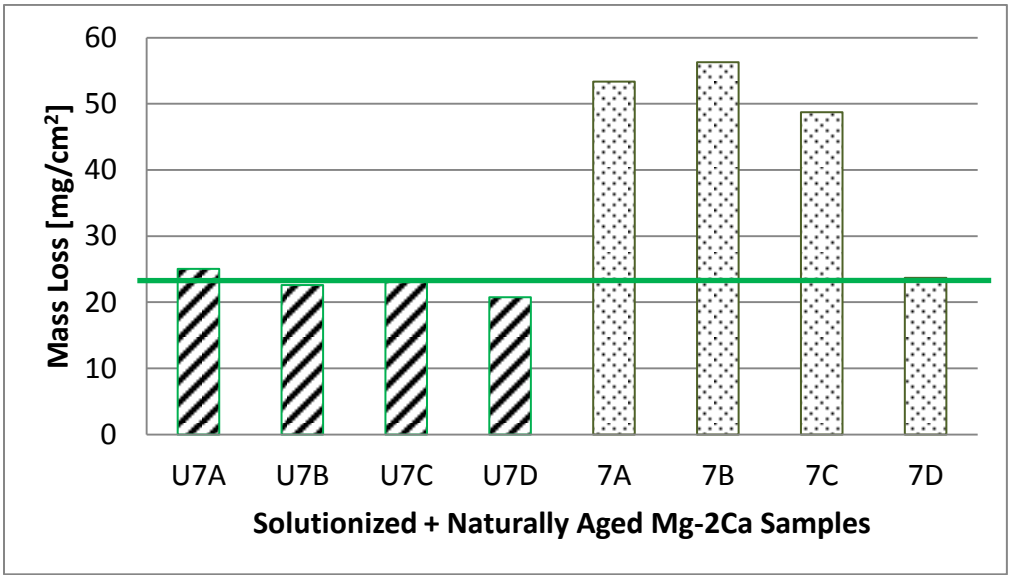

Figure 55: Individual mass loss results of uncoated samples and samples with Ag deposition that were immersed for 168 hours

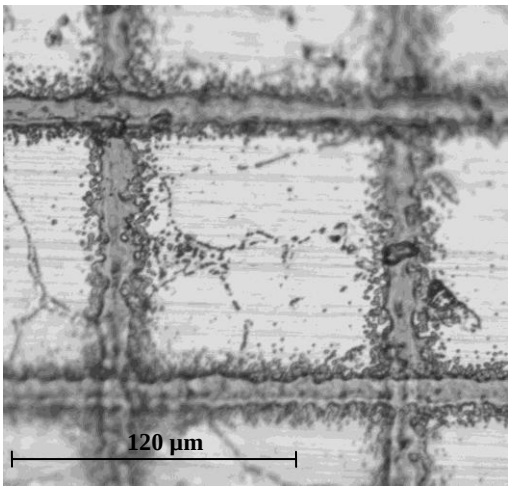

S&NA Mg-2Ca Sample 7A

Mass Loss: 53.3711 mg/cm^2

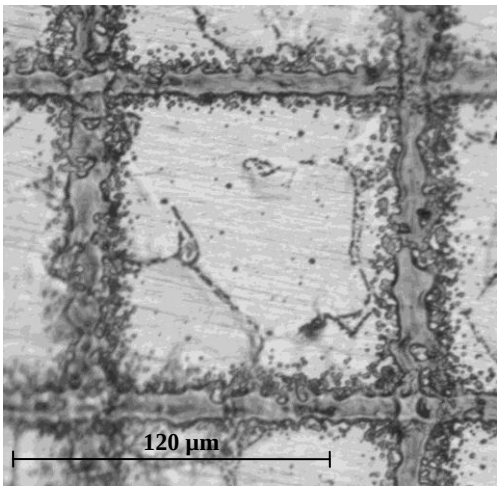

S&NA Mg-2Ca Sample 7B

Highest Mass Loss

Mass Loss: 56.3014 mg/cm^2

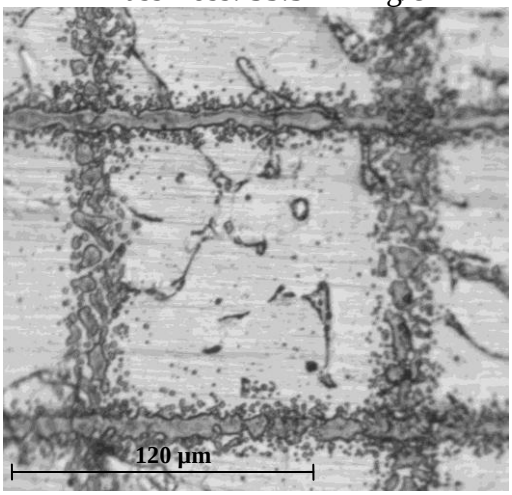

S&NA Mg-2Ca Sample 7C

Mass Loss: 48.7432 mg/cm^2

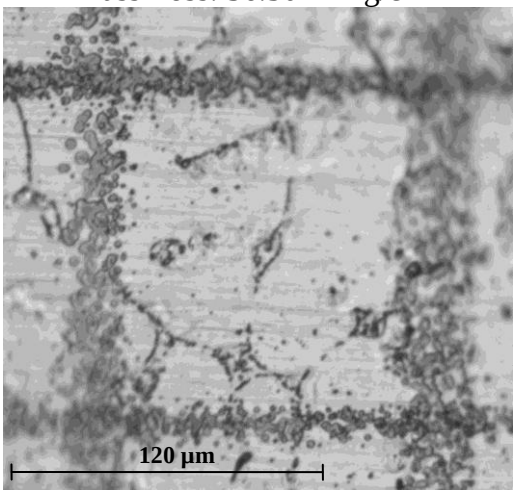

S&NA Mg-2Ca Sample 7D

Lowest Mass Loss

Mass Loss: 23.6947 mg/cm^2

Figure 56: Optical microscope images of the Ag tracks on the S&NA Mg-2Ca samples prior to immersion for 168 hours

The idea that different Ag track characteristics could affect the corrosion behaviour was further supported by considering the surface morphology of the corroded samples. Figure 57 shows the surface of an uncoated sample (U7C) after the removal of the

corrosion products, while Figure 58 shows the surfaces of the corresponding Mg-2Ca samples with Ag deposition after immersion. The surface morphology of the sample with thin Ag tracks (Sample 7D in Figure 58) quite closely resembles that of an uncoated sample (Figure 57), appearing to corrode in a similar manner, while the samples with thicker, denser, and more solid Ag tracks clearly corroded much more severely.

Figure 57: Surface of a corroded Mg-2Ca sample (without Ag deposition) after 168 hours of immersion

S&NA Mg-2Ca Sample 7A

Mass Loss: 53.3711 mg/cm^2

S&NA Mg-2Ca Sample 7B
Highest Mass Loss
Mass Loss: 56.3014 mg/cm^2

S&NA Mg-2Ca Sample 7C

Mass Loss: 48.7432 mg/cm^2

S&NA Mg-2Ca Sample 7D
Lowest Mass Loss
Mass Loss: 23.6947 mg/cm^2

Figure 58: Surfaces of corroded Mg-2Ca samples (with Ag deposition) after 168 hours of immersion

For these S&NA Mg-2Ca samples immersed for 168 hours (from Figure 58), it was obvious that three of the Ag-deposited samples had Ag tracks that were similar to one another, with one sample (7D) having very different Ag track characteristics. If Sample 7D were temporarily disregarded, and the mass loss results of the remaining Ag-deposited samples in that group were compared to those of the uncoated samples, it was then found that the mass loss of the Ag-deposited samples was significantly higher ($p < 0.05$) than that of the uncoated samples (Figure 59).

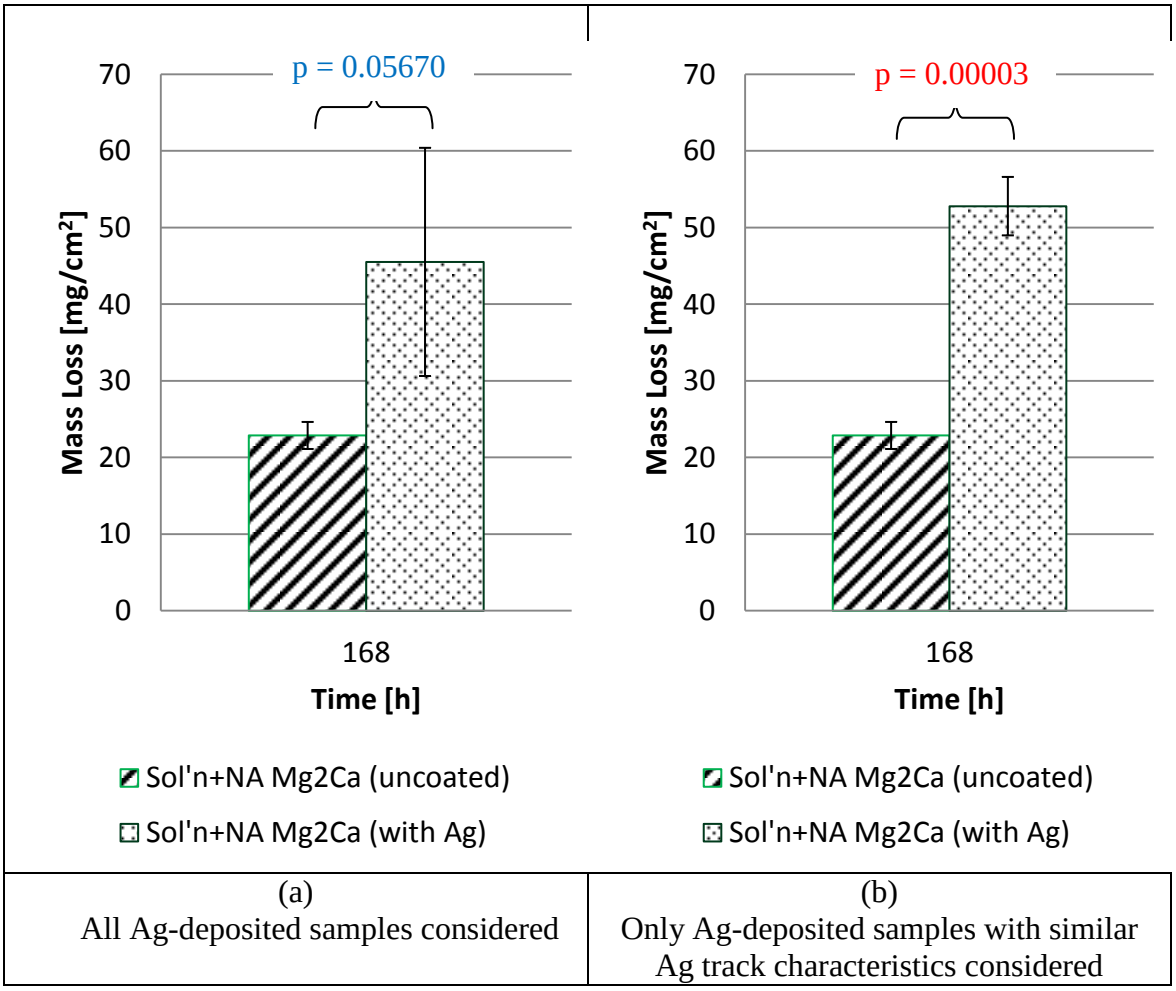

(a) All Ag-deposited samples considered

(b) Only Ag-deposited samples with similar Ag track characteristics considered

Figure 59: Mass loss results of S&NA Mg-2Ca samples (uncoated and with Ag-deposition) immersed for 168 hours

Considering this, it was speculated that depositing Ag nanoparticles on Mg (and Mg-based) substrates indeed had an effect on corrosion. In the cases where the Ag tracks were thick, dense, and solid, corrosion behaviour was significantly worse than corresponding samples without Ag deposition. However, when the Ag tracks were thinner/smaller, the corrosion behaviour of an Ag-deposited sample more closely resembled its corresponding uncoated sample.

It should be noted that the large variation in mass loss results associated with the Ag-deposited samples could be minimized through better control of the Ag depositions during the sample fabrication stage. Before the immersion tests were performed in this work, it was unclear how much the different Ag track characteristics could affect the corrosion/mass loss results, if at all. However, after reviewing all of the results, the extent to which different Ag track characteristics can affect corrosion seemed very apparent, and appeared to have quite a large effect on the corrosion/mass loss results. Knowing this, it would beneficial in the future to examine and characterize the Ag tracks on each and every sample after deposition, and reject samples that have Ag tracks that do not fit certain prescribed criteria (for example, track thickness must be within a certain range). In doing so, any sample with inferior Ag tracks could be eliminated from the sample group, which would likely lead to corrosion/mass loss results with smaller variation. However, there has been some benefit from the variation that has arisen in the present work due to the differences in the Ag track characteristics. The current results indicate that if the Ag depositions are controlled well enough to be thin/sparse, then the subsequent corrosion behaviour will not be affected greatly.

Ag has been thought to be beneficial to the mechanical properties when added to Mg alloys by improving its age hardening ability [67]. However, results presented by Shaw [68] indicated that when Ag is alloyed with Mg, the corrosion rate of this binary alloy in NaCl solution increases with increasing Ag content.

Also, Ben-Hamu *et al.* [69] studied the effects of the additions of Ag (up to 3 wt. %) on the corrosion behaviour of Mg-6Zn alloys. Similarly, it was found that the addition of Ag to these alloys resulted in increased corrosion rates when compared with binary Mg-6Zn (Figure 60) [69]. The lowered corrosion resistance of the alloys with Ag was attributed to the presence of the $Ag_{17}Mg_{54}$ phase, which acted as local cathodes to the α-Mg due to the electrochemical potential difference between the two phases [69].

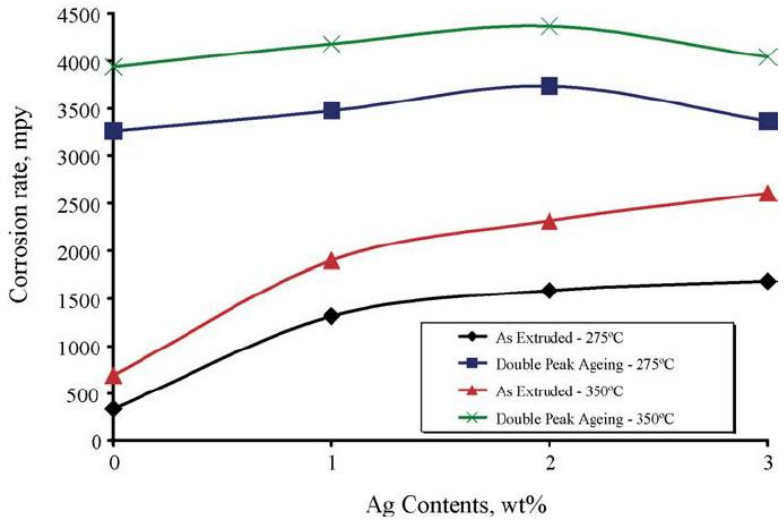

Figure 60: Corrosion results showing the effect of Ag additions to Mg-6Zn alloy [69]

Reprinted from Materials Science and Engineering A, 435-436, Ben-Hamu, G., Eliezer, D., Kaya, A., Na, Y.G., Shin, K.S., Microstructure and corrosion behavior of Mg-Zn-Ag alloys, Pages 579-587, Copyright (2006), with permission from Elsevier.

Because of the electrochemical potential difference between Mg and Ag, galvanic couples were created on the surfaces of the Ag-deposited samples in the present work. The Ag tracks would serve as local cathodes while the exposed Mg substrate served as local anodes, which would result in the preferential corrosion of the exposed Mg areas. Because this galvanic couple was obviously not present on the uncoated samples, it seemed reasonable that the corrosion of the Ag-deposited samples would be more severe than that of the uncoated samples. It was also noticed that corrosion seemed to be much worse when the Ag tracks were thick and solid compared to when the Ag tracks were thin and had a splattered appearance. This might well be explained by the fact that the ratios of anode (Mg) to cathode (Ag) area are different when Ag tracks are thick and dense versus thin and 'splattered'. Indeed, it has been said that as the ratio of the cathodic area to the anodic area increases, corrosion of the anode becomes increasingly rapid and severe [70], which would explain why the samples with thicker Ag tracks (i.e., higher cathode-to-anode ratio) corroded more severely than the samples with thinner Ag tracks (i.e., smaller cathode-to-anode ratio).

Another factor that likely contributed to the variation in mass loss results within a group of samples was the existence of inhomogeneities in the substrate material. This was particularly evident for the alloy materials. During the polishing step of the sample fabrication process of the Mg-2Ca and Mg-2Ca-1Zn alloy samples, small and irregular areas of roughness were frequently observed across the freshly polished surfaces (Figure 61 (a) and (b)). Upon examining these surfaces under SEM (Figure 61 (c) and (d)), it was

revealed that these areas were in fact areas of micro-porosity that had formed during the casting of the raw material.

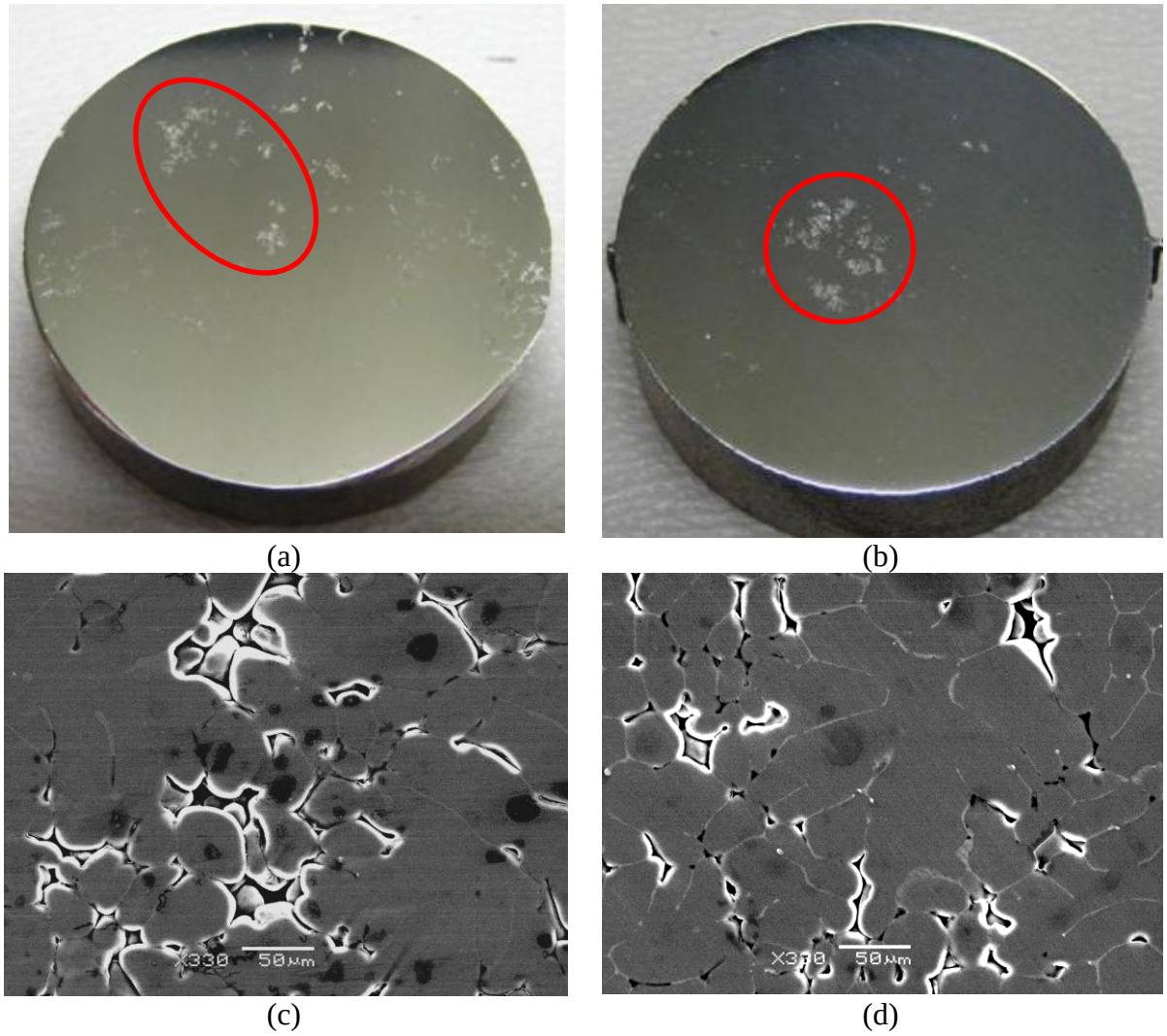

Figure 61: Areas of roughness on (a) Mg-2Ca and (b) Mg-2Ca-1Zn surfaces after polishing. Corresponding SEM images of (c) Mg-2Ca and (d) Mg-2Ca-1Zn samples showing micro-porosity

It has been said that micro-porosity would have severe negative effects on the corrosion behaviour of Mg alloys [71]. Understandably, more corrosion would occur at a

region of micro-porosity because the actual surface area at such a region is greater [71], resulting in more severe local corrosion.

As was mentioned, the alloy samples were cut into quarter-circle shapes from discs of the cast rods. Because the areas of porosity were not evenly distributed over the face of the cast rods, it was clear that some samples would have had larger areas of porosity than others within a sample group. It was therefore reasonable to suggest that the variation in mass loss results could be partly attributed to uneven areas of porosity within the cast structure of the alloy samples.

4.2 Corrosion Products and Corrosion Product Morphology

As mentioned in Chapter 4, samples were removed from the Hanks' solution after immersion for prescribed amounts of time, rinsed gently with distilled water, and dried in a light stream of air. The dried corroded samples possessed a layer of loosely adhered corrosion products that appeared white and powdery. As an example, an as-cast Mg-2Ca sample immersed for 336 hours is shown in Figure 62.

Figure 62: White corrosion products on the surface of an as-cast Mg-2Ca sample after 336 hours of immersion

4.2.1 Corrosion Product Morphology

Before corrosion product removal, corroded surfaces were viewed under SEM to obtain some understanding of the corrosion products. The corrosion product morphology was very similar across all samples (regardless of substrate type), showing large amounts of round corrosion product particles building up on a crackled surface, such as that seen in Figure 63. This crackled surface (with corrosion products) is typical of corroded Mg surfaces after immersion tests and has been observed by several other researchers [32,63]. The crackled appearance has been attributed to dehydration of the surface layer (during drying of the sample after immersion) and to the vacuum inside the SEM chamber [72]. It was worth noting that the physical characteristics of the corrosion products were typical for both uncoated samples as well as samples with Ag deposition; that is, under the SEM, the Ag tracks could not be seen (Figure 64), as they were covered by the growing

corrosion products. It is also likely that some of the Ag reacted and was incorporated into the corrosion products.

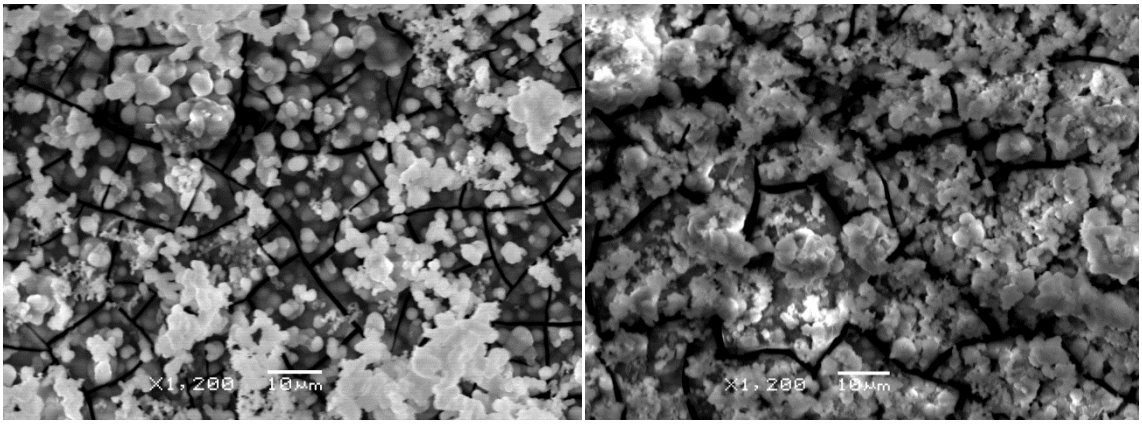

(a) (b)

Figure 63: SEM images of corroded surfaces of (a) Mg-2Ca after 48 hours of immersion and (b) uncoated Mg-2Ca-1Zn after 14 days immersion

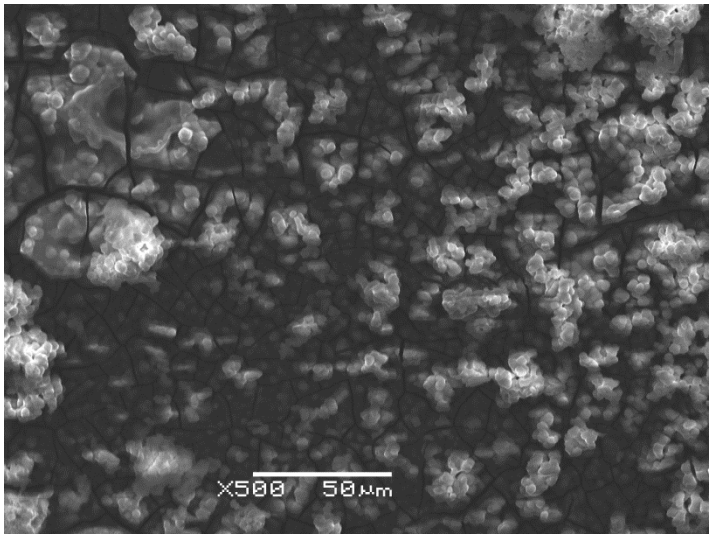

Figure 64: SEM image of Mg-2Ca-1Zn sample with Ag deposition after 48 hours of immersion

Although the corroded surfaces of all the samples largely resembled those in Figure 63 and Figure 64 (with more white corrosion products built up for samples with faster

corrosion rates and/or samples immersed for longer periods of time), needle-like formations were found upon closer inspection with the SEM. These needle-like formations were formed among the round corrosion product particles in very small areas on almost all of the samples. Majority of these needle-like formations were seen as clusters in seemingly isolated areas (Figure 65 (a)), while in other areas, the needle-like formations appeared to have grown across larger surfaces (Figure 65 (b) and (c)).

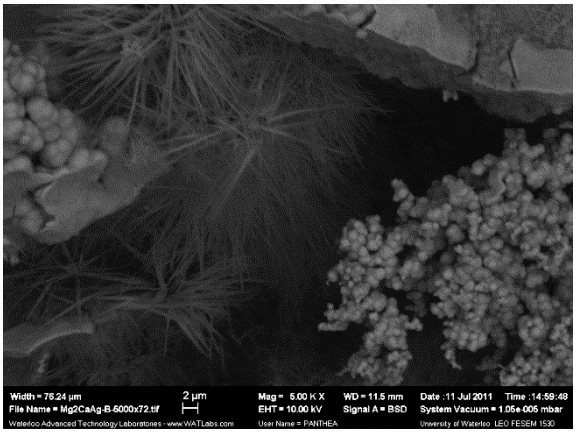

(a)

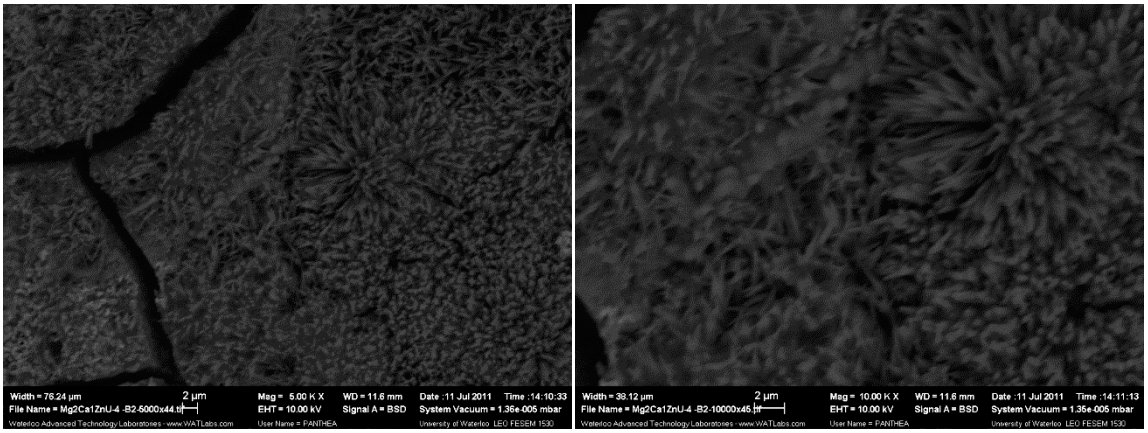

(b) (c)

Figure 65: SEM images showing needle-like formations on various corroded samples.

4.2.2 Identification of the Corrosion Products

XRD performed on the corrosion products formed during immersion revealed that the main corrosion product was magnesium hydroxide ($Mg(OH)_2$) (Figure 66), and was present on all of the samples tested, regardless of alloy and regardless of whether the samples were uncoated or had Ag deposition. The formation of $Mg(OH)_2$ was expected, since the corrosion reaction of Mg in aqueous environments has been illustrated by the chemical equation below [19] (which shows $Mg(OH)_2$ as a corrosion product along with hydrogen gas):

$$Mg_{(s)} + 2H_2O_{(aq)} \leftrightarrow Mg(OH)_{2(s)} + H_{2(g)}$$

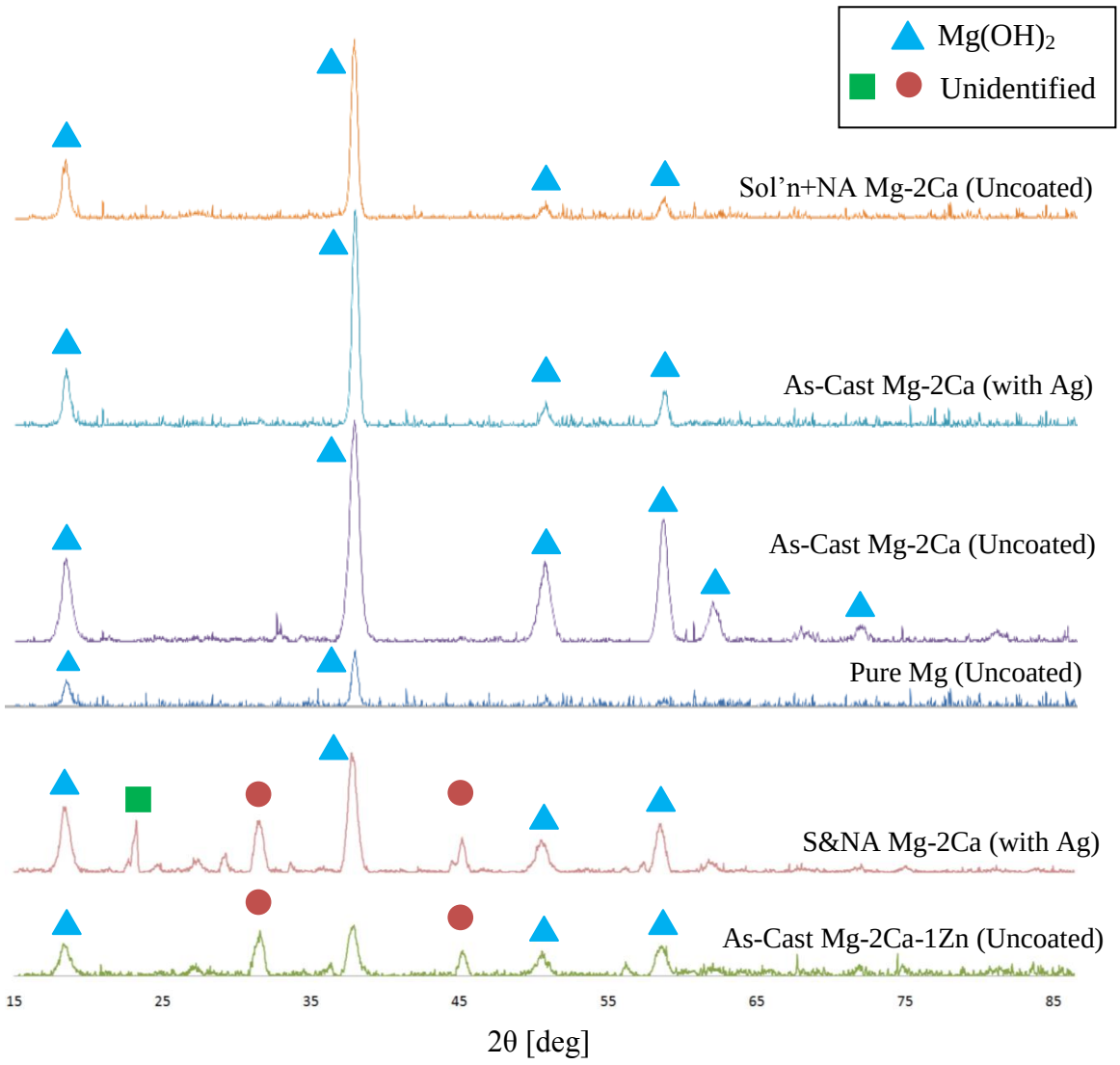

Figure 66: XRD patterns of the corrosion products

However, XRD also revealed several other peaks on two of the tested samples that could not be identified conclusively (seen on the last two traces in Figure 66). It was possible that these peaks represented certain compounds that were not contained in the database that was used for identification. The peak labelled with the green square for the S&NA Mg-2Ca (with Ag) sample may be due to the Ag deposition (for example, the possible formation of an Ag salt), as this peak was not present on any of the other traces.

EDX performed on the corrosion products consistently showed the presence of other elements in the corrosion products as well (Table 17). In addition to magnesium and oxygen, significant amounts of calcium and phosphorus were detected, as well as small amounts of carbon, and even smaller amounts of sodium and chloride (but not in all areas). This therefore indicated that the corrosion products consisted of other compounds as well (i.e., in addition to $Mg(OH)_2$) but were not successfully detected or identified by XRD analysis.

Table 17: EDX results of the corrosion products formed on corroded samples

Sample Type		Elements						
		C	O	Na	Mg	P	Cl	Ca
Without Ag Deposition	Pure Mg	11.11	36.65	1.92	17.51	14.01	1.78	18.02
	Mg-2Ca	10.68	42.09	1.12	5.56	15.77	--	24.77
	Mg-2Ca-1Zn	21.31	34.42	0.99	1.67	15.37	--	26.24
With Ag Deposition	Pure Mg	11.83	42.73	2.57	5.17	13.51	2.20	22.00
	Mg-2Ca	11.80	39.57	0.78	4.79	16.76	--	26.30
	Mg-2Ca-1Zn	18.95	37.65	1.09	2.21	14.53	--	25.56
Needle-like formations		--	45.32	--	44.65	--	10.03	--

In the work by Li *et al*. [27], in which as-cast Mg-1Ca and Mg-2Ca alloys were immersed in simulated body fluid, the formation of both $Mg(OH)_2$ and hydroxyapatite on the surfaces was confirmed by XRD (Figure 67). Chemical analysis on the corrosion products also revealed the presence of carbon, oxygen, magnesium, phosphorus, and calcium [27], much like the EDX results in the present work.

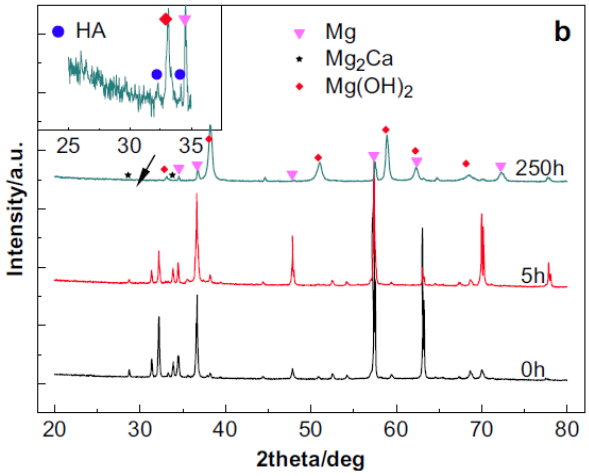

Figure 67: XRD results of the corrosion products formed on Mg-2Ca, confirming the presence of $Mg(OH)_2$ and hydroxyapatite [27]

Reprinted from Biomaterials, 29, Li, Z., Gu, X., Lou, S., Zheng, Y., The development of binary Mg-Ca alloys for use as biodegradable materials within bone, Pages 1329-1344, Copyright (2008), with permission from Elsevier.

Similarly, in the work by Zhang *et al.* [73], Mg-6Zn alloy was immersed in simulated body fluid for 30 days. XRD performed on the corroded samples also confirmed the presence of $Mg(OH)_2$ and hydroxyapatite as the corrosion products [73] (Figure 68).

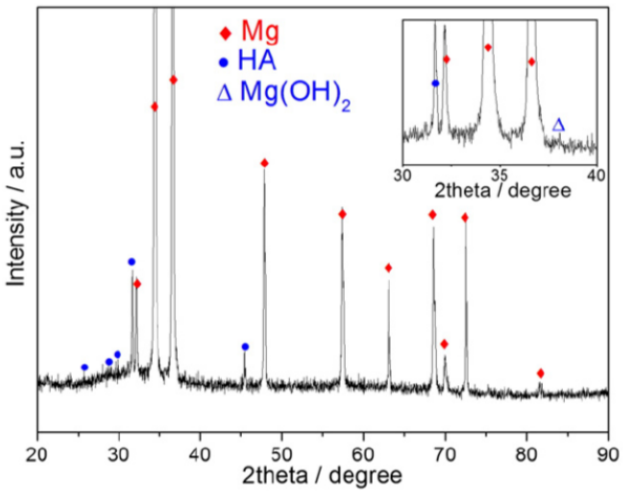

Figure 68: XRD results of corrosion products formed on Mg-6Zn, confirming the presence of $Mg(OH)_2$ and hydroxyapatite [73]

Reprinted from Materials Science and Engineering C, 29, Zhang, S., Li, J., Song, Y., Zhao, C., Zhang, X., Xie, C., Zhang, Y., Tao, H., He, Y., Jiang, Y., Bian, Y., In vitro degradation, hemolysis and MC3T3-E1 cell adhesion of biodegradable Mg-Zn alloy, Pages 1907-1912, Copyright (2009), with permission from Elsevier.

Wang *et al.* [74] also found that hydroxyapatite and $Mg(OH)_2$ had formed in the corrosion products after pure Mg substrates were immersed in simulated body fluids. In addition, they also found needle-like clusters on the surfaces of the samples [74], shown in Figure 69 . Chemical analysis performed on these clusters revealed a relatively high Cl content (along with high Mg and O content), leading the authors to suggest that the clusters might contain $MgCl_2$ [74]. This is plausible since the Cl^- ions present in simulated body fluids can transform $Mg(OH)_2$ into $MgCl_2$ via the following chemical equation [14]:

$$Mg(OH)_2 + 2Cl^- \rightarrow MgCl_2 + 2OH^-$$

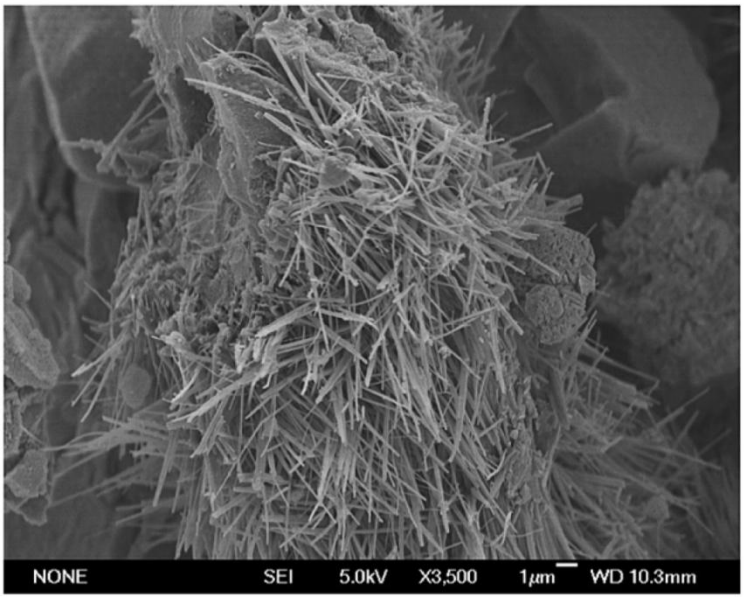

Figure 69: Needle-like clusters formed on surfaces of pure Mg after 3 days of immersion in simulated body fluid [74]

Reprinted from Materials Letters, 62, Wang, Y., Wei, M., Gao, J., Hu, J., Zhang, Y., Corrosion process of pure magnesium in simulated body fluid, Pages 2181-2184, Copyright (2008), with permission from Elsevier.

Given the fact that EDX performed on the needle-like formations in the present work also revealed relatively large amounts of Mg, O, and Cl (Table 17), it was conceivable that $MgCl_2$ was also present in the needle-like formations.

In an investigation by Hiromoto *et al.* [75], hydroxyapatite crystals were intentionally grown on the surfaces of pure Mg and AZ31 alloy in order to evaluate the effect of the hydroxyapatite coating on corrosion behaviour. The SEM images of the hydroxyapatite-coated surfaces obtained by Hiromoto *et al*. are shown in Figure 70.

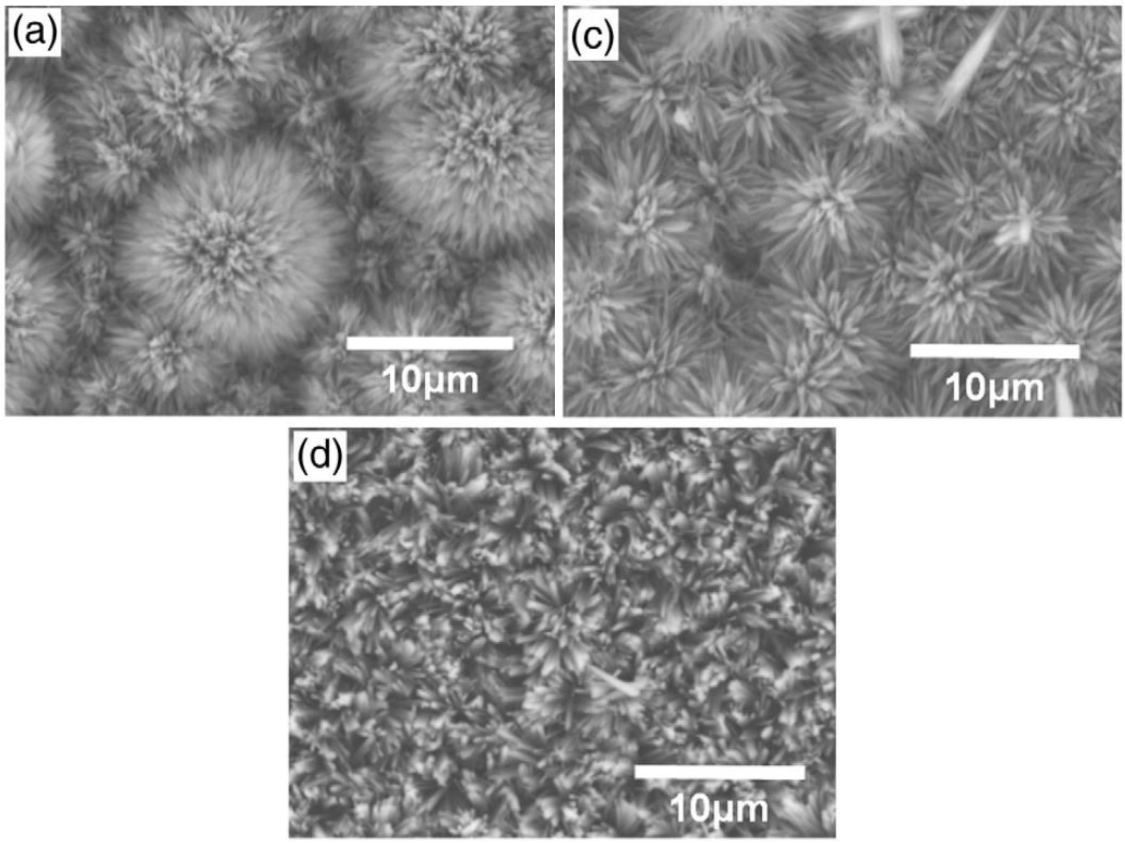

Figure 70: Hydroxyapatite grown on surfaces of AZ31 (a,c) and pure Mg (d) [75]

Reprinted from Surface & Coatings Technology, 205, Hiromoto, S., Tomozawa, M., Hydroxyapatite coating of AZ31 magnesium alloy by a solution treatment and its corrosion behavior in NaCl solution, Pages 4711-4719, Copyright (2011), with permission from Elsevier.

The hydroxyapatite crystals in Figure 70 bear a close resemblance to the needle-like formations found on the corroded samples of the present work (Figure 65). It has been reported that hydroxyapatite can precipitate in simulated body fluids after immersion for certain amounts of time [74], so it is very likely that hydroxyapatite had indeed formed after long periods of immersion in this work.

It was also possible that Mg- and/or Ca-containing phosphates were present in the corrosion products. Mg- and Ca-containing phosphates have been reported as corrosion

products from several other researchers [32,63]. For example, Yang *et al.* [63] immersed Mg-1Mn-1Zn alloy samples in Hanks' solution, and the resultant corroded surface is shown in Figure 71 (a). EDX analysis showed the presence of Mg, Ca, P, and O, and XRD analysis indicated the presence of $Ca_3Mg_3(PO_4)_4$ in the corrosion products (Figure 71 (b)) [63].

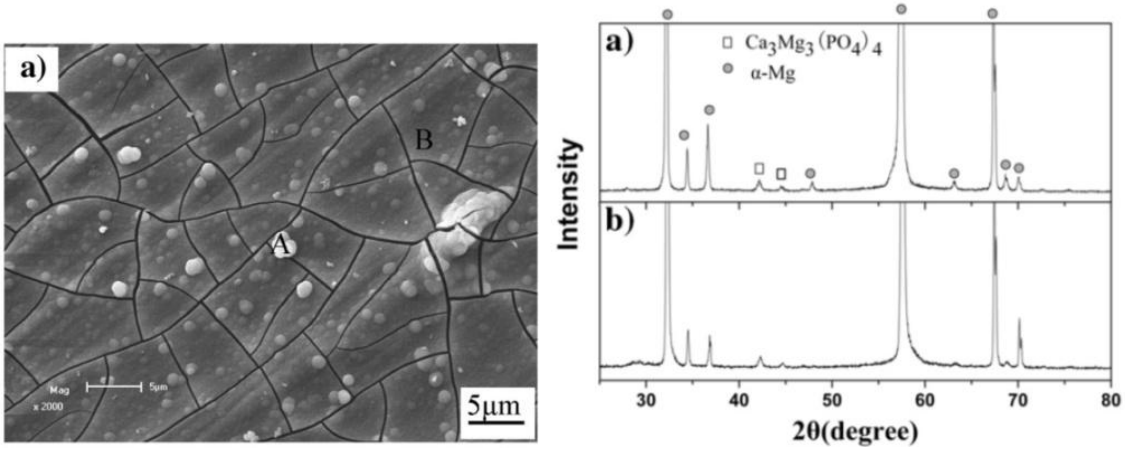

(a) (b)

Figure 71: (a) Corroded surface of Mg-1Mn-1Zn after immersion in Hanks' solution, and XRD results of the formed corrosion products [63]

Likewise, Du *et al.* [32] also believed that Mg- and Ca-phosphates were present in the corrosion products after their investigation involving the immersion of Mg-3Ca-2Zn alloys in Hanks' solution (resultant corroded surface is shown in Figure 72). Chemical analysis revealed the presence of Mg, Ca, P, and O [32]. The authors suggested that the Mg and Ca ions released from the alloy during the corrosion reaction could have

combined with the phosphate ions from the Hanks' solution to form the Mg- and Ca-containing phosphates [32].

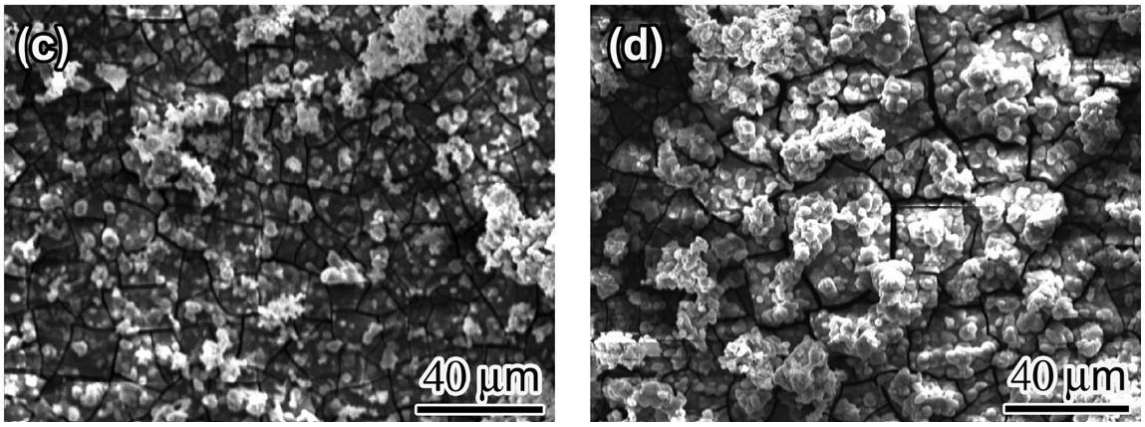

Figure 72: Corroded surface of Mg-3Ca-2Zn after immersion in Hanks' solution for different times [32]

Reprinted from Materials Chemistry and Physics, 125, Du, H., Wei, Z., Liu, X., Zhang, E., Effects of Zn on the microstructure, mechanical property and bio-corrosion property of Mg-3Ca alloys for biomedical application, Pages 568-575, Copyright (2011), with permission from Elsevier.

Finally, in the work of Zhang *et al.* [35], Mg-*x*Zn-1Ca alloys (with varying Zn contents) were immersed in Hanks' solution. XRD analysis performed on the corrosion products revealed that $Mg(OH)_2$, hydroxyapatite, *and* a type of Mg- and Ca-containing phosphates had all formed on the surfaces of the samples (Figure 73) [35].

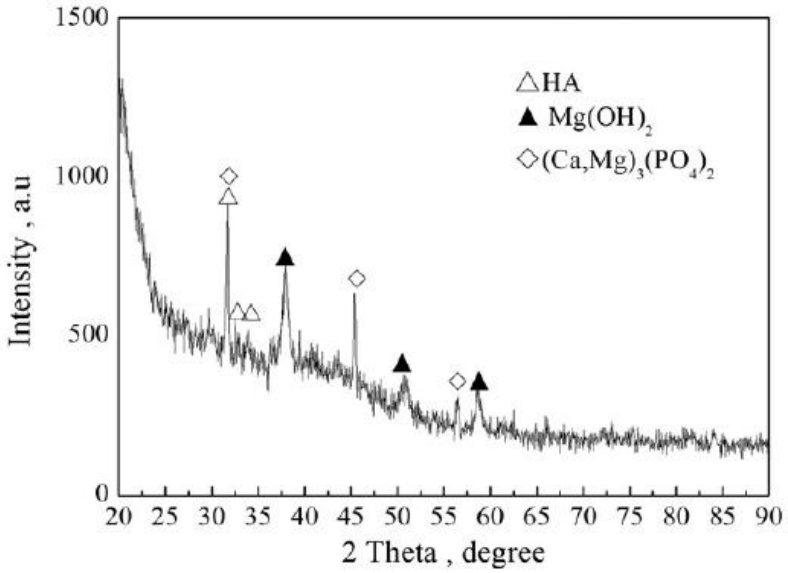

Figure 73: XRD results of the corrosion products formed on Mg-*x*Zn-1Ca alloys [35]

Reprinted from Materials Science and Engineering C, 31, Zhang, B., Hou, Y., Wang, X., Wang, Y., Geng, L., Mechanical properties, degradation performance and cytotoxicity of Mg-Zn-Ca biomedical alloys with different compositions, Pages 1667-1673, Copyright (2011), with permission from Elsevier.

Given the similarities among the immersion tests and results of the present work and those presented in the literature, it was possible that the corrosion products formed in the present work (along with the already confirmed $Mg(OH)_2$) could have been a type of Mg- and/or Ca-containing phosphate, $MgCl_2$, and/or hydroxyapatite. Further examination would confirm this. The formation of a larger amount of corrosion products (via longer immersion times) before examination with XRD would be recommended, as it was believed that the limited amount of corrosion products that had formed and were available for XRD examination in the present work was not sufficient and thus hindered the ability to successfully detect the other compounds within the corrosion products.

Chapter 5

Conclusions

The corrosion behaviour of pure Mg, Mg-2Ca, and Mg-2Ca-1Zn has been studied in this work using static immersion tests in Hanks' solution. The effect of Ag nanoparticle deposition on corrosion behaviour was also studied. As well, the characteristics of the corrosion products were examined using SEM, EDX, and XRD.

The mass loss of the as-cast uncoated Mg-2Ca was shown to be statistically significantly higher than that of as-cast uncoated pure Mg and Mg-2Ca-1Zn. More severe corrosion of the Mg-2Ca alloy was attributed to the presence of the Mg_2Ca phase. The addition of 1 wt. % Zn to the Mg-2Ca alloy improved the corrosion behaviour significantly.

Solutionized and naturally aged Mg-2Ca samples exhibited statistically significantly less mass loss than as-cast Mg-2Ca samples during the earlier stages of immersion, but no statistically significant differences were detected at longer immersion times. For the Mg-2Ca-1Zn alloy, the solutionizing and natural aging treatment did not appear to enhance corrosion resistance for any length of immersion.

Ag depositions indeed seemed to have an effect on the corrosion behaviour. The corrosion behaviour of the substrates seemed to be very sensitive to the Ag track characteristics; the extent to which Ag depositions can affect corrosion depended on the characteristics of the Ag tracks. When more Ag was present on the substrates (i.e., the Ag tracks were sufficiently thick and dense, and thus, the sample possessed a higher cathode-to-anode ratio), the mass loss values were statistically significantly higher than corresponding

samples without any Ag deposition. However, if the Ag tracks were thin and sparse (i.e., the sample possessed a smaller cathode-to-anode ratio), then the mass loss values of those Ag-deposited samples tended to be closer to corresponding uncoated samples and statistically significant differences were not detected. Therefore, it was believed that Ag deposition could be a suitable surface modification for antibacterial purposes if the Ag track characteristics were very carefully controlled.

White and powdery corrosion products formed on all of the samples tested. The corrosion product morphology appeared to be very similar for samples with and without Ag deposition. Small needle-like formations were also found on certain areas of the corroded samples. XRD analysis indicated that the main corrosion product was $Mg(OH)_2$. However, EDX analysis consistently revealed other elements in the corrosion products as well (Mg, Ca, O, P, small amounts of C, and sometimes Cl). As such, it was probable that other compounds (possibly hydroxyapatite, $MgCl_2$, and/or Mg- and Ca-containing phosphates) were also present in the corrosion products along with $Mg(OH)_2$ but could not be detected. This was possibly due to reasons pertaining to sample preparation (e.g., the amount of corrosion product that could be collected after a feasible time period for corrosion was insufficient).

Chapter 6

Recommendations for Future Work

Because the corrosion behaviour of Mg and Mg alloys was sensitive to the characteristics of the Ag tracks, it is recommended to perform corrosion tests to determine what the Ag track characteristics would have to be (e.g., how thin or thick) in order to consistently cause a significant difference in corrosion behaviour (when compared to uncoated samples). These key track characteristics could then be used to create Ag-deposited samples with thinner/smaller Ag tracks so that the corrosion behaviour is not significantly deteriorated. Also, because corrosion behaviour did not appear to significantly deteriorate if the Ag tracks were thin, *in vitro* bacterial culture tests would be recommended to determine if the small amount of Ag (not causing a significant difference in corrosion) is enough to have an antibacterial effect.

References

[1] Paital, S.R., Dahotre, N.B. Calcium phosphate coatings for bio-implant applications: Materials, performance factors, and methodologies. Materials Science and Engineering R 66 (2009) 1-70.

[2] Erdmann, N., Bondarenko, A., Hewicker-Trautwein, M., Angrisani, N., Reifenrath, J., Lucas, A., Meyer-Lindenberg, A. Evaluation of the soft tissue biocompatibility of MgCa0.8 and surgical steel 316L in vivo: a comparative study in rabbits. BioMedical Engineering OnLine 9:63 (2010)

[3] Staiger, M.P., Pietak, A.M., Huadmai, J., Dias, G. Magnesium and its alloys as orthopedic biomaterials: a review. Biomaterials 27 (2006) 1728-1734.

[4] Dee, K.C., Puleo, D.A., Bizios, R. (2002). *An introduction to tissue-biomaterial interactions*. New Jersey: John Wiley & Sons, Inc.

[5] Silverthorn, D.U. (2007). *Human physiology: An integrated approach*. (4). San Francisco: Pearson Education, Inc. (Benjamin Cummings).

[6] Vormann, J. Magnesium: nutrition and metabolism. Molecular Aspects of Medicine 24 (2003) 27-37.

[7] M. Kontani, A. Hara, S. Ohta, T. Ikeda. Hypermagnesemia induced by massive cathartic ingestion in an elderly woman without pre-existing renal dysfunction. Internal Medicine 44 (2005) 448-452.

[8] Brar, H.S., Platt, M.O., Sarntinoranont, M., Martin, P.I., Manuel, M.V. Magnesium as a biodegradable and bioabsorbable material for medical implants. JOM 61 (2009) 31-34.

[9] Song, G. Control of biodegradation of biocompatible magnesium alloys. Corrosion Science 49 (2007) 1696-1701.

[10] Gosheger, G., Hardes, J., Ahrens, H., Streitburger, A., Buerger, H., Erren, M., Gunsel, A., Kemper, F.H., Winkelmann, W., von Eiff, C. Silver-coated megaendoprostheses in a rabbit model – an analysis of the infection rate and toxicological side effects. Biomaterials 25 (2004) 5547-5556.

[11] Witte, F., Kaese, V., Haferkamp, H., Switzer, E., Meyer-Lindenberg, A., Wirth, C.J., Windhagen, H. In vivo corrosion of four magnesium alloys and the associated bone response. Biomaterials 26 (2005) 3557-3563.

[12] Zeng, R., Dietzel, W., Witte, F., Hort, N., Blawert, C. Progress and challenge for magnesium alloys as biomaterials. Advanced Engineering Materials 10 (2008) B3-B14.

[13] Peeters, P., Bosiers, M., Verbist, J., Deloose, K., Heublein, B. Preliminary results after application of absorbable metal stents in patients with critical limb ischemia. Journal of Endovascular Therapy 12 (2005) 1-5.

[14] Wang, Y., Lim, C.S., Lim, C.V., Yong, M.S., Teo, E.K., Moh, L.N. In vitro degradation behavior of M1A magnesium alloy in protein-containing simulated body fluid. Materials Science and Engineering C 31 (2011) 579-587.

[15] Waksman, R., Pakala, R., Kuchulakanti, P.K., Baffour, R., Hellinga, D., Seabron, R., Tio, F.O., Wittchow, E., Hartwig, S., Harder, C., Rohde, R., Heublein, B., Andreae, A., Waldmann, K.H., Haverich, A. Safety and efficacy of bioabsorbable magnesium alloy stents in porcine coronary arteries. Catheterization and Cardiovascular Interventions 68 (2006) 607-617.

[16] Xin, Y., Liu, C., Zhang, X., Tang, G., Tian, X., Chu, P.K. Corrosion behavior of biomedical AZ91 magnesium alloy in simulated body fluids. Journal of Materials Research 22 (2007) 2004-2011.

[17] Liu, C., Xin, Y., Tang, G., Chu, P.K. Influence of heat treatment on degradation behaviour of bio-degradable die-cast AZ63 magnesium alloy in simulated body fluid. Materials Science and Engineering A 456 (2007) 350-357.

[18] Quach, N.C., Uggowitzer, P.J., Schmutz, P. Corrosion behaviour of an Mg-Y-RE alloy used in biomedical applications studied by electrochemical techniques. Comptes Rendus Chimie 11 (2008) 1043-1054.

[19] Witte, F., Hort, N., Vogt, C., Cohen, S., Kainer, K.U., Willumeit, R., Feyerabend, F. Degradable biomaterials based on magnesium corrosion. Current Opinion in Solid State and Materials Science 12 (2008) 63-72.

[20] Song, G., Atrens, A. Understanding magnesium corrosion: A framework for improved alloy performance. Advanced Engineering Materials 5 (2003) 837-858

[21] McLachlan, D.R.C. Aluminium and the risk for Alzheimer's disease. Environmetrics 6 (1995) 233-275.

[22] Song, Y., Shan, D., Chen, R., Zhang, F., Han, E.H.. Biodegradable behaviors of AZ31 magnesium alloy in simulated body fluid. Materials Science and Engineering C 29 (2009) 1039-1045.

[23] Zhang, E., He, W., Du, H., Yang, K. Microstructure, mechanical properties and corrosion properties of Mg-Zn-Y alloys with low Zn content. Materials Science and Engineering A 488 (2008) 102-111.

[24] Wu, G., Fan, Y., Gao, H., Zhai, C., Zhu, Y.P. The effect of Ca and rare earth elements on the microstructure, mechanical properties and corrosion behavior of AZ91D. Materials Science and Engineering A 408 (2005) 255-263.

[25] Zhang, E., Yang, L. Microstructure, mechanical properties and bio-corrosion properties of Mg-Zn-Mn-Ca alloy for biomedical application. Materials Science and Engineering A 497 (2008) 111-118.

[26] Wan, Y., Xiong, G., Luo, H., He, F., Huang, Y., Zhou, X. Preparation and characterization of a new biomedical magnesium-calcium alloy. Materials and Design 29 (2008) 2034-2037.

[27] Li, Z., Gu, X., Lou, S., Zheng, Y. The development of binary Mg-Ca alloys for use as biodegradable materials within bone. Biomaterials 29 (2008) 1329-1344.

[28] Denkena, B., Lucas, A. Biocompatible magnesium alloys as absorbable implant materials – Adjusted surface and subsurface properties by machining processes. CIRP Annals – Manufacturing Technology 56 (2007) 113-116.

[29] Kirkland, N.T., Birbilis, N., Walker, J., Woodfield, T., Dias, G.J., Staiger, M.P. *In-vitro* dissolution of magnesium-calcium binary alloys: Clarifying the unique role of calcium additions in bioresorbable magnesium implant alloys. Journal of Biomedical Materials Research B: Applied Biomaterials 95B (2010) 91-100.

[30] von der Höh, N., von Rechenberg, B., Bormann, D., Lucas, A., Meyer-Lindenberg, A. Influence of different surface machining treatments of resorbable magnesium alloy implants on degradation – EDX-analysis and histology results. Materialwissenschaft und Werkstofftechnik 40 (2009) 88-93.

[31] You, B.S., Park, W.W., Chung, I.S. The effect of calcium additions on the oxidation behavior in magnesium alloys. Scripta Materialia 42 (2000) 1089-1094.

[32] Du, H., Wei, Z., Liu, X., Zhang, E. Effects of Zn on the microstructure, mechanical property and bio-corrosion property of Mg-3Ca alloys for biomedical application. Materials Chemistry and Physics 125 (2011) 568-575.

[33] Rad, H.R.B., Idris, M.H., Kadir, M.R.A., Farahany, S., Fereidouni, A., Yahya, M.Y. Characterization and corrosion behavior of biodegradable Mg-Ca and Mg-Ca-Zn implant alloys. Applied Mechanics and Materials 121-126 (2012) 568-572.

[34] Xu, Z., Smith, C., Chen, S., Sankar, J. Development and microstructural characterizations of Mg-Zn-Ca alloys for biomedical applications. Materials Science & Engineering B 176 (2011) 1660-1665.

[35] Zhang, B., Hou, Y., Wang, X., Wang, Y., Geng, L. Mechanical properties, degradation performance and cytotoxicity of Mg-Zn-Ca biomedical alloys with different compositions. Materials Science and Engineering C 31 (2011) 1667-1673.

[36] Gao, J.H., Guan, S.K., Ren, Z.W., Sun Y.F., Zhu, S.J., Wang, B. Homogeneous corrosion of high pressure torsion treated Mg-Zn-Ca alloy in simulated body fluid. Materials Letters 65 (2011) 691-693.

[37] Ouyang, C., Lei, T., Wang, L., Li, N.F., Zhou, L.S. Corrosion behaviours of ternary Mg-Zn-Ca alloy biomaterials. The Chinese Journal of Nonferrous Metals 20 (2010) 891-897.

[38] Sun, Y., Zhang, B., Wang, Y., Geng, L., Jiao, X.. Preparation and characterization of a new biomedical Mg-Zn-Ca alloy. Materials and Design 34 (2012) 58-64.

[39] Langelier, B., Esmaeili, S. (2010). The effect of Zn additions on precipitation hardening of Mg-Ca alloys, in *Magnesium Technology 2010: Proceedings of a Symposium Sponsored by the Magnesium Committee of the Light Metals Division of TMS*, February 14-18, 2010, Seattle, 505-510. Wiley, John & Sons, Incorporated.

[40] Bamberger, M., Levi, G., Vander Sande, J.B.. Precipitation hardening in Mg-Ca-Zn alloys. Metallurgical and Materials Transactions A 37A (2006) 481-487.

[41] Langelier, B., Wang, X., Esmaeili, S. Evolution of precipitation during non-isothermal ageing of an Mg-Ca-Zn alloy with high Ca content. Materials Science and Engineering A 538 (2012) 246-251.

[42] Geng, L., Zhang, B.P., Li, A.B., Dong, C.C. Microstructure and mechanical properties of Mg-4.0Zn-0.5Ca alloy. Materials Letters 63 (2009) 557-559.

[43] Gu, X., Zheng, Y., Zhong, S., Xi, T., Wang, J., Wang, W. Corrosion of, and cellular responses to Mg-Zn-Ca bulk metallic glasses. Biomaterials 31 (2010) 1093-1103.

[44] Gray, J.E., Luan, B. Protective coatings on magnesium and its alloys – a critical review. Journal of Alloys and Compounds 336 (2002) 88-113.

[45] Gray-Munro, J.E., Seguin, C., Strong, M. Influence of surface modification on the in vitro corrosion rate of magnesium alloy AZ31. Journal of Biomedical Materials Research Part A 91A (2009) 221-230.

[46] Cui, F.Z., Yang, J.X., Jiao, Y.P., Yin, Q.S., Zhang, Y., Lee, I.S. Calcium phosphate coating on magnesium alloy for modification of degradation behavior. Frontiers of Materials Science in China 2 (2008) 143-148.

[47] Hiromoto, S., Yamamoto, A. Control of degradation rate of bioabsorbable magnesium by anodization and steam treatment. Materials Science and Engineering C 30 (2010) 1085-1093.

[48] Wang, H., Shi, Z.. In vitro biodegradation behavior of magnesium and magnesium alloy. Journal of Biomedical Materials Research Part B: Applied Biomaterials 98B (2011) 203-209.

[49] Hiromoto, S., Shishido, T., Yamamoto, A., Maruyama, N., Somekawa, H., Mukai, T. Precipitation control of calcium phosphate on pure magnesium by anodization. Corrosion Science 50 (2008) 2906-2913.

[50] Zhang, X.P., Zhao, Z.P., Wu, F.M., Wang, Y.L. Corrosion and wear resistance of AZ91D magnesium alloy with and without microarc oxidation coating in Hank's solution. Journal of Materials Science 42 (2007) 8523-8528.

[51] Shi, P., Ng, W.F., Wong, M.H., Cheng, F.T. Improvement of corrosion resistance of pure magnesium in Hanks' solution by microarc oxidation with sol-gel TiO_2 sealing. Journal of Alloys and Compounds 469 (2009) 286-292.

[52] Hanawa, T. In vivo metallic biomaterials and surface modification. Materials Science and Engineering A 267 (1999) 260-266.

[53] Wan, Y.Z., Xiong, G.Y., Luo, H.L., He, F., Huang, Y., Wang, Y.L. Influence of zinc ion implantation on surface nanomechanical performance and corrosion resistance of biomedical magnesium-calcium alloys. Applied Surface Science 254 (2008) 5514-5516.

[54] Mao, L., Wang, Y., Wan, Y., He, F., Huang, Y. Corrosion resistance of Ag-ion implanted Mg-Ca-Zn alloys in SBF. Rare Metal Materials and Engineering 39 (2010) 2075-2078.

[55] Bosetti, M., Massè, A., Tobin, E., Cannas, M. Silver coated materials for external fixation devices: in vitro biocompatibility and genotoxicity. Biomaterials 23 (2002) 887-892.

[56] Colmano, G., Edwards, S.S., Barranco, S.D. Activation of antibacterial silver coatings on surgical implants by direct current: preliminary studies in rabbits. American Journal of Veterinary Research 41 (1980) 964-966.

[57] Chen, W., Liu, Y., Courtney, H.S., Bettenga, M., Agrawal, C.M., Bumgardner, J.D., Ong, J.L. In vitro anti-bacterial and biological properties of magnetron co-sputtered silver-containing hydroxyapatite coating. Biomaterials 27 (2006) 5512-5517.

[58] Bai, X., More, K., Rouleau, C.M., Rabiei, A. Functionally graded hydroxyapatite coatings doped with antibacterial components. Acta Biomaterialia 6 (2010) 2264-2273.

[59] Choi, C.H., Hagvall, S.H., Wu, B.M., Dunn, J.C.Y., Beygui, R.E., Kim, C.J. Cell interaction with three-dimensional sharp-tip nanotopography. Biomaterials 28 (2007) 1672-1679.

[60] Teixeira, A.I., McKie, G.A., Foley, J.D., Bertics, P.J., Nealey, P.F., Murphy, C.J. The effect of environmental factors on the response of human corneal epithelial cells to nanoscale substrate topography. Biomaterials 27 (2006) 3945-3954.

[61] Shi, Z., Huang, X., Cai, Y., Tang, R., Yang, D. Size effect of hydroxyapatite nanoparticles on proliferation and apoptosis of osteoblast-like cells. Acta Biomaterialia 5 (2009) 338-345.

[62] Alemohammad, H., Aminfar, O., Toyserkani, E. Morphology and microstructure analysis of nano-silver thin films deposited by laser-assisted maskless microdeposition. Journal of Micromechanics and Microengineering 18 (2008) 1-12.

[63] Yang, L., Zhang, E. Biocorrosion behavior of magnesium alloy in different simulated fluids for biomedical application. Materials Science and Engineering C 29 (2009) 1691-1696.

[64] He, W., Zhang, E., Yang, K. Effect of Y on the bio-corrosion behavior of extruded Mg-Zn-Mn alloy in Hank's solution. Materials Science and Engineering C 30 (2010) 167-174.

[65] Gerasimov, V.V., Rozenfeld, I.L. Effect of temperature on the rate of corrosion of metals. Russian Chemical Bulletin 6 (1957) 1192-1197.

[66] Südholz, A.D., Kirkland, N.T., Buchheit, R.G., Birbilis, N. Electrochemical properties of intermetallic phases and common impurity elements in Mg alloys. Electrochemical and Solid-State Letters 14 (2011) C5-C7.

[67] Avedesian, M.M., Baker, H. (1999). *Magnesium and magnesium alloys: ASM specialty handbook*. (2). Materials Park, OH: ASM International.

[68] Shaw, B.A. Corrosion Resistance of Magnesium Alloys. ASM Handbook, Volume 13A Corrosion: Fundamentals, Testing, and Protection (#06494G) ASM International (2003) 692-696.

[69] Ben-Hamu, G., Eliezer, D., Kaya, A., Na, Y.G., Shin, K.S. Microstructure and corrosion behavior of Mg-Zn-Ag alloys. Materials Science and Engineering A 435-436 (2006) 579-587.

[70] Dexter, S.C. Galvanic Corrosion. Sea Grant Publication.

[71] Song, G., Atrens, A. Corrosion mechanisms of magnesium alloys. Advanced Engineering Materials 1 (1999) 11-33.

[72] Baril, G., Pébère, N. The corrosion of pure magnesium in aerated and deaerated sodium sulphate solutions. Corrosion Science 43 (2001) 471-484.

[73] Zhang, S., Li, J., Song, Y., Zhao, C., Zhang, X., Xie, C., Zhang, Y., Tao, H., He, Y., Jiang, Y., Bian, Y. In vitro degradation, hemolysis and MC3T3-E1 cell adhesion of biodegradable Mg-Zn alloy. Materials Science and Engineering C 29 (2009) 1907-1912.

[74] Wang, Y., Wei, M., Gao, J., Hu, J., Zhang, Y. Corrosion process of pure magnesium in simulated body fluid. Materials Letters 62 (2008) 2181-2184.

[75] Hiromoto, S., Tomozawa, M. Hydroxyapatite coating of AZ31 magnesium alloy by a solution treatment and its corrosion behavior in NaCl solution. Surface & Coatings Technology 205 (2011) 4711-4719.